SIZE CONTROLLED REVERSE MICELLE SYNTHESIS OF METALLIC COBALT NANOPARTICLES

By

KEVIN NAKIA BARBER

Bachelor of Science Chemical Engineering

University of Oklahoma

Norman, Oklahoma

1999

Submitted to the Faculty of the
Graduate College of the
Oklahoma State University
in partial fulfillment of
the requirements for
the Degree of
MASTER OF SCIENCE
July, 2005

SIZE CONTROLLED REVERSE

MICELLE SYNTHESIS OF METALLIC

COBALT NANOPARTICLES

Thesis Approved:

Dr. James E. Smay

Thesis Adviser

Dr. Allen Apblett

Dr. A. Johannes

A. Gordon Emslie

Dean of the Graduate College

TABLE OF CONTENTS

LIST OF TABLES

LIST OF FIGURES

ACKNOWLEDGEMENTS

This thesis is dedicated to the memories of Mrs. Cammie (Malone) Virden (1906-1998) and Garner Dale Maggard (1927-2003), two people, without whom, I am sure, I would never have come this far.

I would like to thank my advisor, Dr. James Smay and my committee members, Dr. "AJ" Johannes and Dr. Allen Apblett for all their help and encouragement. I would also like to thank Dr. Khaled Gasem, Dr. Sundar Madihali, Dr. Shushing Tan, and Phoebe Doss for all their encouragement and assistance. I would also like to thank my parents, Charles and Juanita Barber, and my aunt Betty Maggard for everything. I must also thank the following people for their friendship and support: Ronetta Kerntke and Family, Joe Hurdle and Augie Bernstein, Regina Heim, Dr. Ronald Heim and Family, Dr. Jerry Newman, Dr. Louis Rose, Mark Deaver, Steve Marino, and Stacy Sanders.

Chapter 1: Introduction

1.1. Introduction

This thesis describes the synthesis and characterization of cobalt nanoparticles by a reverse micelle route. A factorially designed set of experiments were used to assess the effect of process variables on nanoparticle composition, size, and polydispersity. The results and analysis presented herein may elucidate controllable parameters leading to improved synthesis of nanoparticle catalyst size and chemistry for applications such as carbon nanotube growth.

1.2. Scope:

This thesis focuses specifically on the synthesis and characterization of cobalt nanoparticles in the size range of 1 to 5 nm diameters by a reverse micelle route. The size and polydispersity analysis was performed using atomic force microscopy and dynamic light scattering.

1.3. Objectives:

The objectives of the work described in this thesis were to:

1. synthesize cobalt nanoparticles with (i) size selectable average diameter in the range of 1-5 nm, (ii) narrow size distribution (+/-10%), and (iii) pure metallic composition.
2. devise a factorial design of experiments to determine the effects of (i) metal salt concentration (ii) reducing agent to metal salt molar ratio, and (iii) water to surfactant molar ratio on the synthesized nanoparticle size, distribution, and composition.
3. characterize the synthesized cobalt nanoparticle size by (i) dynamic light scattering, (ii) tapping mode atomic force microscopy, and
4. elucidate an experimental correlation relating the process variables to the particle size and polydispersity.

Chapter 2: Background

2. Background:

Metal nanoparticles have found numerous applications in a wide variety of interdisciplinary fields. This background section highlights select applications where properties and performance depend critically on the size and composition of the particles. Next, several synthesis routes for obtaining metal nanoparticles are reviewed with comparison of the techniques. Finally, methods for refining and characterizing the particle size distribution are presented. Special attention is given to science underlying the phase behavior of surfactant liquid mixtures that form micellar solutions. This background section is concluded with a discussion of current reverse micelle synthesis processes and the fundamental understanding of the governing physical principles.

2.1. Applications of Metal Nanoparticles:

2.1.1. Catalysis:

Metal nanoparticles are ideal candidates for many catalytic applications because of (i) large surface area to volume ratio that results in increased activity per gram of catalyst and a greater fraction of active surface sites per particle; (ii) ease of functionalization that allows for deposition onto a substrate for gas phase reaction applications or dispersion in a liquid phase reaction system; (iii) controllable particle

diameter that allows for greater control of downstream products, such as single wall carbon nanotubes synthesized by chemical vapor deposition (CVD).

Metallic nanoparticles have been used as catalysts in applications such as hydrogenation[1]; enantioselective hydrogenation[2]; hydropyrolysis[3]; hydrogenolysis[3]; hydrosilylation[4]; oxidative acetoxylation[5]; oxidation of CO[6]; oxidation of CO/H_2[6]; 3 + 2 cycloaddition reactions[7]; Suzuki[8] and Heck-Type[9] couplings; and carbon nanotube synthesis by CVD.

One of the more interesting of these reactions from a size-tailored nanoparticle catalyst standpoint is the single wall carbon nanotube synthesis by CVD. The CVD process entails gas phase thermal decomposition of a carbon containing gas such as methane or acetylene (or disproportionation of carbon monoxide) over a transition metal catalyst (Co, Ni, Fe, Co-Mo Alloy[10-15], etc.) on a metal oxide substrate. The catalyst/substrate can be prepared with a variety of methods, resulting in nanosized particles of metal embedded in the surface of the substrate.

The carbon from the decomposed (or disproportioned) gas is then deposited onto the metal particle. The deposited carbon is thought to form an intermetallic carbide phase with the catalyst metal until the metal becomes saturated with carbon. The carbon is then precipitated on the surface of the particle in the form of a hemifullerine cap that becomes the Single Wall Carbon Nanotube (SWCNT) tip. As more carbon is added to and precipitated from the particle, the carbon is added equatorially to the interface between

the hemifullerine cap and the particle. At this point one of two things happen, either (i) the particle-substrate interaction is sufficiently strong to anchor the particle to the substrate in which case the SWCNT grows off the metal particle, this is known as the "base growth" mechanism, or (ii) the particle-substrate interaction is not sufficiently strong to anchor the particle to the substrate in which case the metal nanoparticle remains in the tip of the SWCNT and is lifted off the substrate surface as the SWCNT grows, this is known as the "tip growth" mechanism.[16, 17]

Observation of SWCNTs grown by the CVD process strongly suggests the diameters of the SWCNTs are closely related to the diameter of the catalytic metal nanoparticles.[16, 17] Hence, numerous studies have been carried out to attempt to control nanoparticle catalyst size. Table 2.1.1-1 compares initial catalyst particle size distribution to the resulting carbon nanotube diameter distribution for CNTs produced via CVD.

Table 2.1.1-1: Tabulated Literature Data for CVD Grown CNTs

Catalyst Metal	Catalyst Particle Size (nm)	Nanotube Type	Nanotube Diameter (nm)	Reference
Fe	1 – 3	SWCNTs, DWCNTs	~1 – 3	[18]
Fe	3.7 +/- 1.1	SWCNTs	3.0 +/- 0.9	[19]
Fe	1.9 +/- 0.3	SWCNTs	1.5 +/- 0.9	[19]
Fe	1.2 +/- 0.5	SWCNTs	1.4 +/- 0.3	[20]
Fe, Mo	2 – 3	SWCNTs	0.9 – 2	[21]
Fe, Mo	1.3	SWCNTs	0.8 – 1.3	[22]
Fe	3.2 +/- 0.8	SWCNTs, DWCNTs	2.6 +/- 0.8	[23]
Fe	9.0 +/- 0.9	MWCNTs, SWCNTs	7.3 +/- 2.2	[23]
Fe	12.6 +/- 1.7	MWCNTs	11.7 +/- 3.2	[23]

The empirical trend of the data in Table 2.1.1-1 suggests that the CNT diameter is a strong function of nanoparticle diameter, and that the variation of CNT diameter from nanoparticle diameter appears to decrease with decreasing nanoparticle diameter. For nanoparticles with diameters larger than ~ 3 nm the resulting product is predominantly MWCNTs of comparable diameter to that of the nanoparticle. A working hypothesis based on this data is that by controlling the size distribution of the metal nanoparticle catalysts it will be possible to control the diameter distribution of the SWCNTs, as well as the diameter dependent properties of SWCNTs such as chirality, and electronic structure.

2.1.2. Biomedical Applications

MRI Contrast Agents

Another potential application for metallic nanoparticles is use as a MRI contrast agent. In order for metallic nanoparticles to be a good candidate for use as an MRI contrast agent they must (i) be biocompatible, i. e., non-toxic *in vivo* and maintain their structure and effectiveness in the human body, (ii) remain active in the body for a sufficient period of time (measured in terms of half-life) to obtain the required diagnostic data, and (iii) in MRI applications, be a superparamagnetic material. Currently, chelates of gadolinium are used for this purpose. [24, 25] However, these Gd chelates typically have a half-life of ~1.5 hours [24-27] resulting in a short time window for data acquisition. For this reason, other contrast agents that may have longer half-lives while

maintaining an acceptable signal enhancement are being sought. One of these agents of particular interest is "ultrasmall superparamagnetic iron oxides" (USPIO).

USPIO's are small iron oxide nanoparticles coated with a surfactant polymer.[28] In a study of USPIOs coated with carboxydextran at three dosage levels[28], the particles were classified by hydrodynamic diameter. The classifications were: 21 nm, 33 nm, 46 nm and 65 nm. In this study, although the single pass signal enhancement was minimal, a significant increase in the half-life of the contrast agent in the body with decreasing particle size resulted in as much as a 25 minute increase in the data acquisition window.

Thus the half-life of the contrast agent increases with decreasing hydrodynamic diameter. This phenomena, coupled with the fact that cobalt nanoparticles are superparamagnetic [29] at sufficiently small diameters suggest that further work should be performed to determine whether < 10 nm cobalt particles could be used as long half-life MRI contrast agents. Additionally, an added benefit of the smaller particles is that they would be sufficiently small (2 – 20 nm) to cross the blood-brain barrier [30, 31] allowing increased contrast MRI data from the brain area. Although bulk cobalt is sufficiently biocompatible to be used in various metal implants[32, 33], it may be necessary to perform additional biocompatibility/toxicity studies of nanophase cobalt metal.

Biosensors:

Colloidal gold nanoparticles have been used extensively in biological applications because of their excellent biocompatibility, optical and electron-beam contrast properties, and their robust protein conjugation methods.[34, 35] Recently, mercaptoalkyl-oligonucleotide-functionalized gold nanoparticles have been used as probes to detect target oligonucleotides. When the Au nanoparticles interact with the target oligonucleotides the aggregate with a resulting color change from red to blue.[36]

Similarly, gold nanoshells (gold coated silica or AuS particles) [37] have been used to perform an immunoassay on blood with no preparation of the blood. In this process the gold nanoshells were tuned for near-IR resonance and functionalized with antibodies that correspond to the target antigens. Upon contact with the target antigens these nanoshells aggregate which caused the in resonant wavelength to shift farther into the IR region.[38] Here the location of the adsorption peak is a function of the diameter of the AuS core and the thickness of the outer Au shell. This is an example of a particle size effect on material properties.

2.1.3. Ultra-High-Density Magnetic Data Storage Medium

Presently hard drives are manufactured by sputtering a Co/Cr/Pt polycrystalline alloy on a glass or aluminum alloy substrate. Upon addition of segregation agents, such as B or Ta, the alloy segregates into single domain magnetic grains on the order of 10 nm

in size. Using this method it is possible to store one bit of information on a cell of about 100 grains. In order to increase the bit density of the recording media it is necessary to decrease the size of the grains. However, as the grain size decreases, thermal fluctuations become sufficient to change the magnetic configuration of the domains. For this reason, there is a lower limit for the grain size under the present scheme.[39]

One possible alternative to the limited present scheme is to make discrete patterned arrays of magnetic elements separated from each other by a distance comparable to the width of the element. The width of the element plus the width of the separation is known as the period. For instance, a periodicity of 50 nm correspond to 25 nm elements spaced 25 nm apart. This 50 nm periodicity corresponds to a bit density of 30 Gbit/cm^2.[39]

Present optical lithographic techniques cannot be used to produce features this size or smaller due to inherent resolution limits. Suggested approaches include electron-beam [40-57] and X-ray lithography [52, 58, 59]coupled with various deposition techniques, templated growth [42, 60-67], and self-assembly of metal nanoparticles.[39] Electron-beam lithography can be used to pattern structures as small as 15 nm (periodicity of 30 nm).[40] X-ray lithography can be used for feature sizes as small as 20 nm (periodicity of 40 nm).[39] Templated growth methods have also been used to create magnetic elements, such as anodizing aluminum to create arrays of alumina regions with pores as small as 11 nm, and depositing magnetic material in the pores via electrodeposition.[42, 60, 61]

Possibly one of the most promising methods for producing patterned arrays of magnetic elements with low-nanometer scale periodicity is the self-assembly of magnetic nanoparticles. One benefit of this method is that there is no need for any type of lithographic mask, hence there is no wavelength limitation on the feature size. The feature size is potentially limited by the size of the nanoparticles used in the process. It is possible to create arrays with a period on the order of 10 nm.[39]

The major issues with this type of method are 1) Control of the size distribution of the particles to ensure uniform properties and highly ordered self-assembly, 2) Protection from oxidation, and 3) Protection from aggregation.[39] Once these limitations are overcome it should be possible to create highly ordered 2-D superlattice monolayers of magnetic nanoparticles with a density of at least an order of magnitude larger than present methods.

2.2. Synthesis of Metal Nanoparticles:

Numerous routes for metal nanoparticle synthesis have been investigated for the late transition metals in groups 9, 10, and 11, particularly Au, Ag, Pd, Pt, Co, Ni, Fe, and Cu. Noble Metals nanoparticles such as Au, Ag, Pd, and Pt are easily synthesized because: (i) They do not readily form oxides under normal conditions and (ii) They bind strongly to protecting groups such as alkanethiols which coat the nanoparticle and sterically inhibit the bare metal particles from coming together and forming larger

aggregates. On the other hand, the more reactive metals such as Co, Ni, Fe, and Cu pose several difficulties in the synthesis of stable metallic nanoparticles due to their relatively high reactivity when compared to the Noble Metals. A brief overview of the synthesis routes and process variables used to make size-controlled nanoparticles of these metals will be described to set the stage for the study described in this thesis to quantify nanoparticle and SWNT size distributions.

2.2.1. Nanoparticles of Noble Metals:

Nanoparticles of noble metals including Au [68-75], Ag [75-83], Pd [75, 83-94] and Pt [75, 83-94] can be synthesized by reducing the metal salts in an organic phase in the presence of chemical stabilizers, such as alkanethiols.[68] The resulting nanoparticle diameters can be very small (e.g. 1-3 nm for Au). Under normal reaction conditions, the size distribution is controlled by two factors: the ratio of stabilizer to salt, and the strength of the reducing agent. Weak reducing agents such as citrate, or tartarate [75, 95-97] yield a slower reaction resulting in small faceted nanoparticles with diameters less than 1 nm. Stronger reducing agents such as o-anisidine or formamide [98, 99] yield a faster reaction with larger more spherical particles.

2.2.2 Nanoparticles of Non-Noble Transition Metals:

The reactivity and robust ligand complex chemistry of metals such as Co, Ni, Fe, that make these materials desirable as catalyst particles also impose difficulty on the

synthesis and handling process. Foremost in these difficulties is the prevention of oxidation and aggregation during synthesis and post synthesis handling. Three predominant methods have been investigated to synthesize narrow, controllable nanoparticle size distributions. These methods include: (i) solution phase reduction of a metal salt with a stabilizer/protecting group, (ii) decomposition of a metal carbonyl complex, and (iii) reverse micelle reduction methods. All three of these methods can be used to synthesize nanoparticles with an average particle size within or near the target range (1-5 nm).

Stabilized Solution Phase Reduction of a Metal Salt

One of the most common and fairly successful synthesis methods is the solution phase reduction of a metal salt in the presence of a stabilizer/protecting agent. Sun and Murray [100] were able to synthesize Co nanoparticles controllable in the range of 2 – 11 nm with a standard deviation, $\sigma < 7\%$. This was carried out by reducing cobalt chloride in a dioctyl ether/oleic acid/trioctylphoshine solution with superhydride ($LiBEt_3H$). The process was carried out at 200 ^{o}C. Trialkylphosphine and oleic acid were used to control the rate of nanoparticle growth and to protect the particles against aggregation and oxidation. The growth reaction was quenched by lowering the temperature.

Coarse size control was carried out by choice of the particular trialkylphosphine. For instance, trioctylphosphine resulted in a particles in the range of (2 - 6 nm), while the smaller tributylphosphine resulted in larger particles in the range of (7 – 11 nm). The

size of the phosphine stabilizer is inversely related to the nanoparticle diameter because the phosphines control the rate of the nanoparticle growth by sterically inhibiting the addition of Co to the nanoparticles. Thus, by increasing or decreasing the diffusion rate of free Co to the particle, the overall rate of particle growth is controlled.

Fine particle size control was carried out by size selective precipitation. Size selective precipitation is performed by adding a small amount of non-solvent to the colloidal suspension. Hence, larger particles precipitate while smaller particles remain suspended. The minimum particle size precipitated can be selected by the amount of non-solvent added to the system. The narrow 7% standard deviation was, therefore, not an effect of the reaction, but of the size-selective precipitation method.

A similar method [101] for Co nanoparticle synthesis, known as the "polyol" process, involves dissolving cobalt acetate, oleic acid, and trioctylphosphine (stabilizer) in diphenyl ether and heated to 250 °C. 1,2-dodecanediol is added as a reducing agent. Coarse diameter control was provided by varying the ratio of the stabilizer to the cobalt acetate. A 1:1 stabilizer to salt ratio produces a diameter distribution of 6-8 nm, while a 2:1 ratio produced a distribution of 3 - 6 nm. This method has also been used to synthesize Ni nanoparticles of 8 - 13 nm, by substituting the cobalt acetate with hydrated nickel acetate.

These methods suffer from a few weaknesses. First, fine control of the particle size and monodispersity requires a size selective precipitation method. Secondly, these

syntheses require relatively high temperatures on the range of 100 °C to 300 °C. Finally, it is necessary to use air-free handling methods throughout the synthesis in order to mitigate oxidation. In comparison to the reverse micelle method, this method is complex and energetically wasteful.

Stabilized Decomposition of a Metal Carbonyl

Puntes et al [102] have synthesized nanoparticles of Co by thermally decomposing cobalt carbonyl [$Co_2(CO)_8$] in anhydrous o-dichlorobenzene in the presence of oleic acid, lauric acid, and trioctylphosphine stabilizers at high temperature. The stabilizers perform a similar function that they did for the reduction of cobalt chloride [100]. They were able to control the size distribution of Co nanoparticles over a range of 3 – 17 nm. No data was reported for standard deviation. The size of the particles produced was controlled by the process variables: precursor/surfactant ratio, reaction temperature, and reaction time.

Other examples of transition metal nanoparticles by decomposition of metal carbonyls include the following: (i) Suslick et al [103] produced Fe nanoparticles in the range of 3-8 nm, by sonochemically decomposing iron pentacarbonyl in the presence of polyvinylpyrrolidone or oleic acid; (ii) Shafi, et al [104] synthesized amorphous Co nanoparticles in the range of 5–10 nm by sonicating $Co(CO)_3(NO)$ in a decane solution with oleic acid. (iii) Hyeon et al [105] synthesized monodisperse Fe nanoparticles on the controllable range of 4-11 nm by aging iron-oleic acid complex at 300 °C. (The iron-

oleic acid complex was synthesized by decomposing iron pentacarbonyl in the presence of oleic acid at 100 °C).

The stabilized decomposition of metal carbonyl method is somewhat simpler than the previously mentioned reduction method, since no reducing agent is required. However, there is still a large energy requirement for decomposition of the metal species, be it thermal, sonic, etc. The particles produced by this appear to be less monodisperse than those synthesized by the reduction methods.

Reverse Micelle Methods

Another method of synthesizing monodisperse metal nanoparticles is to add enough surfactant and aqueous salt solution to a nonpolar organic solvent to produce spherical inverted micellular structures around the target size of the nanoparticles. A reducing agent is then added to the system which in turn reduces the aqueous salt into the metal. The reverse micelles act as nanoreactors and keep the forming nanoparticles from aggregating into larger structures. After the reaction, the surfactant remains adsorbed to the surface of the nanoparticles stabilizing them against aggregation and oxidation.

Pileni, et al [106-108] synthesized Cu nanoparticles on the range of 2 – 20 nm by dissolving copper bis(2-ethylhexyl)-sulfosuccinate ($Cu(AOT)_2$) in a mixture of cyclohexane, isooctane and sodium bis(2-ethylhexyl)-sulfosuccinate (NaAOT). An aqueous solution of hydrazine was added as a reducing agent. The size distribution was

determined to be controlled by a number of factors: 1. Average diameter and polydispersity increases with water content, 2. Average particle size increases with Cu ion concentration, 3. Average particle size increases with increasing reducing agent concentration for intermediate water content.

Chen et al [109] synthesized Co nanoparticles in the range of 1.8 to 4.4 nm diameter via borohydride reduction of $CoCl_2$ in a reverse micelle system of toluene and didodecyldimethyl ammonium bromide (DDAB). For this synthesis $CoCl_2$ was dissolved in an 11 wt% mixture of DDAB in toluene. An aqueous solution of $NaBH_4$ (sodium borohydride) was injected into the system to reduce the Co^{2+} to cobalt metal. According to the literature the particle size was controlled by controlling the Co^{2+} concentration. Care must be taken to keep the $[H_2O]$/[DDAB] ratio less than 1.5, or else cobalt boride will form.[109-111]

2.3. Size Based Separation Methods:

Although the scope of this project was to control the particle size distribution of metal nanoparticles by control of reaction parameters alone, there are a few methods to further narrow the particle size distribution, post synthesis. These methods were not explored in this thesis and are mentioned for the sake of completeness. These methods can be classified as high or low yield methods. Higher yield methods include filtration[112], size selective precipitation[113-115], and ultra centrifugation[116], while

the lower yield, more time intensive methods include size exclusion chromatography[117-119] and gel electrophoresis.[120]

2.4. Characterization Methods:

The size distributions, compositions, and properties of metallic nanoparticles can be characterized a variety of ways. The primary characterization methods used in this thesis were Dynamic Light Scattering (DLS)[121-130], X-Ray Diffraction (XRD), transmission electron microscopy (TEM)[109-111, 116, 122, 124, 126, 127, 131-137], and atomic force microscopy (AFM)[132, 138, 139]. Other notable methods for metallic nanoparticle size characterization include small-angle X-ray scattering (SAXS)[123, 125, 131, 134, 139], and small-angle neutron scattering (SANS).[123, 125, 131]

2.4.1. Dynamic Light Scattering[125, 140]:

Light passing through a suspension of particles will be scattered if the polarizability of the particles is different than that of the bulk solution. The following description of Dynamic Light Scattering (DLS) was adopted from refs. [130] and [145]. The intensity of the scattered light will be a function of the polarization of the incident light, the scattering angle, and the bulk solvent parameters. The intensity of scattered light, I_s, from a single spherical particle of diameter much smaller than the wavelength of the incident light, λ, suspended in a solvent is given by

$$I_s(1) = \frac{4\pi^2 M^2 (\sin^2 \phi)(dn/dc)^2 I_o}{N_A^2 \lambda^4 R^2} \qquad \textbf{(2.4.1-1)}$$

Where M is the mass of the particle in Daltons, $\varphi = (90^\circ - \theta)$ is the scattering angle from the incident direction, (dn/dc) is the rate of change of the index of refraction of the suspension with concentration, I_0 is the incident light intensity, N_A is Avogadro's number, λ is the wavelength of the incident light, and R is the distance from the scattering point to the point of observation.

In the case where the scattering sample contains a set of N spherical particles of similar size, it is necessary to represent the scattered light in terms of its electric field. The scattered field, E, can be represented by the vector sum of the scattered fields from each particle. Each individual field can be represented by a magnitude and scattering angle, δ, or more conveniently by their "x" and "y" components.

(x-component) $$E_{x,i} = E_s \sum_{i=1}^{N} (\cos \delta_i) \qquad \textbf{(2.4.1-2)}$$

(y-component) $$E_{y,i} = E_s \sum_{i=1}^{N} (\sin \delta_i) \qquad \textbf{(2.4.1-3)}$$

The scattered intensity can then be determined from the electric fields by

$$I_s = \frac{1}{377} E_s^2 \left[\left(\sum_{i=1}^{N} \cos \delta_i \right)^2 + \left(\sum \sum_{i=1}^{N} \sin \delta_i \right)^2 \right] \text{ (=) W/m}^2 \qquad \textbf{(2.4.1-4)}$$

The total scattering intensity can be rewritten in general as

$$I_s = I_s(1)\left[N + 2\sum_{j>i=1}^{N} \cos\left(\delta_i - \delta_j\right) \right] \qquad \textbf{(2.4.1-5)}$$

where the second bracketed term contains the time dependent fluctuations in intensity due to random particle movement by Brownian motion. The time average of this term is zero such that $I_{s,avg} = NI_s(1)$, however it is the fluctuation term that contains the most information about the particle size through the correlation function.

The intensity signal is transformed to an intensity-intensity time correlation function of the form

$$G(\tau) = \lim_{T\to\infty} \frac{1}{2T}\int_{-T}^{T} I(t)I(t+\tau)dt \qquad \textbf{(2.4.1-6)}$$

which simplifies to

$$G(\tau) = 1 + f(n_{coh})e^{-2Dq\tau} \qquad \textbf{(2.4.1-7)}$$

where $q = (4\pi/\lambda) \sin(\theta/2)$, τ is the intensity time, $f(n_{coh})$ is a function of the coherence factor which can be approximated by $f(n_{coh}) = 2.5/n_{coh}$, and D is the effective diffusion coefficient. D is related to the particles hydrodynamic radius by the Stokes-Einstein relation

$$D = \frac{k_B T}{6\pi\eta r_h} \qquad \textbf{(2.4.1-8)}$$

where k_B is Boltzmann's constant, T is temperature, η is viscosity, and r_h is the hydrodynamic radius of the particle.

2.4.2. X-Ray Diffraction[141]:

X-ray diffraction is a well-known technique used to determine the crystal structure of crystalline solids. This atomic plane separation distance, called the d-spacing is dependant upon the size of the atoms, the interatomic spacing between atoms, and the crystalline structure of the sample. The following description of XRD is included for completeness and is adapted from ref [146].

In order to understand how XRD works it is necessary to understand Bragg's Law. Crystalline materials are comprised of parallel layers of atoms stacked upon one another, called planes. (The exact crystalline structure of the material depends how these layers are stacked.) Figure 2.4.2-1 is a simple schematic of two planes A and B separated by some distance d. The rays 1-1' and 2-2' represent two X-ray beams which are reflected by the adjacent planes. From inspection it is apparent that beam 2-2' must necessarily travel farther than beam 1-1'. The difference is the length xyz. Because of this distance the beams will either be in or out of phase. If they in phase they will constructively interfere resulting in increased intensity, and if they are out of phase they

will destructively interfere resulting in decreased intensity. In order for the two beams to be in phase the xyz distance must be some integer multiple of the wavelength of the X-ray.

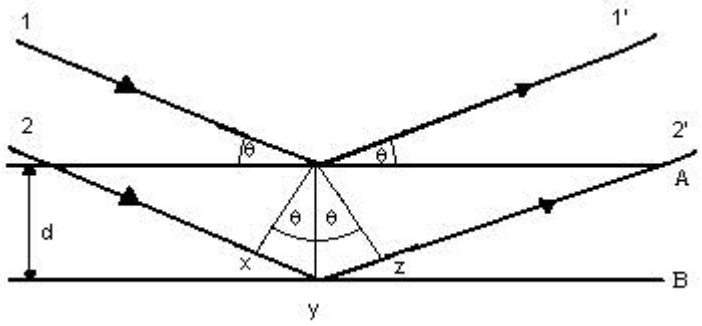

Figure 2.4.2-1: "Derivation of Bragg's Law"

In order for Bragg's Law to be satisfied, the two beams must be in phase such that

$$xy = yz = d\sin\theta \qquad \textbf{(2.4.2-1)}$$

therefore

$$\text{Bragg's Law:} \qquad xyz = n\lambda = 2d\sin\theta \qquad \textbf{(2.4.2-2)}$$

where θ is the angle of incidence or the Bragg angle, and n is an integer number which is customarily set to one. Now it is possible to determine the d-spacing of the crystal by measuring the angle at which the intensity is maximized.

Typically modern XRD apparatus use a solid state detector to measure the intensity as a function of angle. The data is then sent to a microprocessor which creates a plot of the X-ray intensity versus the angle. The data analysis software may have a library of XRD data against which to compare the sample for the non-expert user.

2.4.3. Microscopy Methods:

Microscopy methods, including AFM, TEM, and SEM can be used to determine the particle size and polydispersity of a set of nanoparticles by directly imaging the particles. These methods provide a good visual picture of the particles, however the sample size is very small when compared to the entire population of particles. Microscopy data may introduce bias into quantitative data as it is only as good as the randomness of the sampling.

2.4.4. Small Angle X-ray Scattering and Small Angle Neutron Scattering[125]:

SANS and SAXS methods are similar to light scattering methods discussed earlier. They consist of measuring the angular dependence of the time averaged scattering intensity as a function of the scattering angle of the incident radiation. X-ray and neutron methods have a resolution advantage over light scattering techniques because of their shorter wavelengths. Neutron wavelengths are around 0.5 nm and X-ray

wavelengths are around 0.1 to 0.2 nm compared to visible light with wavelengths on the order of hundreds of nanometers.

For SANS and SAXS the scattered intensity, $I_s(q)$, is proportional to two factors; a structure factor, S(q), and a form factor, P(q)

$$I_s(q) \propto S(q)P(q) \qquad \textbf{(2.4.4-1)}$$

The structure factor is given in terms of the pair correlation function, g(τ), by

$$S(q) = 1 + \frac{4\pi}{N}\int \tau\left[g(\tau) - 1\right]\sin(qr)dr \qquad \textbf{(2.4.4-2)}$$

For the hard sphere model S(q) can be approximated for a zero scattering angle and finite concentration, C, by the Percus-Yevick Approximation as

$$S(q = 0, C) = (1 - \alpha)^4 (1 + 2\alpha)^{-2} \qquad \textbf{(2.4.4-3)}$$

where

$$\alpha = \left(\frac{4\pi R_{HS}^3}{3M}\right) N_A C \qquad \textbf{(2.4.4-4)}$$

where R_{HS} is the hard sphere radius of the particle.

Similarly, the form factor can be determined based of the type of particle under analysis. For example, P(q) for a set of solid spheres of radius R, is given as

$$P(q,R) = \int_0^\infty \left[\frac{3}{(qR)^3} \{\sin(qR) - [(qR)\cos(qR)]\} \right]^2 dR \qquad \textbf{(2.4.4-5)}$$

Once the structure factor and form factor are determined for the system it is necessary to determine the proportionality between $I_s(q)$, S(q), and P(q) by calibration.

2.5. Surfactant Science

A reverse micelle process was chosen to synthesize the cobalt nanoparticles in this work. To understand the reverse micelle process, an understanding of surfactant behavior in mixtures of immiscible fluids is required. In the following sections qualitative and quantitative details of reverse micelle solutions are described. The discussion starts by defining surfactants in 2.5.1. Next, the various self-assembling structures of surfactants in solution, including micelles and reverse micelles, are discussed in 2.5.2. Sections 2.5.3-2.5.5 focus on reverse micelles and the system parameters that influence their structure.

2.5.1. Surfactants:

Surfactants are surface active molecules that lower the interfacial free energy of a multi-phase system. The interfacial free energy is the minimum amount of work necessary to create the interface, W_{min}, and can be calculated from the interfacial (or surface) tension, $\gamma_{I,}$ and the change in interfacial area, $\Delta A_{I,}$ from the relation: [142]

$$W_{\min} = \gamma_I \times \Delta A_I \qquad \textbf{(2.5.1-1)}$$

At the interface between two dissimilar liquid phases, the molecules at the surface of each phase are at higher potential energy than those in the bulk phase and at different potential energy than those across the interface. For two dissimilar liquid phases, a and b, where a is a polar liquid such as water and b is a less polar solvent such as toluene, the potential E_{aa} represents the interaction potential between interfacial a molecules and bulk a molecules, E_{bb} represents the interaction potential between interfacial b molecules and bulk b molecules, and E_{ab} represents the interaction potential between interfacial a and interfacial b molecules across the interface. It is possible to determine the increased potential of the interfacial molecules compared with those of the bulk as

$$(E_{aa}\text{-}E_{ab}) + (E_{bb}\text{-}E_{ab}) = E_{aa} + E_{bb} - 2E_{ab} \qquad \textbf{(2.5.1-2)}$$

which is equal to the energy required to create the interface, ΔG_I, resulting in an interfacial tension:

$$\gamma_I = \gamma_a + \gamma_b - 2\gamma_{ab} \qquad \textbf{(2.5.1-3)}$$

where γ_a and γ_b are the surface free energies per unit area for the pure component liquids and γ_{ab} is the energy per unit area of the a-b interaction across the interface.

As evident from (2.5.1-2) and (2.5.1-3), if the interaction potential across the interface should increase such that $2E_{ab} > E_{aa} + E_{ab}$, then the ΔG_I and γ_I will become negative and the two phases will merge together to become a homogeneous solution. If $2E_{ab} < E_{aa} + E_{bb,}$ then the two liquids are immiscible and can form micro-emulsions. Large ΔG_I results in large spherical drops. As ΔG_I decreases, the minimum size of a stable droplet decreases.

Addition of surfactants to the liquid-liquid system previously discussed results in the surfactant adsorbing to the interface and orienting its hydrophilic end toward the polar (water) side of the interface and its hydrophobic end toward the less polar (toluene) side of the interface. When the surfactant replaces the toluene molecules at the interface, the E_{ab} interaction is no longer between the water and toluene molecules, but between the water and the surfactant molecules, which is a much stronger interaction, which results in a significant decrease in the surface free energy and surface tension of the system.[142]

The surface active properties of surfactants are determined by their structure. In general, surfactants consist of two types of functional groups, (i) hydrophilic (or

lycophobic) groups which are polar and easily associate with polar solvents such as water, and do not associate with non-polar solvents such as hydrocarbons, these are commonly referred to as “head groups”; and (ii) hydrophobic (or lycophillic) groups which are non-polar and easily associate with non-polar solvents, but not with polar solvents, these are commonly referred to as “tail groups”. Surfactants are classified as ionic or non-ionic based on whether or not they ionize in the solvent. Ionics and non-ionics also differ slightly in the manner in which the polar head groups associate with the polar solvent molecules.

Ionic surfactants can be: anionic, cationic, or zwitterionic. Anionic and cationic surfactants both typically have one head group that is ionic in nature. The head group ionizes with a negative charge, in the case of an anionic surfactant, or a positive charge in the case of a cationic surfactant. Anionics adsorb to positively charged surfaces or interfaces while cationics adsorb to negative ones. Zwitterionic surfactants have two polar head groups one anionic and one cationic. This allows the surfactant to adsorb to either positively charged of negatively charged interfaces.

Anionic and cationic surfactants can be viewed as large organic salts. For example, the anionic surfactant, sodium dodecyl sulfate (SDS), can be classified as an organic sulfate salt of the formula: $[C_{12}H_{25}SO_4]^-\ Na^+$. SDS is an n-dodecyl chain covalently bonded to an ionic sulfate group and balanced with a sodium counterion. The sulfate functional group is the polar head group, and the n-dodecyl chain the non-polar tail group. The cationic dodecyldimethylammonium bromide (DDAB) is classified as a

quaternary ammonium salt of the formula $[(C_{12}H_{25}N)_2^+(CH_3)_2]$ Br^-. Here the ammonium is the polar head group and the alkyl chains are the tail group.

2.5.2. Micelles and Amphoteric Structures:

When surfactants are dissolved in a solvent in sufficient concentration the surfactant molecules begin to associate into self-assembled mesostructures. If the solvent is polar, the lycophillic tails associate to minimize their exposure to the solvent molecules. Similarly, head association occurs in non-polar solvents. For a simple binary system, the shape of the amphoteric structures formed is dependent upon (i) the molecular geometry of the surfactant, (ii) the concentration of the surfactant in the solvent, and (iii) the nature of the solvent. If a polar and nonpolar mixture of solvents is used, the geometry of the amphoteric structures are also dependent on the concentration of the second solvent.[142]

Possible amphoteric structures include: (i) spherical micelles, (ii) cylindrical micelles, (iii) lamellar structures, and (iv) reverse micelles. Spherical and cylindrical micelles (lycophillic tail association) are exclusively formed in polar solvents while reverse micelles (lycophobic head association) are strictly a non polar phenomena. Lamellar phases are observed in both types of systems. The interior of the spherical micelles (regular or reverse) offer an isolated microenvironment of polar or nonpolar character, respectively. The spherical morphology of micelles and reverse micelles

makes them ideal for synthesis of nanoparticles. Hence, the remainder of this chapter will focus on these structures.

Surfactant molecular geometry determines the packing efficiency and morphology of the micelle. The characteristic packing parameter (CPP) is related to the molecular volume of the surfactant tail, V_{st}, the cross-sectional area of the polar head group, A_h, and the length of the tail, L_{st}, by the following relation: [142]

$$CPP = \frac{V_{st}}{A_h L_{st}} \qquad \textbf{(2.5.2-1)}$$

The CCP and its use in amphoteric structure determination are based upon theory set forth by Israelachvili, Mitchell, and Ninham. The theory, hereafter referred to as IMN Theory, relates the CPP to the structure in the following way: [142]

Table 2.5.2-1: Amphoteric Structures and Resulting CPP Ranges[142, 143]

Range of CPP Value	Amphoteric Structure
0 < CPP < 1/3	Spherical micelles in polar solvent
1/3 < CPP < ½	Cylindrical micelles in polar solvent
½ < CPP < 1	Lamellar in polar solvent
1< CPP < 3	Inverse lamellar structures
3< CPP	Reverse micelles in non-polar solvent (w = 0)
1< CPP	Reverse micelles in non-polar solvent (w > 0)

When literature data V_{st}, and L_{st} are not readily available, it is possible to estimate those values using the following empirical equations. [142]

$$V_{st} = 27.4 + 26.9n \qquad \textbf{(2.5.2-2)}$$

$$L_{st} \leq 1.5 + 1.265n \qquad \textbf{(2.5.2-3)}$$

where V_{st}, is in units of cubic angstroms, L_{st} is in units of angstroms and n is the number of carbon atoms in the hydrophobic tail.

2.5.3. Reverse Micelles Structures:

When the ionic surfactant didodecyldimethylammonium bromide (DDAB) is dissolved in anhydrous toluene the hydrophilic head groups associate to form reverse micelles. Water additions to this system diffuse into the hydrophilic cores of the reverse micelles causing them to swell. The resulting system is known as a water in oil microemulsion system. The water/surfactant/oil system can be characterized in the ternary phase diagram of Figure 2.5.3-1.

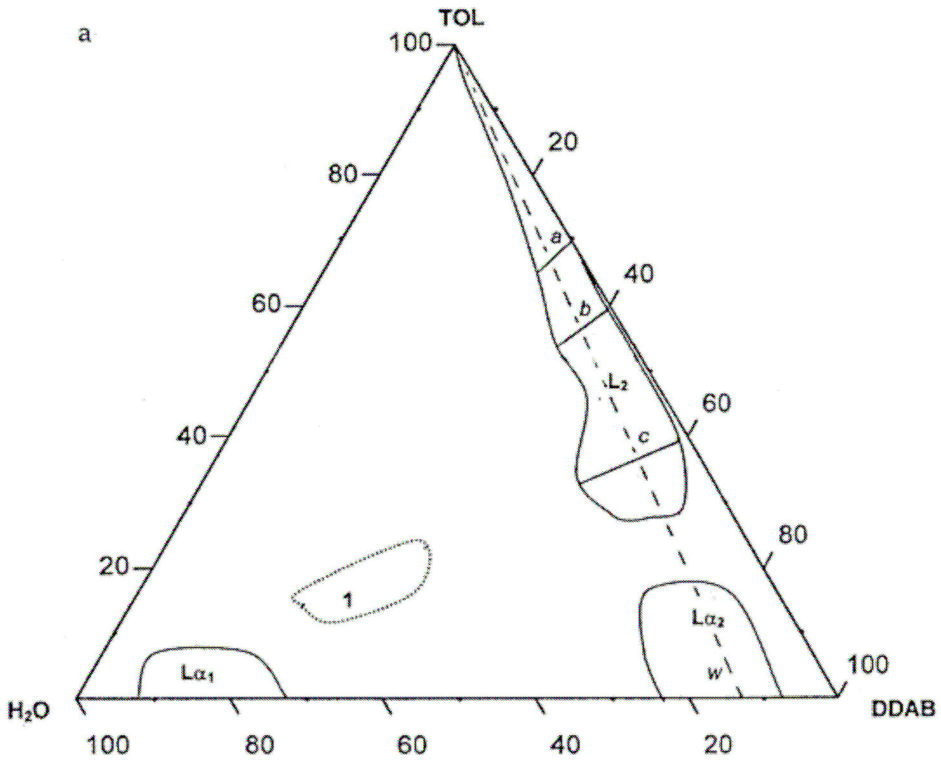

Figure 2.5.3-1: Phase Diagram of the DDAB/H_2O/Toluene System (adopted from [144])

Regions $L_{\alpha 1}$ & $L_{\alpha 2}$ correspond to lamellar phases; Region L_2 corresponds to the "water in oil" microemulsion phase containing the reverse micelles; Region 1 corresponds to creamy emulsion phase. In the L_2 region, the lowercase letters a, b, c, d correspond "water dilution lines" expressed in terms of the surfactant to toluene weight ratios (s/o): a = 3/7, b = 4/6, c = 6/4. The dashed line represents the "oil dilution line" expressed as the weight ratio of water to surfactant, (w/s).[144]

The size of the water pool interior of the reverse micelle is determined by the parameter known as the water content, *w*, which is defined as the molar ratio of the water to the surfactant:

$$w = \frac{[water]}{[surfactant]} \qquad \textbf{(2.5.3-1)}$$

The following calculations will show that the diameter of the water pool is linearly proportional to w by a constant system parameter k, and will provide a theoretical value for that constant[145].

From the initial assumption that the reverse micelles are spherical over the region of interest and w > 0, the effective CPP must be equal to at least 1. The radius of the water pool at the limiting case of effective CPP = 1 can be expressed as

$$R_w = \frac{3V_w}{SA_w} \qquad \textbf{(2.5.3-2)}$$

where R_w is the radius of the water pool, V_w is the volume of the water pool, and SA_w is the surface area of the water pool.

The volume of water in the water pool can be represented as the number of water molecules in the droplet, N_w, multiplied by the molecular volume of a single water molecule, V_{aq}:

$$V_w = N_w V_{aq} \qquad \textbf{(2.5.3-3)}$$

Similarly, the surface area of the water droplet, SA_w, can be represented as the by the cross-sectional area of the surfactant polar head group, A_h, multiplied by the total number of surfactant molecules present at the water pool/non-polar solvent interface, N_{agg}; however, if the number of surfactant molecules in the micellular phase is >> the

number of surfactant molecules that are not associated, N_{agg} is approximately equal to the total number of surfactant molecules in the system per micelle denoted N_s.

$$SA_w = A_h N_s \qquad \textbf{(2.5.3-4)}$$

Substituting (2.5.3-3) and (2.5.3-4) into (2.5.3-2) results in the following relation:

$$R_w = \frac{3V_{aq} N_w}{A_h N_s} \qquad \textbf{(2.5.3-5)}$$

but

$$\frac{N_w}{N_s} = \frac{[water]}{[surfactant]} = w \qquad \textbf{(2.5.3-6)}$$

therefore,

$$R_w = \left(\frac{3V_{aq}}{A_h} \right) w \qquad \textbf{(2.5.3-7)}$$

or

$$D_w = \left(\frac{6V_{aq}}{A_h} \right) w = kw \qquad \textbf{(2.5.3-8)}$$

Therefore the diameter of the water pool inside the reverse micelle is a direct linear function or the water content, w. The value of the constant k is a parameter of the particular surfactant used.

For DDAB: [146, 147]

$$A_h = 68\ \text{Å}^2$$

$$L_s = L_c = 12.5\ \text{Å}$$

$$V_{st} = 700\ \text{Å}^3$$

$$CPP = 0.82$$

Using these values it is possible to determine the size of the water pools as a function of water content for DDAB reverse micelles in the Water/DDAB/toluene system. Based on the A_h value it is possible to obtain a k-value for the system:

$$k = 2.64\ \text{Å} \qquad \textbf{(2.5.3-9)}$$

Utilizing this k-value, the relation between the water content and the water pool diameter is given by the expression:

$$d_w = 2.64w \qquad \textbf{(2.5.3-10)}$$

The literature value for the CPP was given as 0.82 which is too small for the presence of reverse micelles according to IMN Theory. It is necessary to take into account the penetration of the solvent into the hydrophobic tail region of the surfactant. Chen et al. [147] states that if the solvent chain length is much less than the length of the hydrophobic tail, the oil will penetrate the hydrophilic layer of the reverse micelle resulting in a higher effective tail volume, $V_{st,\ eff}$, and an increased effective CPP value.

For the DDAB/H_2O/Toluene system, the hydrophobic tail is comprised of two long dodecyl chains (12 carbons). The solvent, toluene, is composed of a benzene ring with a single methyl group, and is much shorter than the dodecyl chain. This suggests penetration. Therefore to be consistent with phase diagram data the effective CPP value must be approximately equal to one.

If the $V_{st,\,eff}$ parameter is recalculated based on a CPP = 1, an A_h = 68 $Å^2$, and a L_{st} = 12.5Å, from a rearranged version of (2)

$$V_{st} = L_{st} A_h (CPP)_{eff} \qquad \textbf{(2.5.3-11)}$$

the result is a corrected tail volume of 850$Å^3$ compared to the value of 700$Å^3$.

2.5.4. Relationship Between w and Water Pool Size:

The IMN Theory, outlined previously, provides a valuable tool to estimate average values of water pool diameters for surfactant/water/oil systems. Table 2.5.4-1 illustrates the relationship between w and the average diameter, d_w, of the water pool, the average volume of the water pool, and the average number of water molecules in each micelle for the DDAB/H_2O/Toluene system as calculated from the IMN Theory. Similar calculations for the AOT/H_2O/Isooctane system, d_w = 3.0w (Å), studied extensively by Marie-Paule Pileni, is summarized in Table 2.5.4-2.

Table 2.5.4-1: Effect of w on d_w for the DDAB/H_2O/Toluene System

w	d_w,	V_w,	$N_{w,avg}$
1	2.64	9.63	0.322
2	5.28	77.1	2.58
3	7.92	260	8.69
4	10.6	617	20.6
5	13.2	1204	40.2
6	15.8	2081	69.6
7	18.5	3304	110
8	21.1	4933	165
9	23.8	7023	235
10	26.4	9634	322
11	29.0	12823	429
12	31.7	16648	556
13	34.3	21166	707
14	37.0	26436	884
15	39.6	32515	1087

Table 2.5.4-2: Effect of w on d_w for the AOT/H_2O/Isooctane System

w	d_w,	V_w,	$N_{w,avg}$
1	3.00	14.1	0.473
2	6.00	113	3.78
3	9.00	382	12.8
4	12.0	905	30.2
5	15.0	1767	59.1
6	18.0	3054	102
7	21.0	4849	162
8	24.0	7238	242
9	27.0	10306	344
10	30.0	14137	473
11	33.0	18817	629
12	36.0	24429	816
13	39.0	31059	1038
14	42.0	38792	1297
15	45.0	47713	1595

For very low w, the average value of the water pool volume is less than that of a single water molecule. As it is not possible to have less than a single water molecule, it is assumed that some reverse micelles are empty at sufficiently low values of w.

2.5.5. Curvature Effects on Reverse Micelles

The spontaneous curvature of the amphoteric structures, C_0, determined by the effective CPP of the surfactant molecules, determines the type of structures.[147] C_0 is defined as positive when bending toward the water and negative when bending toward the oil. Therefore all reverse amphoteric structures have negative curvature. For reverse systems, the absolute curvature increases with CPP as lamellar < cylindrical < spherical.

For a reverse micelle system of fixed surfactant concentration and constant oil to water interfacial area, the bending energy increases as the micelle is swollen (with water, ions, nanoparticles, etc). The bending energy component is given by: [148, 149]

$$\Delta G_b = 16\pi K\left(1-\frac{R}{R_0}\right)^2 \qquad \textbf{(2.5.5-1)}$$

This bending term serves to lower the surface free energy as the radius of the reverse micelle, R, approaches the natural radius, R_0. If R becomes much larger than R_0, the surface free energy increases until the emulsion breaks and water is purged into a separate phase resulting in a two phase system with reverse micelles of radius R_0 and a separate water phase[148, 149].

What this means is that the curvature of the reverse micelle, which is a function of the surfactant parameters as well as the molar volume of the solvent, places an upper limit on the size of the micelle. The radius of the micelle will increase with water content until the bending energy becomes too large and the reverse micelle must expel some of the water into a second water phase in order to lower its energy.

2.5.6. Effect of Intermicellular Potential on the Reverse Micelle System

The total free energy of a reverse micellular system can be broken down into the sum of the surface or interfacial free energy, ΔG_I, the bending energy, ΔG_b, and a function of the intermicellular potential, Φ_{Total} , which itself consists of an attractive term Φ_{Att}, and a repulsive term, Φ_{Rep}. The overall relationship is given by

$$\Delta G_T = \Delta G_I + \Delta G_B + f(\Phi_{Total}) \qquad \textbf{(2.5.6-1)}$$

$$\Phi_{Total} = \Phi_{Att} + \Phi_{\mathrm{Re}\,p} \qquad \textbf{(2.5.6-2)}$$

The first two terms are already determined and have been discussed in the previous sections. The attractive and repulsive terms are necessary to determine a complete model for this system and can be determined using an interaction model.

2.6. Reverse Micelle Process

2.6.1. Reverse Micelle Process in General

Reverse micelles have been used to synthesize a wide variety of nanoparticles including metallic, bimetallic, metal oxide and semiconducting particles. The general process consists of formulating a water in oil microemulsion from a ternary water/oil/surfactant system such as the DDAB/water/toluene or AOT/water/isooctane. Next, the desired reaction precursor(s), such as a water soluble metal salt for metallic nanoparticles, are dissolved into the aqueous centers of the micelle. A reducing agent, is then added, either by simple injection, or dispersed in analogous reverse micelles and added to the system. When the salt is reduced by the reducing agent, active metal nuclei are formed. The nuclei-containing micelles then collide under Brownian motion and may exchange their contents causing the metal particles to grow. The greater the average number of successful collisions, the larger the particles. Figure 2.6.1-1 illustrates the dynamic exchange mechanism for nanoparticle growth.

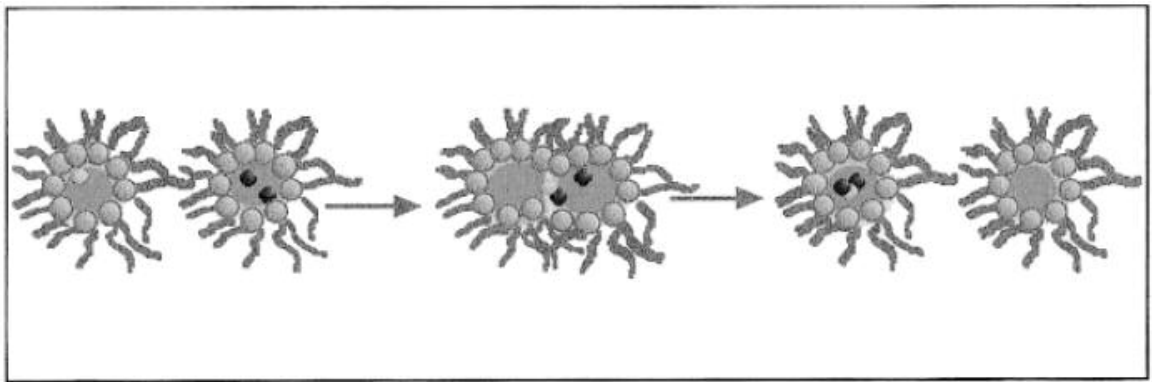

Figure 2.6.1-1: Dynamic Exchange Mechanism for Growth of Nanoparticles Synthesized in Reverse Micelles (adopted from ref [152])

The ultimate size of the nanoparticles seems to be a function of both the average number of micelle exchanges, which depends upon the intermicellular potential, and the rigidity of the interface. A more attractive net intermicellular potential tends to favor more growth interactions resulting in larger particles. Conversely, a less attractive potential results in fewer successful micelle exchanges, favoring smaller particles. A more rigid interface requires a larger collision energy to affect a successful micelle exchange. Therefore the more rigid the interface, the fewer successful exchange collisions and the smaller the resulting particle.[145, 150, 151]

The intermicellular potential is influenced by a number of factors, such as micelle size, solvent molar volume, salinity, electrostatic charge, etc. The rigidity of the interface can be influenced by curvature, solvent penetration, surfactant solute interaction, etc.[151] Most of these factors will be addressed, directly or indirectly within this chapter.

2.6.2. Factors Affecting the Ultimate Particle Size

Water Content

As shown in Section 2.4, for a ternary water/oil/surfactant surfactant system, the initial size of the reverse micelles is linearly related to the water content, w, as illustrated in Tables 2.5.4-1 and 2.5.4-2 for the DDAB/water/toluene and AOT/water/isooctane

systems respectively. As the water content increases for a constant surfactant concentration, the reverse micelle size increases. With increasing diameter of the reverse micelle, three important things happen:

(i) The attractive component of the intermicellular potential increases. Taken by itself, this would result in a larger ultimate particle size.

(ii) The radius of curvature increases resulting in an increase in interfacial rigidity[148, 149, 151]. This factor taken alone would result in a smaller ultimate particle size.

(iii) The proportion of "tightly bound" water decreases because the added water helps to hydrate the surfactant head and lowers the interaction energy between the water and the surfactant[151]. This results in a decrease in interfacial rigidity, and taken alone would serve to increase the ultimate particle size.

Most reverse micelle syntheses have shown that the ultimate particle size increases with water content; typically up to a limiting, or critical, value after which the particle size remains constant and the polydispersity of the particles increase. The increase in polydispersity may result from "breakage of the emulsion", at which time the curvature rigidity reaches its limit with increasing water content, and the excess water and other material is purged from the interior of the reverse micelle to a separate aqueous phase. [148, 149] The critical value of w depends upon the net effect of the three previously

mentioned components (i), (ii), and (iii) which, phenomenologically, make up the net contribution of water content factor, as well the other factors, such that the overall energy of the system is minimized.

Collision Frequency

The ultimate particle size is related to the collision frequency of the micelles containing the active metal nuclei. The greater the number of collisions between reverse micelles the greater the number of successful micellular exchanges resulting in the growth of the nanoparticles. The collision frequency is a function of the reverse micelle size, solvent parameters, and attractive and repulsive intermicellular interactions.

Solvent Molar Volume

The molar volume of the solvent, relative to the surfactant length also influences the ultimate particle size and polydispersity on the nanoparticles. If the molar volume of the solvent is sufficiently small with respect to the surfactant length the solvent will adsorb into the hydrophobic outer layer of the reverse micelle, a phenomena referred to as solvent penetration. When the solvent adsorbs into the hydrophobic region, increased steric interactions result from an increased volume in the hydrophobic layer. These steric interactions between the surfactant tails and the adsorbed solvent serve to effectively increase the CPP of the surfactant thus decreasing the radius of curvature and resulting in

an increase in interfacial rigidity. This increase in interfacial rigidity with decreasing solvent molar volume would, all else equal, result in a smaller ultimate particle size.

Number Density of Total Micelles in System

An increase in the total number of reverse micelles per unit volume, while constraining the size, results in a decrease in the collision energy of the micelle-micelle interactions[151]. Thus, increasing the total number density of the reverse micelles will result in a smaller ultimate nanoparticle diameter.

Concentration of Metal Salt

The concentration of the metal salt also influences the ultimate particle size. A higher concentration of salt in the system will result in:

(i) A larger fraction of reverse micelles containing cobalt ion, in the case where the cobalt concentration is not sufficient for all reverse micelles to contain cobalt ion. In this case the increase in concentration will result in a higher fraction of micelles containing nuclei, and thus a greater probability of filled-filled micelle exchange interactions. This will result in an increase in the ultimate particle size.

(ii) Larger cobalt nuclei in the reverse micelles, in the case where the cobalt ion concentration is sufficiently large ensure that all reverse micelles contain cobalt.

In this case the increase in cobalt ion concentration will result in a larger ultimate particle size as interaction produces a larger intermediate product.

Therefore, for either scenario, an increase in concentration of Co^{2+} will result in a larger particle size if all other process variables are held constant.

2.7. Structure and Chemistry of Cobalt in Micelles of Low w

In aqueous solutions, cobalt occurs predominantly in two oxidation states, Co^{II} and Co^{III}. Cobalt (II) chloride hexahydrate, in its non-dissociated state, has the formula: $[Co^{II}(Cl)_2(OH_2)]2H_2O$, where the inner coordination sphere contains 2 Cl^- and 4 H_2O ligands directly complexed to the core cobalt atom. The other two H_2O molecules are in the outer coordination sphere. These are not bonded to the cobalt, but reside in the lattice in interstitial positions. [152, 153]

Upon dissolution in a sufficiently dilute aqueous concentration, the Cl^- ligands are displaced by the OH_2 ligands, forming the cationic complex, $[Co^{II}(OH_2)_6]^{2+}$ known as hexa-aquacobalt(II). Hexa-aquacobalt(II) is an octahedral six-coordinate complex that appears pale pink in aqueous solution. However, if cobalt (II) chloride hexahydrate is dissolved in an aqueous solution that contains a sufficient chloride ion concentration, some of the hexa-aquacobalt(II) reacts with the available chloride to form a second species, $[Co^{II}(Cl)_4]^{2-}$, an anionic tetrahedral four-coordinate complex. This species appears an intense brilliant blue in solution. [152, 154]

The reaction is given by:

$$[Co^{II}(OH_2)_6]^{2+} + 4Cl^- \rightleftharpoons [Co^{II}(Cl)_4]^{2-} + 4\ H_2O\ [153] \qquad \textbf{(2.7-1)}$$

The equilibrium constant for this reaction, K_{eq} is given by:

$$K_{eq} = \frac{\left[Co_{II}(Cl)_4^{2-}\right]\left[H_2O\right]^4}{\left[Co_{II}(OH_2)_6^{2+}\right]\left[Cl^-\right]^4} \qquad \textbf{(2.7-2)}$$

Upon addition of cobalt (II) chloride hexahydrate salt to the DDAB/H_2O/Toluene system at w ~ 1, an intense blue color is expected in the solution, which suggests that some $[Co^{II}(Cl)_4]^{2-}$ may be present. This should be intuitive from the reaction equation (30) and the small water pool volume at w = 1 for the DDAB/H_2O/Toluene system. For very low w, there is not enough H_2O in the reverse micelle to sufficiently hydrate the polar head groups of the surfactants. For this reason the interaction between the polar groups and the water molecules is very strong. This interaction is so strong that the water can be considered "bound" to the surfactant and thus not available to participate in the reverse reaction of (2.7-1). It is very likely that the bromide from the surfactant is also present in the complex, such that the actual ion is a four-coordinate chloro-, bromo-, compound of the form $[Co^{II}(Cl)_x(Br)_y]^{2-}$, where x + y = 4.

2.8. Statistical Design of Experiments [155, 156]

Statistical Design of Experiments (SDE) is a technique aimed at obtaining sensitivities of a process to numerous variables using a limited set of well chosen experiments. SDE is best suited for situations where a reasonably large number of variables may influence the outcome of some process metric. In order to discuss SDE it is necessary to include a few definitions.

Factors – Factors are the controllable input parameters to the experimental process.

Responses – Responses are the measured output variables of interest.

Levels – Levels are the particular settings of the input factor (i.e. reaction temperature at T = 700 °C, 800 °C and 900 °C; each temperature is a level).

Factor Effects – The change in response resulting from change in the level of the factors.

Interaction Effects – The change in response resulting from the combined effect of two or more factors.

The SDE method allows the experimenter to screen a large number of Factors which may or may not influence the responses of interest. Also, the SDE method allows the observer to determine the relative magnitudes and directions of the effects of each factor. Finally it allows the experimenter to observe interaction effects of factors that might not be evident using other methods.

The most basic type of SDE is a full factorial design. The full factorial design allows the observer to analyze all factor effects and multiple interactions. The full factorial is usually a two or three level experiment. A two level full factorial is usually sufficient for screening if the levels are taken far enough apart. The number of runs increases with increasing number of factors and levels as:

$$R = L^F \qquad \textbf{(2.8-1)}$$

where R= # of runs; L = # of levels; F = # factors

Once the number of factors and levels have been selected, it is possible to codify the experiment in the form of a table. Table 2.8-1 is an example for a 4 factor, two level full factorial experiment where A, B, C, and D represent the factors being studied. The 1 and –1 represent high and low levels of the factors. The 2^{nd}, 3^{rd}, and 4^{th} order interactions are represented by multiple letters (i.e. AB is the 2^{nd} order interaction of factors A and B). The levels only have a literal meaning for the main factor (or 1^{st} order) interactions. The levels for the 2^{nd} and 3^{rd} order interactions are calculated as the product of the levels of the 1^{st} order components. ABCD is usually negligible and taken as a measure as the average, or background noise in the experiment.

Table 2.8-1: Example of an Experimental Matrix for a 2^4 Factorial Screening Experiment

Run	A	B	C	D	AB	AC	AD	BC	BD	CD	ABC	ABD	ACD	BCD	ABCD
1	1	1	1	1	1	1	1	1	1	1	1	1	1	1	1
2	1	1	1	-1	1	1	-1	1	-1	-1	1	-1	-1	-1	-1
3	1	1	-1	1	1	-1	1	-1	1	-1	-1	1	-1	-1	-1
4	1	1	-1	-1	1	-1	-1	-1	-1	1	-1	-1	1	1	1
5	1	-1	1	1	-1	1	1	-1	-1	1	-1	-1	1	-1	-1
6	1	-1	1	-1	-1	1	-1	-1	1	-1	-1	1	-1	1	1
7	1	-1	-1	1	-1	-1	1	1	-1	-1	1	-1	-1	1	1
8	1	-1	-1	-1	-1	-1	-1	1	1	1	1	1	1	-1	-1
9	-1	1	1	1	-1	-1	-1	1	1	1	-1	-1	-1	1	-1
10	-1	1	1	-1	-1	-1	1	1	-1	-1	-1	1	1	-1	1
11	-1	1	-1	1	-1	1	-1	-1	1	-1	1	-1	1	-1	1
12	-1	1	-1	-1	-1	1	1	-1	-1	1	1	1	-1	1	-1
13	-1	-1	1	1	1	-1	-1	-1	-1	1	1	1	-1	-1	1
14	-1	-1	1	-1	1	-1	1	-1	1	-1	1	-1	1	1	-1
15	-1	-1	-1	1	1	1	-1	1	-1	-1	-1	1	1	1	-1
16	-1	-1	-1	-1	1	1	1	1	1	1	-1	-1	-1	-1	1

It is possible to decrease the number of required runs by splitting the full factorial into two half factorials and running either of them. This is done by splitting the ABCD column such that the runs with ABCD = 1 being one half factorial and the runs with ABCD = -1 being the other. However, for any experimental system there are R-1 degrees of freedom (in this case 15), thus there are only 15 different unique pieces of information recoverable. In the full factorial case these are the 4 1^{st} order interactions, the 6 2^{nd} order interactions, the 4 3^{rd} order interactions, and the 4^{th} order interaction/background (ABCD). If the experiment is reduced to 8 runs there are only 7 degrees of freedom, this results in the effects from various interactions becoming confounded, or mathematically inseparable from each other. For a 4 factor 2 level experiment the confounding schedule is:

A=BCD B=ACD C=ABD D=ABC AB=CD AC=BD AD=BC ABCD=Average

The half factorial case could be sufficient in the case that the experimenter is reasonably certain that the 2^{nd} and 3^{rd} interactions are not significant.

Once the experiment had been designed and completed, each response variable can be evaluated as a function of the level of any factor or set of factor interactions. Hence, certain factors may arise as significant whereas others may be ignored in future experiments due to insignificant response magnitude.

2.9. Analysis of Variance [157]

When comparing ensembles of experimental data, such as particle size distributions, where the average values are statistically close and the distributions overlap, the evaluation of sameness of the distribution is best treated by statistical methods. In the case of designing nanoparticle synthesis methods where the goal is a narrow distribution, statistical comparison between populations is particularly germane. A number of statistical tests have been developed for comparing populations. These include the t-test, the f-test, and the ANOVA.

t-test

The t-test is an analysis method that compares the average values of two data sets of similar variance to determine whether or not there is a significant difference between to two means. That is, are the data sets members of the same population, and merely

differ because of random effects, or are they members of two different populations, and therefore differ because of the change the level of one of the factors (independent variables).

ANOVA

The ANOVA is a type of test known as an f-test which compares a set of multiple means to determine whether or not they all come from the same population. This is best suited to determine whether or not a set of factors influence a particular response variable. In order to carry out the ANOVA it is necessary to have n observations for m runs. Using this method, it will be necessary to perform an ANOVA for each factor or interaction. The following chart is a simplified example of the one-way ANOVA:

Table 2.9-1: Example of Simplified ANOVA Procedure

Factor A	Run:	1	2	…	m
Observation:	1	X_{11}	X_{21}	…	X_{m1}
	2	X_{12}	X_{22}	…	X_{m2}
	3	…	…	…	…
	4	X_{1n}	X_{2n}	…	X_{mn}
Totals		ΣX_1	ΣX_2	…	ΣX_m
Mean		X'_1	X'_2	…	X'_m

The data for each observation are tabulated in columns according to the run and the mean value of observations is determined. A grand mean, X_{GM}, the mean of the means, is then calculated by

$$X_{GM} = (X_{1M} + X_{2M} + \ldots + X_{mM})/(m\text{-}1) \qquad \textbf{(2.9-1)}$$

The *between-means variance*, s_b^2, (the observed variance about the grand mean) is given by:

$$s_b^2 = \{ (X_{1M} - X_{GM})^2 + (X_{2M} - X_{GM})^2 + \ldots + (X_{nM} - X_{GM})^2\}/(m\text{-}1) \qquad \textbf{(2.9-2)}$$

The *within-means variance*, s_w^2, is given by:

$$s_w^2 = \{(X_{1,1} - X'_1)^2 + (X_{1,2} - X'_1)^2 + \ldots + (X_{m,n} - X'_m)^2\}/\{m(n\text{-}1)\}. \qquad \textbf{(2.9-3)}$$

The F value is then calculated by:

$$F = ns_b^2/s_w^2 \qquad \textbf{(2.9-4)}$$

with the F indices of $\Phi_1 = m - 1$ and $\Phi_2 = m(n - 1)$. If the calculated value for F > the chart value for F based on the desired confidence interval, then it is likely within the confidence limits that some of the values are significantly different. If this is the case it will be necessary to do a t-test to determine which particular data sets are significantly different.

t-Test

The t-test is used to compare two sets of data to determine whether or not two data sets are significantly different. The assumption inherent in this test is that the variance of the two data points is similar. The following example illustrates the use of the t-test:

For two random samples of n_1 and n_2 units and means X_1' and X_2', respectively, one can express the t value as:

$$t = \frac{\left|X'_1 - X'_2\right|}{\sqrt{s_{n1}^2 + s_{n2}^2}} \qquad \textbf{(2.9-5)}$$

where

$$s = \sqrt{\frac{\Sigma(X'_1 - X'_2)}{n_1 + n_2 - 2}} \qquad \textbf{(2.9-6)}$$

If the two samples have the same variance, this simplifies to:

$$t_\alpha = \frac{\left|X'_1 - X'_2\right|}{\sqrt{\frac{n_1 + n_2}{n_1 n_2}}} \qquad \textbf{(2.9-7)}$$

Note: [158] The ANOVA and t-test assumes that the data being analyzed is at least "approximately" normal. The data needs to be examined for normality and if necessary transformed before use of the ANOVA and t-tests or analyzed by a

nonparametric significance analysis such as Kruskal-Wallis analysis of ranks and/or the Median test.

Chapter 3: Experimental

3.1. Experimental Methods

This section describes in detail the experiments preformed for this work. These experiments include, I. The materials and reverse micelle synthesis procedure for cobalt nanoparticles, II. An AFM analysis of the effect of the concentration of the cobalt salt on the resulting particle sizes of the of the cobalt nanoparticles under two conditions, with and without NaOH stabilizer for the reducing agent, III. An XRD analysis of the nanoparticle composition, and IV. A screening experiment in which the effects of several variables on the resulting particle size are examined and their relative effects determined.

3.1.1. Materials

The materials used for these experiments were as follows toluene from Sigma-Aldrich, St. Louis, MO, (HPLC grade, liquid), cobalt chloride hexahydrate from Spectrum, New Brunswick, NJ, (A.C.S. Reagent Grade, Crystalline), didodecyldimethylammonium bromide (DDAB) from Acros, New Jersey, (99%, solid), sodium borohydride from Sigma-Aldrich, St. Louis, MO, (99%, Crystalline) and acetone from Sigma-Aldrich, St. Louis, MO, (Reagent Grade, Liquid).

3.1.2. AFM Examination of Particle Size Dependency on Cobalt Salt Concentration

Experimental Design

For this experiment, the dependency of the particle size on cobalt salt concentration was examined for two cases. In the first case NaOH was not used to stabilize the reducing agent solution, this results in a less stable reducing solution which must be used immediately after being made. In the second case 14 M NaOH was used to stabilize the borohydride solution resulting in a more stable longer lived solution.

AFM Technique

The AFM samples were prepared by first diluting the particle suspension 20:1 in toluene in order to lower the particle density and avoid aggregation of particles upon drying on the AFM slide. The particle suspension was then loaded on the AFM slide by adding a drop to the surface and allowing the toluene to evaporate under ambient conditions. The AFM slide consisted of a flat sheet of mica attached to a steel AFM slug. The mica and the slug were provided by the AFM Lab.

AFM data was collected on the Digital Instruments Nanoscope IIIa Multimode Scanning Probe Microscope. The microscope, operated in AFM-Tapping Mode by Kevin Barber, was used to image the synthesized particles by measuring the Z-height of the surface of the sample. Because the tip of the AFM probe was much larger than the

diameter of the nanoparticles, it was necessary to assume the particles were spherical and that the Z-height was representative of the diameter.

Synthesis without NaOH stabilizer

Concentrations of $CoCl_2$ hexahydrate were prepared in 30 ml glass septum bottles in the range of 0.003M to 0.006M in an 11 wt% solution of DDAB in toluene. The volume of each preparation was 10 ml. This was carried out by first making up a stock solution of 11 wt% DDAB in toluene. A volume of this stock solution was then used to make a 0.03M solution of the $CoCl_2$ in DDAB. It was necessary to make a stock solution of the salt solution at 0.03M in order to ensure precision in the mass measurement of the $CoCl_2$. The Salt stock was then diluted with the DDAB Toluene stock as needed to prepare the required concentrations for the samples.

A 5.4 M concentration of $NaBH_4$ was prepared by dissolving the required amount of $NaBH_4$ in deionized H_2O and magnetically stirring until all of the solids were dissolved. Each sample was magnetically stirred and injected with 35 ul of the reducing solution.

Upon injection of the reducing solution the $CoCl_2$ solution reacted, as evidences by a color change from blue to green to black. The color change appeared to be complete after about two hours, however the samples were left on the stir plate for at least 12 hours to ensure completion of the reaction.

AFM analysis of the synthesized product was performed according to the standard technique described previously. Statistical analysis of the resulting AFM images was performed.

Synthesis with NaOH stabilizer

The concentration range of interest was narrowed in this set of experiments to 3.1 to 3.25 mM based on data collected from the synthesis without NaOH stabilizer. This concentration range was predicted to yield a nanoparticle diameter range of 1-3 nm. Three concentrations were synthesized in a similar manner to the previous experiment. The DDAB concentration in the toluene remained at 11 wt%. The reducing agent concentration was maintained at 5.4 M $NaBH_4$ in an aqueous solution of 14 M NaOH, such that the injection volume, and thus the water content remained constant. The $[NaBH_4]$:$[Co^{2+}]$ ratio was maintained at approximately 6:1. The reaction samples were reacted as previously mentioned, allowed five days to reach equilibrium, diluted 20:1 by volume in toluene and placed on an AFM slide. Statistical testing via ANOVA, and regression analysis were performed on the resulting data.

3.1.3. XRD Analysis of Particle Composition

In order to determine the crystal structure of the particles, it was necessary to perform an XRD analysis of the sample. A representative sample of nanoparticles was

precipitated out of the toluene by addition of acetone (Sigma-Aldrich, St. Louis, MO, Reagent Grade, Liquid). (a non-solvent) to the suspension. The precipitate, containing DDAB surfactant and cobalt nanoparticles were then isolated and dried in a watch glass under ambient conditions. The XRD analysis was performed by Dr. Allen Apblett, in the department of Chemistry at Oklahoma State University, Stillwater, OK using a Brucker Advance D-8 model diffractometer with Cu-k_a radiation.

3.1.3. DLS Factorial Analysis of Particle size as a Function of Co^{2+} Concentration, Water Content and Reducing Agent to Co^{2+} Ratio

Experiment Design

For this experiment, a three-factor two-level full factorial design was used to determine the effects of the Co^{2+} concentration, the water content, and the reducing agent to Co^{2+} ratio. Table 3.1.3-1 is the codified experimental matrix for this experiment. The dummy variables 0 and 1 are used to represent low and high values respectively of each factor. For this experiment Factor A is defined as the concentration of the cobalt ion in terms of the total volume, [Co^{2+}]. Factor B is defined as the water to DDAB ratio or water content, w. Factor C is defined as the molar ratio of the sodium borohydride ratio to the cobalt ion concentration.

Table 3.1.3-1: Experimental Matrix for DLS Screening Experiment

Run	A	B	C	AB	AC	BC	ABC
1	1	1	1	1	1	1	1
2	1	1	0	1	0	0	0
3	1	0	1	0	1	0	0
4	1	0	0	0	0	1	1
5	0	1	1	0	0	1	0
6	0	1	0	0	1	0	1
7	0	0	1	1	0	0	1
8	0	0	0	1	1	1	0

Table 3.1.3-2: Low and High Values for Factors A, B, and C.

Factor	Low	High
A	0.003 M	0.006 M
B	3:1	5:1
C	1.25:1	0.8:1

Experimental Method

Eight 10 ml samples numbered 1 through 8 were made according to the experimental matrix by adding the required amount of $CoCl_2 \cdot 6H_2O$ to a 11 wt % solution of DDAB in toluene in 30 ml glass screw top bottles. These bottles were placed on a magnetic stirrer. As the samples were stirred, each top was removed and the required amount of NaOH stabilized $NaBH_4$ was injected into the bottle, and the bottle was quickly capped. Upon addition of the reducing solution, the sample changed color form a light blue to a green, to finally a black color. After a 48 hour equilibrium time, the particles were then filtered through a 22 nm nitrocellulose syringe filter from Millipore.

The filtration was employed in order to remove dust particles from the sample, as a clean-room environment was not available for sample preparation. The samples were then placed in a quartz glass cuvette and analyzed with a Malvern High Performance Particle Sizer (HPPS-5001) Dynamic Light Scattering Analyzer. Thirty runs were performed for each sample. The resulting data was obtained in the form of a particle size distribution by volume. From this distribution the average particle size and peak width was determined. The peak width is defined as the width of the distribution at one half its height. The required viscosity data for the solvent was determined to be 12.510 cP from viscometry analysis on a Bohlin Instruments C-VOR rheometer using a double gap fixture. The sample viscosity was analyzed at a constant shear rate.

Data Analysis

The resulting DLS data was subjected to a semi-log transformation and analyzed using SAS General Linear Model to perform an ANOVA to determine the effect and significance of the factors and factor interactions on the particle diameter and polydispersity response (embodied in the peak width). In addition, confounded factor interactions were de-convoluted using the least square means, and a multiple regression was performed to determine an experimental linear correlation relating the factors and interactions to the response variables. This model is characterized by a set of linear parameter coefficients for each factor and interaction.

The data analysis for this paper was generated using SAS software, Version 9.1.

Chapter 4: Results and Discussion

4.1. AFM Analysis of Co nanoparticles synthesized without NaOH stabilizer

The data from the NaOH-free experiment was collected using a Nanoscope III Atomic Force Microscope. The resulting micrographs were analyzed on the Nanoscope software using the sectioning tool, which allows the user to obtain a moving cross-section of the surface of the sample slide. Figures 4.1-1 and 4.1-2 illustrate a typical sample slide and use of the sectioning tool to measure a nanoparticle, respectively. Because the AFM tip is significantly larger than the particles, the particles were assumed to be spherical, and the Z-height was taken to be equivalent to the particle diameter.

The diameter data for each concentration were tabulated, tested for significance using a statistical program known as the SAS General Linear Model (GLM), plotted and fit to a model. Because the particle size distributions were log-normal in nature, the raw diameter data had to first be transformed to its natural logarithm before it could be analyzed.

After the determination of the means and significance testing, the average diameter values were transformed back to linear:

$$\bar{x}_{linear} = \exp\left(\bar{x}_{\log}\right) \quad \textbf{(4.1-1)}$$

The variance was also transformed back to linear:

$$\left(\bar{x} + 2\sigma\right)_{linear} = \exp\left[\left(\bar{x} + 2\sigma\right)_{\log}\right] \quad \textbf{(4.1-2)}$$

and

$$\left(\bar{x} - 2\sigma\right)_{linear} = \exp\left[\left(\bar{x} - 2\sigma\right)_{\log}\right] \quad \textbf{(4.1-3)}$$

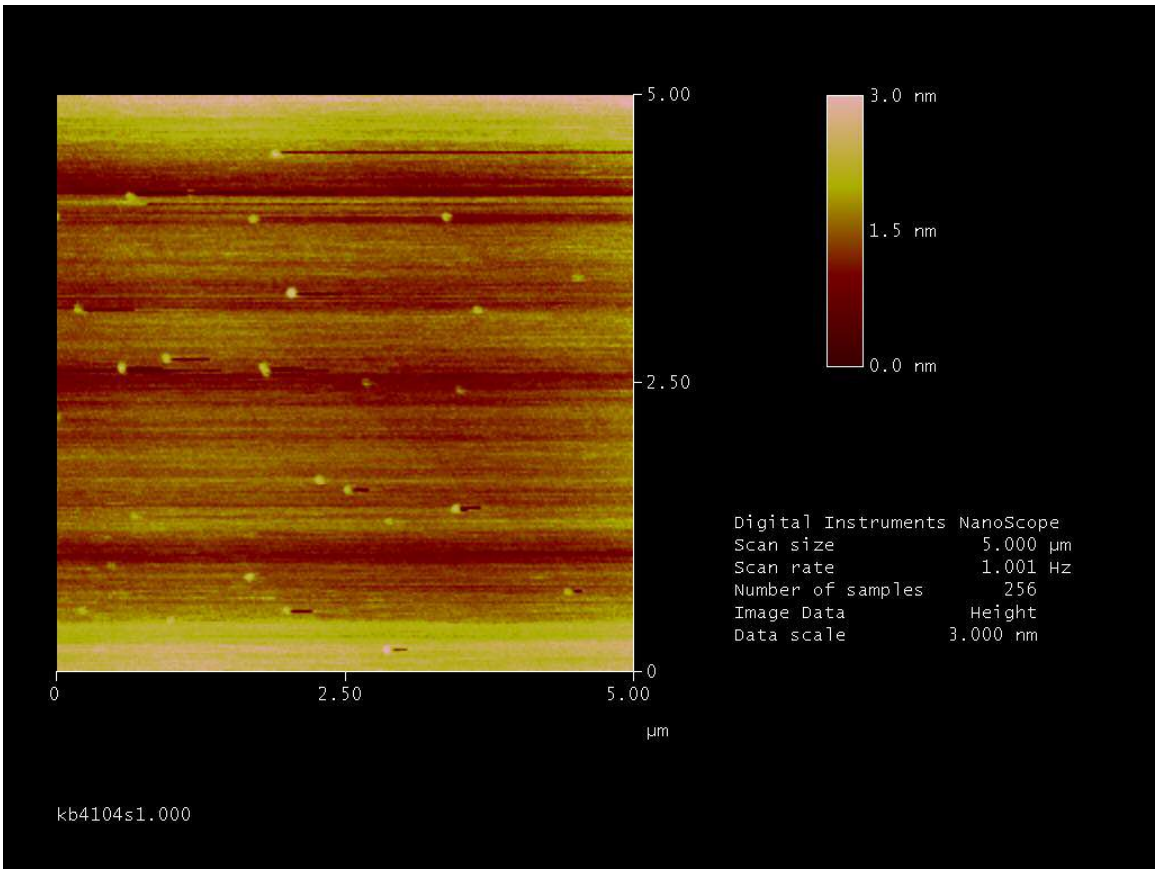

Figure 4.1-1: Representative AFM Micrograph of Discrete Cobalt Nanoparticles Synthesized by this Process.

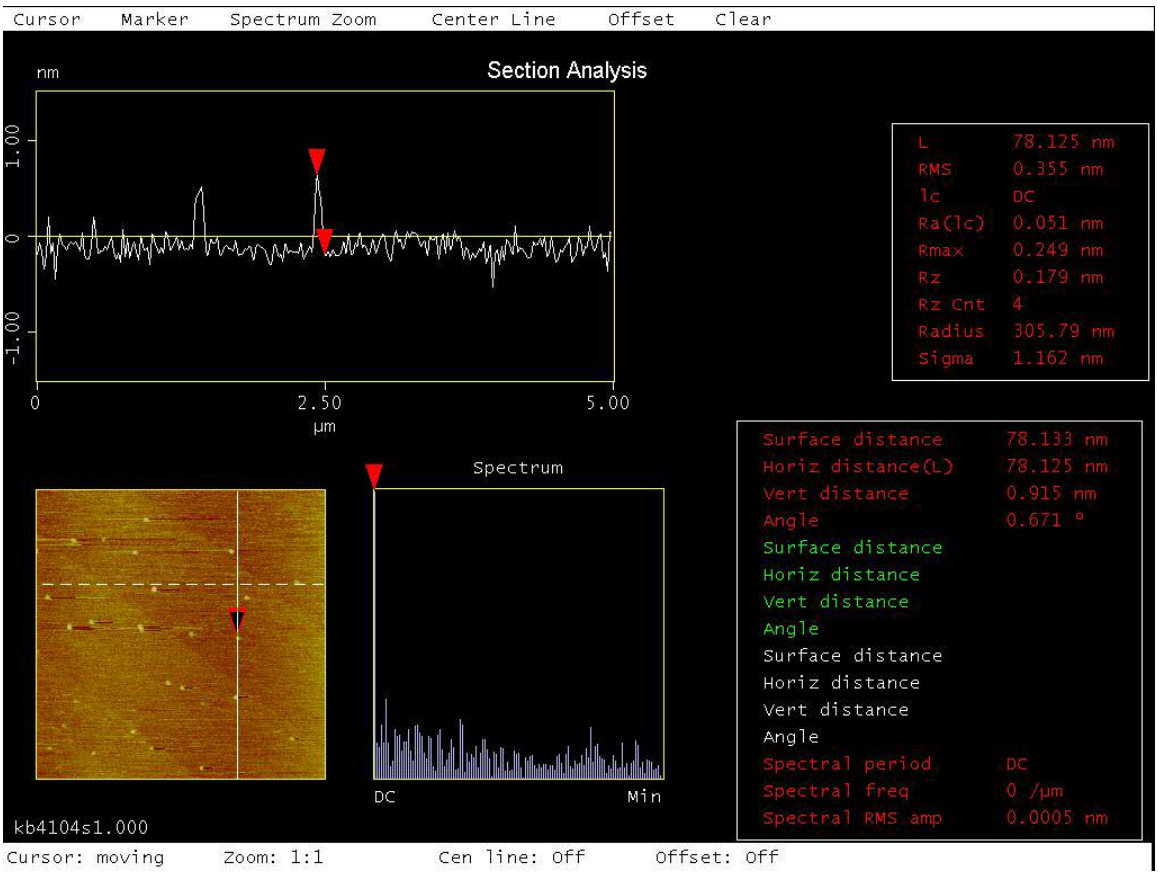

Figure 4.1-2: Screen Capture of Sectioning Tool Used to Determine Nanoparticle Diameter.

The t-test ANOVA preformed using the SAS GLM Procedure determined that all four of the diameter vs. concentration means obtained in this experiment were significantly different at the 0.05 level. The full statistical analysis is provided in the appendix of this thesis.

The following Figure 4.1-3 is a plot of the diameter vs. concentration data for this experiment. This data was taken at four levels and appears to be linear on a semi-log plot.

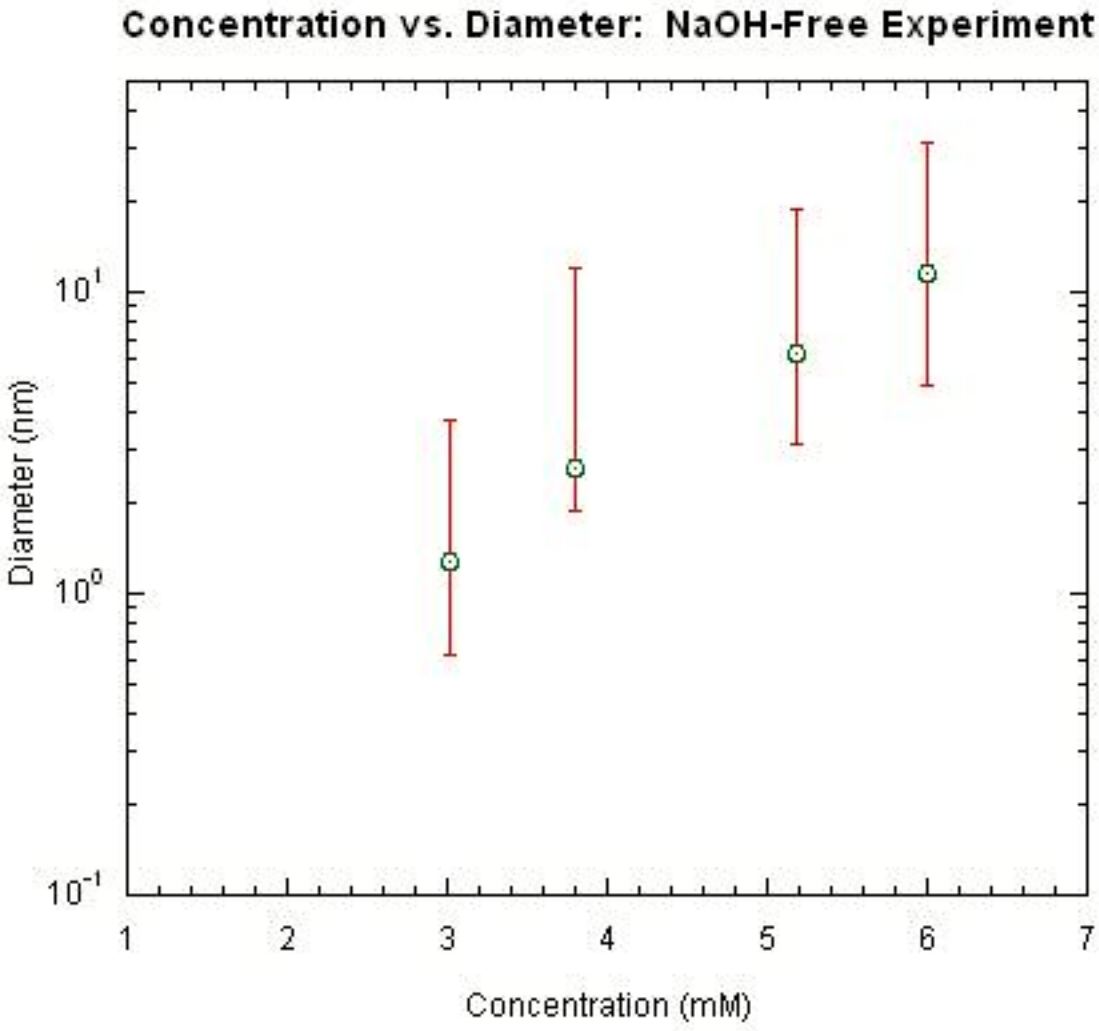

Figure 4.1-3: Semi-log Plot of Co^{2+} vs. Cobalt Nanoparticle Diameter for the NaOH-Free Experiment.

The data was fit to an exponential model function using the curve fit application in the KaleidaGraph plotting software. The natural logarithm of the average diameter vs. Co^{2+} concentration was plotted. The software then used a linear regression algorithm to

determine the pre-exponential and exponential coefficients for the fit. The resulting equation follows :

$$d = 0.15e^{0.72c} \quad \textbf{(4.1-4)}$$

where d is the measured particle diameter in nm, and c is the Co^{2+} concentration in mM.

4.2. AFM Analysis of Co nanoparticles synthesized with NaOH stabilizer

The AFM data from the NaOH stabilized experiments were collected and analyzed in the same manner as that from the NaOH-free experiment. Likewise, significance testing and regression analysis were performed on the data. Significance tests for the NaOH stabilized experiment determined that there was no significant difference between the 3.10 mM data and the 3.24 mM data for the 95% confidence interval. However there was a significant difference between both the 3.10 mM and 3.30 mM data and the 3.24 mM and 3.3 mM data. This may suggest that the two means are too close together in comparison to the variance to allow them to be significantly differentiated.

The diameter vs. concentration data from the NaOH stabilized experiment was plotted in Figure 4.2-1 and fit to an exponential curve in a similar manner to the previous experiment.

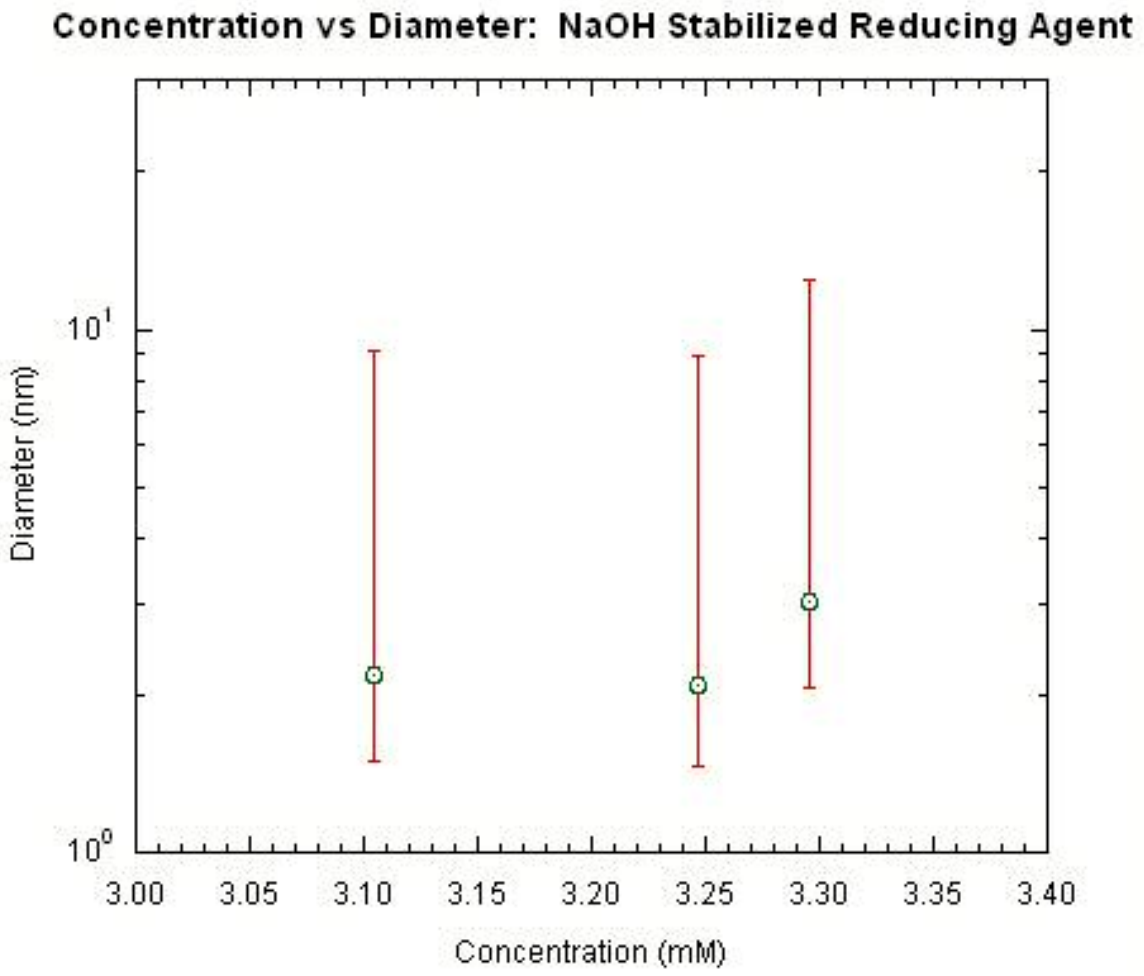

Figure 4.2-1: Semi-log Plot of Co $^{2+}$ Concentration vs. Cobalt Nanoparticle Diameter for the NaOH-Stabilized Reducing Agent Experiment.

The following model equation resulted from the exponential curve fit of the data. The data was fit by the same method as above.

$$d = 0.039e^{1.3c} \qquad \textbf{(4.2-1)}$$

Based on the data from both the stabilized and non-stabilized reducing agent experiments it can be concluded that the relationship between the particle size and the cobalt ion concentration can be fit to an exponential function with the following caveat. Initially, it was assumed that the only two factors that influenced the particle size were the water content and the cobalt concentration. Under this assumption, in these early experiments, the concentration and injection volume of the reducing agent was held constant for convenience. This resulted in the reducing agent to cobalt ion ratio varying. For the NaOH stabilized case any error that may have been introduced was mitigated by the short range examined. However for the non-stabilized case the reducing agent to salt ratio differs by a factor of two from the highest to lowest value and may be significant.

4.3. XRD Analysis of Particles

The X-ray diffraction method was not sensitive enough to detect the cobalt nanoparticles present in the DDAB. This is because the particle size and concentration were too low. The composition of the particles are assumed to be cobalt metal because the color change observed were consistent with the literature for cobalt nanoparticles at or near our size range.

4.4. Factorial DLS Analysis of Particle Size and Polydispersity

For the factorial experiment the data was collected on a Malvern HPPS Dynamic Light Scattering particle size analyzer. Thirty runs were performed for each sample

resulting in eight sets of diameter data and peak width data. Each run consisted of 20-30 machine observations of the correlation function. The actual number of machine observations for each run was determined by the machine automatically. The resulting data for both responses were analyzed by a Two-Way ANOVA procedure in SAS GLM, which determined the diameter and peak width responses to each of the factors and multi-factor interactions as well as the significance of those responses. The resulting multi-factor interactions were then analyzed Finally, multiple linear regression models were determined for both particle diameter and peak width (full width at half height) with the aid of the SAS Multiple Regression Procedure.

4.4.1 Analysis of Diameter Data

In order to discuss the analysis of the diameter data for this factorial experiment, it is helpful to review the factors analyzed in this experiment. The following table provides a factor identifier label for each factor analyzed, as well as the high and low ends of the factor range for the experiment. The high and low values for each factor are represented by the dummy variables 1 and 0 respectively.

Table 4.4.1-1: Factors, Identifiers, and High-Low Range for Dummy Variables

Label	Factor	High	Low
A	$[Co^{2+}]$	6 mM	3 mM
B	$[BH_4]$:$[Co^{2+}]$	3:1	6:1
C	$[H_2O]$:[DDAB]	1.25:1	0.75:1

From the ANOVA it was determined, that factors A, B, and C, as well as the B-C two-way interaction significantly effect the diameter response over the range of the experiment on a confidence interval greater than 95%. The Appendix contains the output from the SAS GLM.

The ANOVA tests the Null Hypothesis for each factor and multifactor interaction, that is it test whether there is a significant difference in the mean value of the response for the high and low values of the factor of interaction. This is done by calculating an F-score for each factor or interaction and comparing it against a tabulated critical value which is dependent upon the number of degrees of freedom and the desired confidence interval. If the F-score for each factor/interaction is greater than the critical F-value, the null hypothesis is rejected, thus the difference in the means due to the factor is significant at the desired level.

SAS GLM model reports the mean effects of the factor/interaction in terms of the least squares means (as not all data was of equal size). The model then used the ANOVA method to determine the significance of the means, reporting the F-score and the p-value which is a measure of the confidence interval. 95% confidence limit is represented by a p-value of 0.05.

The magnitude and direction of the diameter response to the factors are represented by the change in the least squares mean of the natural log of the diameter for

high and low values of each significant factor and interaction as summarized in Table 4.4.1.-3.

Table 4.4.1-2: Least Square Means for ln(Diameter)

Factor	Level	Mean d (nm)	Mean ln(d)	95% Confidence Limits	
A	0	3.8	1.3	1.3	1.4
	1	4.2	1.4	1.4	1.5
B	0	4.9	1.6	1.5	1.6
	1	3.2	1.2	1.1	1.2
C	0	3.7	1.3	1.3	1.4
	1	4.3	1.5	1.4	1.5
B-C	0, 0	5.4	1.7	1.6	1.7
	0, 1	4.4	1.5	1.4	1.5
	1, 0	2.5	0.93	0.88	0.99
	1, 1	4.1	1.4	1.4	1.5

The mean log diameter values for the main effects (A, B, C) are an average of the four values for which each effect was high or low. For instance, for main factor A = 0, the mean log diameter value was determined by taking an average value for all four runs in which factor A was at the low level. The mean log diameter values for each set of levels of the interaction (e.g. B-C) is an average of two values. For instance, for interaction B-C = 0, 0, the mean log diameter value was determined by taking the average value for the two runs in which both B and C were at the low level.

It is important to note that no repetitions were run for these experiments. Additional repetitions would have provided better average values for the responses.

Figure 4.4.1.-1 Graphically represents the effect of the main interactions on the average of the log of the nanoparticle diameter.

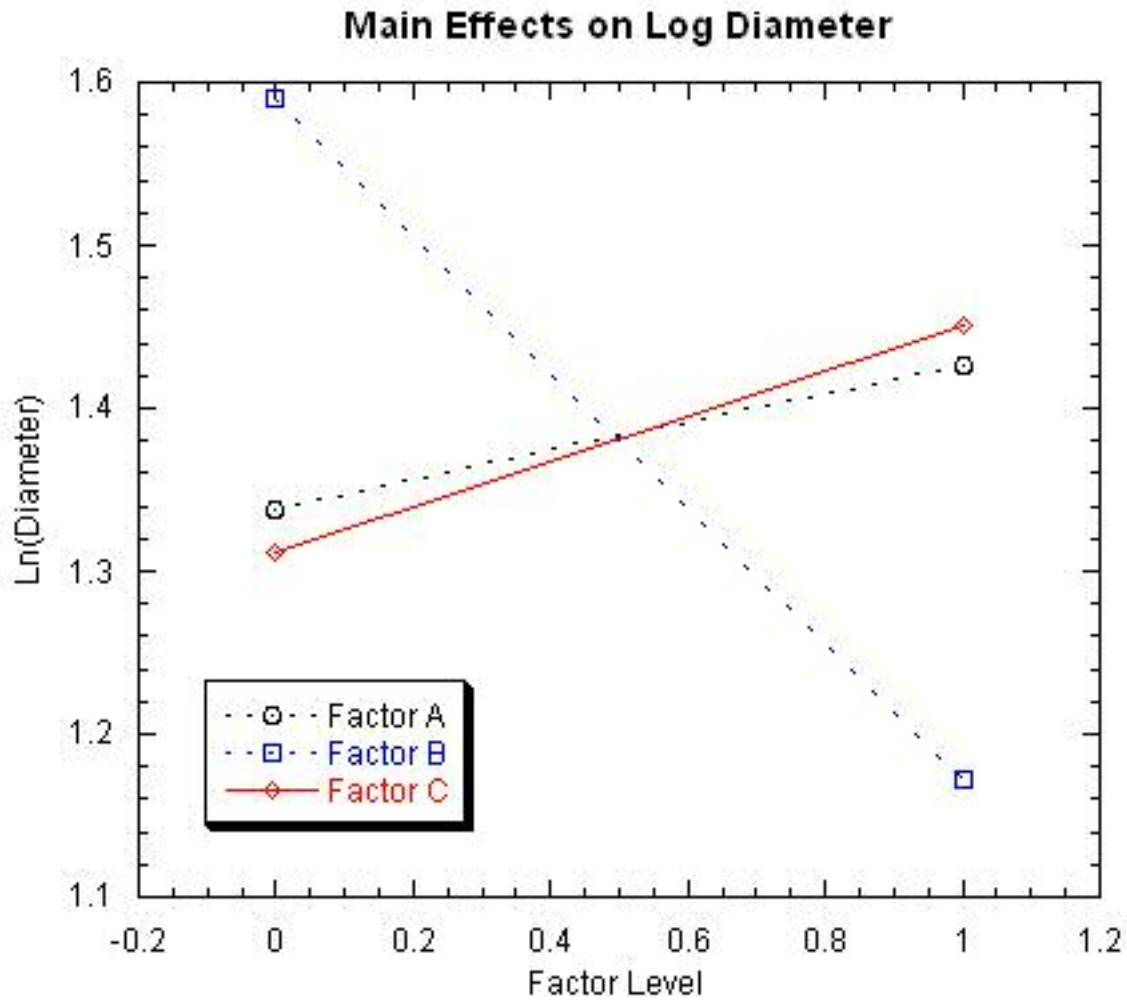

Figure 4.4.1-1: Main Factor Effects on Log Diameter of Nanoparticles.

Over the experimental range the average particle size increases with an increase in the Co^{2+} concentration (Factor A). As the concentration of Co^{2+} increases from 3 mM to 6 mM, the average particle size increases from 3.8 nm to 4.2 nm. For the case of the Co^{2+} concentration effect on the diameter, there is no indication of a significant interaction effect involving this factor, therefore the main effect of Co^{2+} is sufficient to characterize its total effect on the diameter.

This observation is at least qualitatively consistent with the literature for Cobalt nanoparticles synthesized in reverse micelles by similar methods, as it provides an increase in particle size with increasing Co^{2+} concentration over the range examined. The increase in particle size with increasing Co^{2+} may be accounted for by an increase in the proportion of cobalt containing reverse micelles which would increase the number of effective growth collisions.

For Factor B, the average particle size was observed to decrease from 4.9 nm to 3.2 nm as the borohydride to Co^{2+} ratio increased from 3:1 to 5:1. This factor is also involved in a two factor interaction with water content, Interaction B-C, which must be elucidated to completely understand the effect of borohydride to Co^{2+} ratio on the nanoparticle diameter.

For Factor C, the water content, w, of molar ratio of DDAB to H_2O, the average diameter of the nanoparticles increased from 3.7 nm to 4.3 nm as the water content increased from 0.80 to 1.25. The water content factor, like the borohydride ratio, also contributes to the B-C Interaction.

The increase in the nanoparticle diameter with increasing water content is also consistent with the observations in the literature for this system. Possible explanations for the increase in particle size with an increase in the water content include, (i) an increase in the initial size of the reverse micelle, (ii) a decrease in the interaction between

the DDAB heads and the bound water, and (iii) an increase in the attractive potential between the reverse micelles resulting in an increase in the number of growth collisions.

While an increase in the absolute size of the reverse micelle seems to be similar to the ultimate particle size for higher water contents, this is not case for the smaller water contents. Therefore the templating effect does not seem to come into play in the very low water content range on the order of w = 1.

For very low water content, all of the water in the reverse micelle is strongly bound to the surfactant. The strength of this bonding may result in an increase in the required collision energy to affect a growth exchange between reverse micelles. As the water content increased, the bonding energy between the bound water molecules are delocalized among the added water, resulting in less energy required to remove a surfactant molecule from the reverse micelle, resulting in a decrease in the energy required to affect a growth collision.

The interaction effects of borohydride to Co^{2+} ratio with water content (B-C Interaction) on the average nanoparticle diameter are not as straightforward at first glance. In order to understand this interaction it is necessary to look at the average effect of B on the interval of 0 to 1, while holding C constant first at 0 and then at 1. The converse analysis could also be performed. If the water content is constrained to the low value, 0.80, and the borohydride to Co^{2+} ratio is increased from 3:1 to 5:1, the average particle size decreases from 5.4 nm to 2.5 nm. If, on the other hand, the water content is

constrained to the high value, 1.25, the average particle size still decreases, but by a much smaller amount from 4.4 nm to 4.1 nm for the came increase in borohydride to Co^{2+} ratio.

Conversely, constraining the borohydride to Co^{2+} ratio to the low value of 3:1 while increasing the water content, results in a decrease in the average diameter from 5.4 nm to 4.4 nm. Constraining the borohydride to Co^{2+} ratio to the high value of 5:1 results in an increase from 2.5 nm to 4.1 nm. The effect of increasing both the borohydride to Co^{2+} ratio and the water content simultaneously from low to high results in a decrease in the average value of the diameter from 5.4 nm to 4.1 nm.

The analysis of the B-C Interaction implies that the rate effect on the diameter experienced by increasing the borohydride ratio is damped by increasing the water content of the system. This suggests that there may be a competing reaction between the borohydride and the H_2O in the system. As part of the borohydride reacts with the water, there is less borohydride reacting with the metal ion, consequently the timescale of the reaction increases, in comparison with the collision timescale. Consequently the negative effect of the increased borohydride ratio is dampened. Here “negative effect” indicates that the effect causes the average particle size to decrease.

Figure 4.4.1-2 Graphically represents the effect of the B-C multi-factor interaction on the average nanoparticle diameter. The line “B, C=0” represents the average value of the natural log of the diameter with level of B for the case where C is constrained to the low level and the line “B, C=1” represents the average value of the natural log of the

diameter with level of B for the case where C is constrained to the high level. Likewise, The line "C, B=0" represents the average value of the natural log of the diameter with level of C for the case where B is constrained to the low level and the line "C, B=1" represents the average value of the natural log of the diameter with level of C for the case where B is constrained to the high level

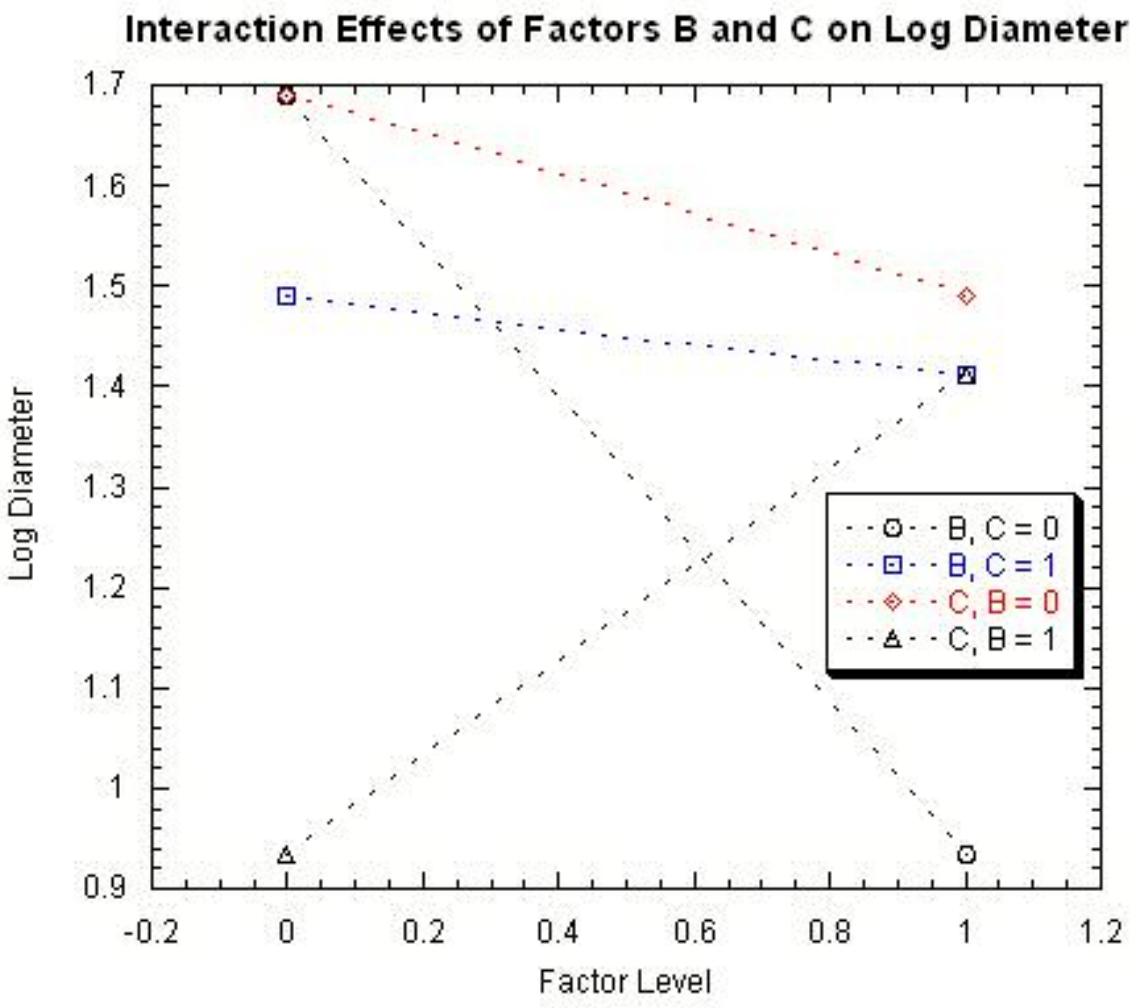

Figure 4.4.1-2: B-C Interaction Effects on the Log of the Diameter.

It was possible to use the regression procedure in SAS to perform a multiple linear regression in order to obtain an experimental model. Since this was a two level

experiment the regression model must be linear in terms of the log of the diameter and therefore exponential in terms of the linear diameter. The linear correlation is of the form:

$$\ln(d) = m + k_A x_A + k_B x_B + k_C x_C + k_{BC} x_{BC} \qquad \textbf{(4.4.1-1)}$$

Where m is the intercept, k is the parameter constant for each factor of interaction, and x is the value of the normalized factor constrained between the high and low values. The following table summarizes the values for the intercept and the parameter constants.

Table 4.4.1-3: Parameter Constants for Diameter Correlation

Parameter	Value	Standard Error
m	1.7	0.033
k_A	0.088	0.029
k_B	-0.76	0.042
k_C	-0.20	0.041
k_{AB}	0.68	0.059

4.4.2. Analysis of Peak Width Data

A similar set of analyses were performed on the peakwidth data. From the ANOVA it was determined that all main factors and interactions had a significant effect on the peak width over the experimental range with a confidence interval of greater than 95%.

Table 4.4.2-1: Least Square Means for Peak Width.

Factor	Level	Mean Peak Width (nm)	95% Confidence Intervals	
A	0	0.41	0.39	0.43
	1	0.59	0.57	0.61
B	0	0.63	0.61	0.65
	1	0.36	0.34	0.38
C	0	0.51	0.49	0.53
	1	0.48	0.47	0.51
A-B	0, 0	0.49	0.46	0.51
	0, 1	0.33	0.30	0.35
	1, 0	0.78	0.75	0.80
	1, 1	0.40	0.37	0.42
A-C	0, 0	0.40	0.38	0.43
	0, 1	0.41	0.39	0.44
	1, 0	0.61	0.58	0.64
	1, 1	0.56	0.54	0.59
B-C	0, 0	0.76	0.73	0.79
	0, 1	0.50	0.48	0.53
	1, 0	0.25	0.23	0.28
	1, 1	0.47	0.45	0.50

The main effects of the factors on the peak width are summarized in Figure 4.4.2-1. Likewise, the effects of the A-B, A-C, and B-C interactions are summarized in Figures 4.4.2-2 through 4.4.2-4.

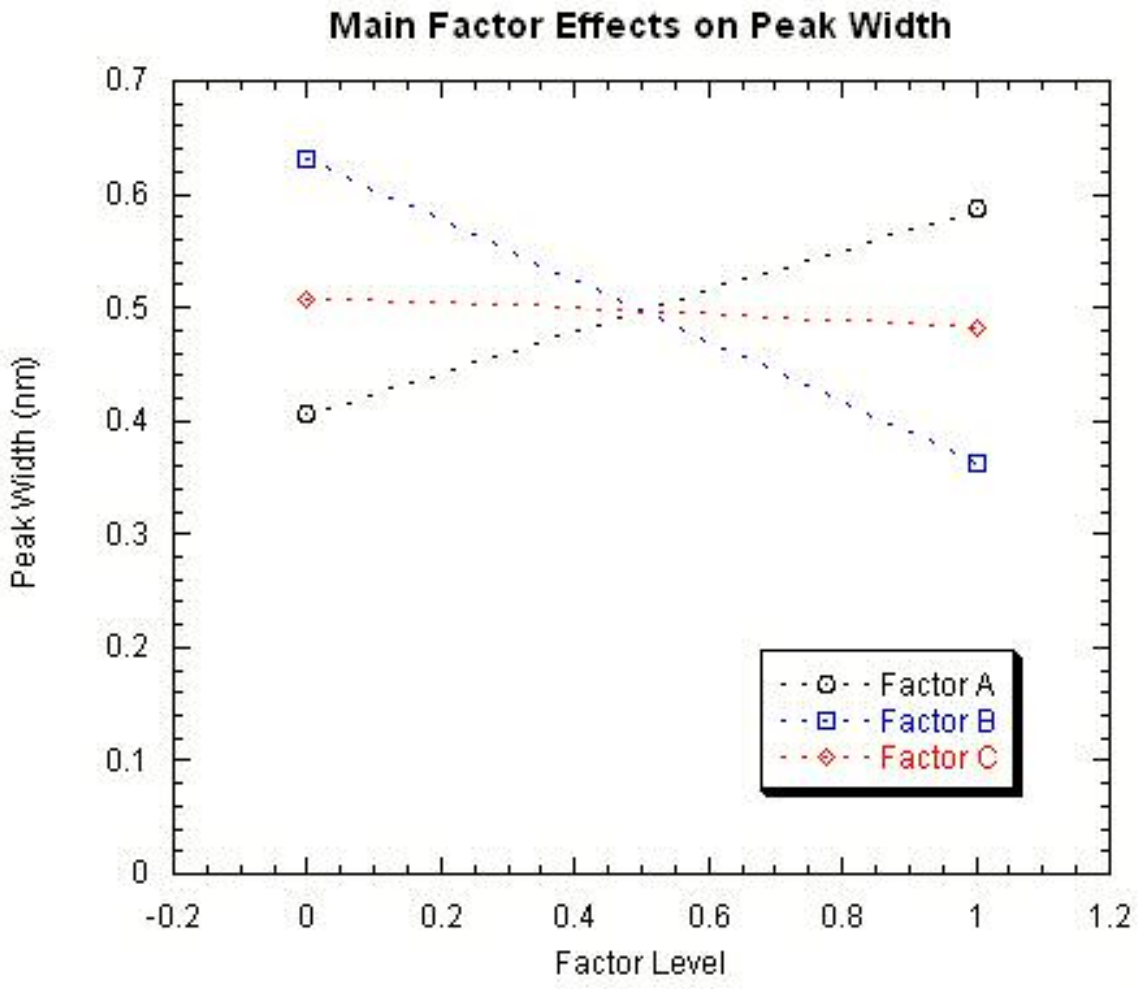

Figure 4.4.2-1: Main Factor Effects on Peak Width of Nanoparticle Size Distribution Data.

The average value of the peak width was observed to increase from 0.41 nm to 0.59 nm with an increase in Co^{2+} concentration (Factor A) from 3 mM to 6mM, while it decreased from 0.63 nm to 0.36 nm as the borohydride to Co^{2+} ratio (Factor B) increased from 3:1 to 5:1, and decreased from 0.51 nm to 0.48 nm as the water content (Factor C) increased from 0.80 to 1.25.

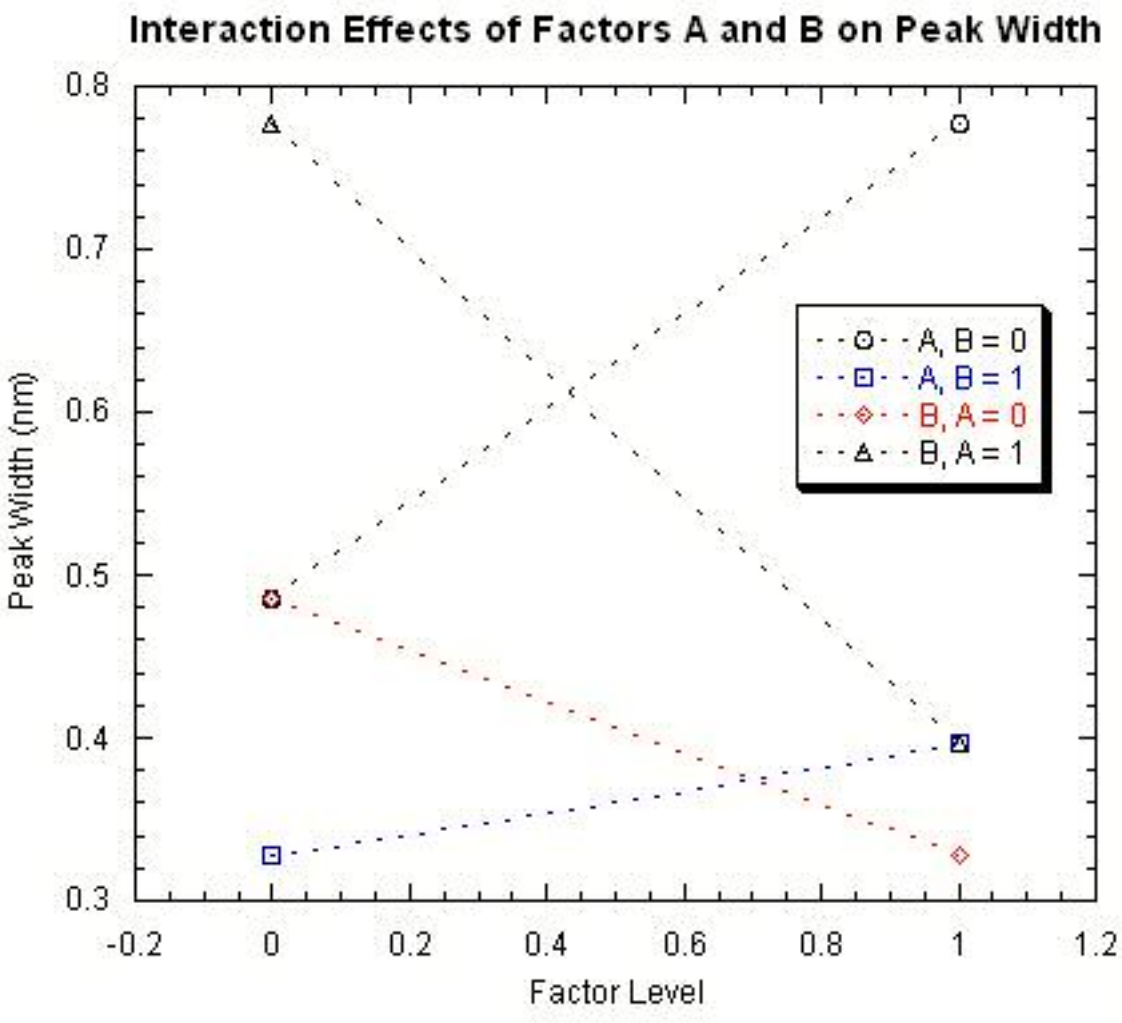

Figure 4.4.2-2: A-B Interaction Effects on Peak Width.

The A-B Interaction effect is summarized in Figure 4.3.2-2. As illustrated, for borohydride ratio constrained at the low value, an increase of Co^{2+} results in a relatively large increase in peak width when compared to the main effect, increasing the average value of the peak width from 0.49 nm to 0.78 nm. However for the borohydride ratio constrained at the high value, the resulting increase in the peak width was substantially damped, resulting in an increased average peak width from 0.33 nm to 0.40 nm.

Conversely, if the Co^{2+} concentration is constrained to the low value an increase in the borohydride ratio results in a decrease in the average value of the peak width from 0.49 nm to 0.33 nm, and for the Co^{2+} concentration constrained to the high level, the resulting change in average peak width is a larger decrease from 0.78 nm to 0.40 nm.

For the A-C Interaction effects on the average peak width, summarized in Figure 4.4.2-3, the effect of Co^{2+} concentration (Factor A) for water content constrained at the low value results in an increase in average peak width from 0.40 nm to 0.61 nm, for water content constrained at the high value the resulting increase, from 0.41 nm to 0.56 nm, is dampened.

Conversely, if the Co^{2+} concentration is constrained to the low value, an increase in the water content results in a small increase in the average peak width from 0.40 nm to 0.41 nm however these two means are not significant at the 95% level as evidences by the overlap in their 95% confidence levels. When the Co^{2+} concentration is constrained to the high value, however, the average peak width is observed to decrease significantly from 0.61 nm to 0.56 nm.

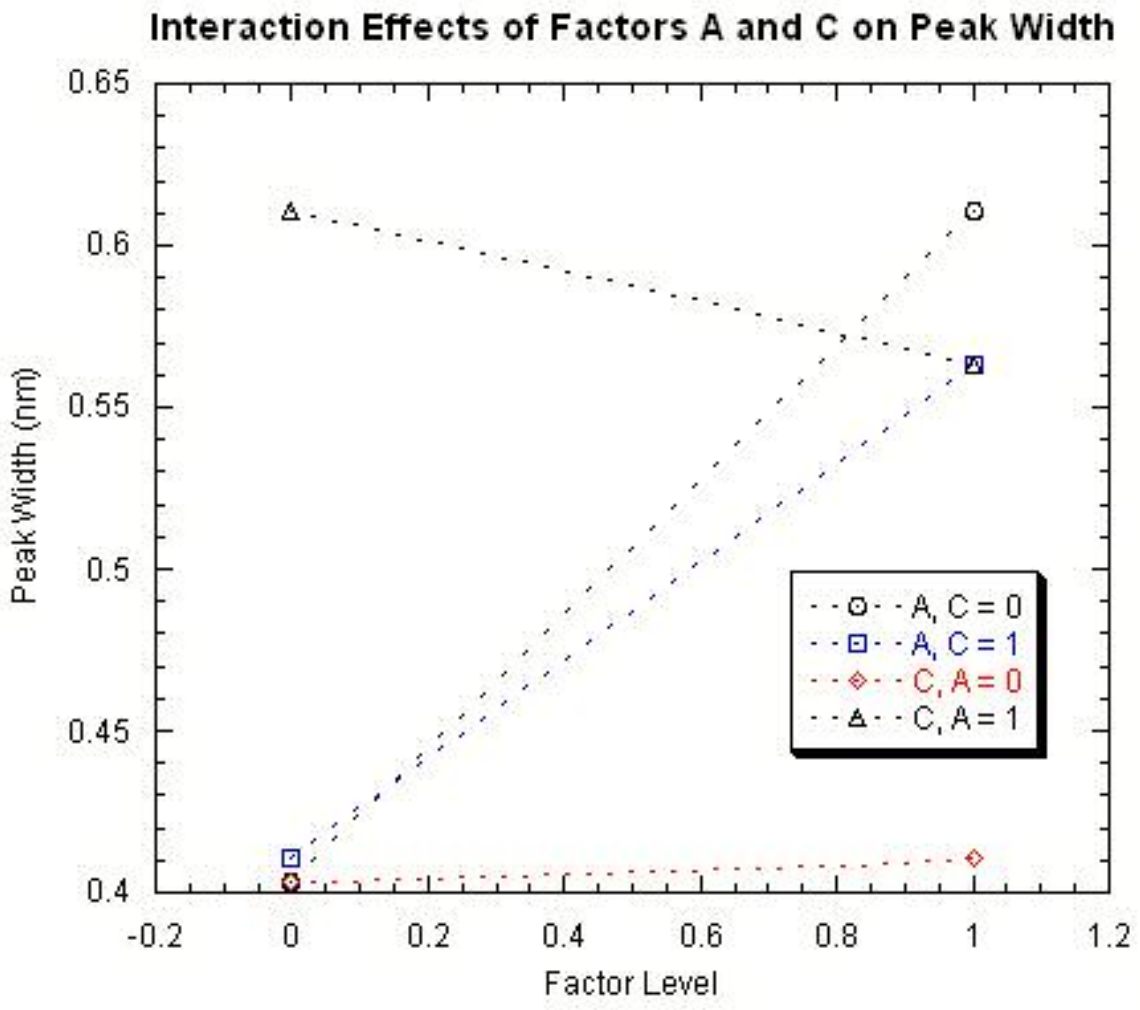

Figure 4.4.2-3: A-C Interaction Effects on Peak Width.

The B-C Interaction effects on the average peak width, are summarized in Figure 4.4.2-4. The effect of increasing the borohydride ratio for the low value of water content results in a decrease in the peak width from 0.76 nm to 0.25 nm. For the high value of water content the increase in the borohydride ratio, from 0.50 nm to 0.47 nm, is damped.

Conversely, increasing water content for low borohydride ratio results in a decrease of average peak width from 0.76 nm to 0.56 nm, while increasing water content for high borohydride ratio results in an increase from 0.25 nm to 0.47 nm.

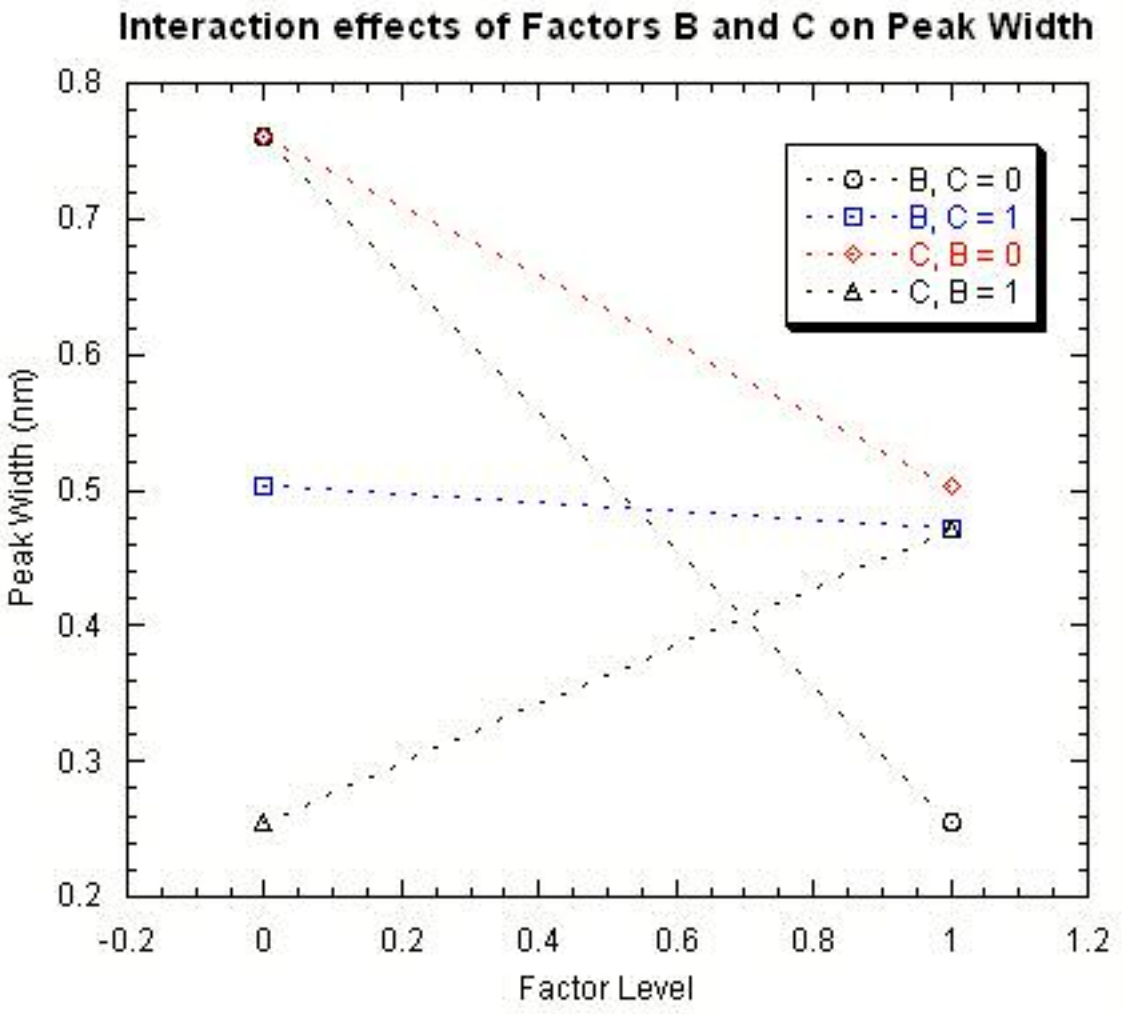

Figure 4.4.2-4: B-C Interaction Effects on Peak Width.

In this case the model from the multiple linear regression is indeed truly linear with respect to the peak width as the data did not require a logarithmic transformation to be normal. The data is characterized by the following equation:

$$PW = m + k_A x_A + k_B x_B + k_C x_C + k_{AB} x_{AB} + k_{AC} x_{AC} + k_{BC} x_{BC} \qquad \textbf{(4.4.2-1)}$$

Where PW is the peak width, and the parameter constants are determined as listed in the following table.

Table 4.4.2-2: Parameter Constants for Peak Width Correlation

Parameter	Value	Standard Error
m	0.60	0.017
k_A	0.32	0.023
k_B	-0.39	0.023
k_C	-0.23	0.023
k_{AB}	-0.22	0.026
k_{AC}	-0.055	0.026
K_{BC}	0.47	0.026

Chapter 5: Conclusions

The following is a summary of the tasks that were performed for the purpose of this thesis:

1. Metallic cobalt nanoparticles were synthesized in the 1 to 5 nm range using a reverse micelle process where a cobalt chloride salt in a DDAB/Toluene solvent was reduced using sodium borohydride.

2. The diameters of these particles were characterized using atomic force microscopy and dynamic light scattering methods.

3. The polydispersity of these particles were characterized in terms of the width at half height using dynamic light scattering methods.

4. The effects of the main factors (Co^{2+} Concentration, Reducing Agent to Metal Ion Molar Ratio, and Water Content) on nanoparticle diameter and polydispersity were determined.

5. The effects of the significant two factor interactions on the nanoparticle diameter and polydispersity were determined.

6. Simple experimental correlations for the effects and interactions on the diameter and polydispersity were constructed based on the analyzed data.

Based on the results detailed in Chapter 4, the following conclusions were drawn:

1. Main Effects of Cobalt Ion Concentration:

   Over the experimental range, the average diameter of the cobalt nanoparticles were shown to increase from 3.8 to 4.2 nm as the cobalt ion concentration increases from 3 to 6 mM. The relationship between diameter and cobalt concentration may be exponential based upon the multilevel experiments. It was also shown that the polydispersity of the nanoparticles increased from an average width at half maximum of 0.41 to 0.59 nm.

2. Main Effects of Borohydride to Cobalt Ion Ratio:

   Over the experimental range, the average diameter of the cobalt nanoparticles were shown to decrease from 4.9 to 3.2 nm as the borohydride to cobalt ion ratio increased from 3:1 to 5:1. The polydispersity of the nanoparticles decreased from an average width at half maximum of 0.63 to 0.36 nm.

3. Main Effects of Water Content:

Over the experimental range, the average diameter of the cobalt nanoparticles were shown to increase from 3.7 to 4.3 nm as the water content increased from 0.8 to 1.25.

4. Interaction Effects Between Cobalt Ion Concentration and Borohydride to Cobalt Ion Ratio:

   For the diameter response, there was no significant effect between cobalt ion concentration and borohydride to cobalt ion ratio as evidenced from the ANOVA. However, for the polydispersity there is a significant set of interactions between cobalt ion concentration and borohydride to cobalt ion ratio. For low values of borohydride ratio (3:1) the average peak width at half maximum height increases from 0.49 nm to 0.78 nm as the cobalt ion concentration increases from 3 mM to 6mM, for high borohydride ratio (5:1) the response is damped with an average peakwidth increase from 0.33 nm to 0.40 nm for the same change in cobalt ion concentration. Conversely, for low values of cobalt ion concentration (3 mM) the average peak width at half maximum height decreases from 0.49 nm to 0.33 nm for an increase in borohydride ratio from 3:1 to 5:1, for high cobalt ion concentration (6 mM) the response is an average peakwidth decrease from 0.78 nm to 0.40 nm for the same change in borohydride ratio.

5. Interaction Effects Between Cobalt Ion Concentration and Water Content:

   For the diameter response, there was no significant effect between cobalt ion concentration and water content as evidenced from the ANOVA. However, for

the polydispersity there is a significant set of interactions between cobalt ion concentration and water content. For low values of water content (0.8) the average peak width at half maximum height increases from 0.40 nm to 0.61 nm as the cobalt ion concentration increases from 3 mM to 6mM, for high water content (1.25) the response is damped with an average peakwidth increase from 0.41 nm to 0.56 nm for the same change in cobalt ion concentration. Conversely, for low values of cobalt ion concentration (3 mM) the average peak width at half maximum height increases from 0.40 nm to 0.41 nm for an increase in water content from 0.8 to 1.25 (this response was determined not significant at the 95% level); for high cobalt ion concentration (6 mM) the response is an average peakwidth decrease from 0.61 nm to 0.56 nm for the same change in borohydride ratio.

6. Interaction Effects Between Borohydride to Cobalt Ion Ratio and Water Content:

   For the diameter response there is a significant set of interactions between borohydride to cobalt ion ratio and water content. For low values of water content (0.8) the average diameter decreases from 5.4 nm to 2.5 nm as the borohydride ratio increases from 3:1 to 5:1, for high water content (1.25) the average diameter decreases from 4.4 nm to 4.1 nm for the same change in borohydride ratio. Conversely, for low values of borohydride ratio (3:1) the average diameter decreases from 5.4 nm to 4.4 nm for an increase in water content from 0.8 to 1.25; for high borohydride ratio (6 mM) the response is an

average diameter increase from 2.5 nm to 4.1 nm for the same change in water content.

For the polydispersity response there is a significant set of interactions between borohydride to cobalt ion ratio and water content. For low values of water content (0.8) the average peak width at half maximum height decreases from 0.76 nm to 0.25 nm as the borohydride ratio increases from 3:1 to 5:1, for high water content (1.25) the response is damped with an average peakwidth decrease from 0.50 nm to 0.47 nm for the same change in borohydride ratio. Conversely, for low values of borohydride ratio (3:1) the average peak width at half maximum height decreases from 0.76 nm to 0.50 nm for an increase in water content from 0.8 to 1.25; for high borohydride ratio (6 mM) the response is an average peakwidth increase from 0.25 nm to 0.47 nm for the same change in water content.

Recommendations for process design:

1. The cobalt ion concentration should be chosen as the variable for fine control for nanoparticle diameter because there are no significant multi factor interactions associated with this variable.

2. The water content should be constrained to around 1.0, which should ensure formation of cobalt metal over cobalt boride.

3. The borohydride ratio could be used for coarse control of the nanoparticle diameter, because with the water content constrained, there are no multifactor interactions (i.e. no interaction between borohydride ratio and cobalt ion concentration).

Future work should focus on the following points:

1. Performing similar statistically designed experiments at three or four levels with multiple repetitions.

2. Determining the effect of different reducing agents on the nanoparticle diameter and polydispersity.

3. Exploring better characterization methods for the particle distribution analysis, such as SAXS, SANS, and High Resolution TEM.

4. Exploring the effect of other factors such as reaction temperature, reaction time, solvent molar volume, surfactant tail length, and reducing agent on nanoparticle size and polydispersity.

REFERENCES

1. Lin, Y., Finke, J., *Novel polyoxoanion- and Bu4N+-stabilized, isolable, and redissolvable, 20-30-.ANG. Ir300-900 nanoclusters: the kinetically controlled synthesis, characterization, and mechanism of formation of organic solvent-soluble, reproducible size, and reproducible catalytic activity metal nanoclusters.* Journal of the American Chemical Society, 1994. **116**: p. 8335-8353.
2. Bonnemann, G.A.B., *Enantioselective hydrogenations on platinum colloids.* Angewandte Chemie, International Edition, English, 1996. **35**: p. 1992-1995.
3. Wilcoxson, J.P., Martino, T., Klavetter, E., Sylwester, A. P., Nanophase Materials, 1994: p. 771-780.
4. Lewis, L.N., Lewis, N., *Platinum-catalyzed hydrosilylation - colloid formation as the essential step.* Journal of the American Chemical Society, 1986. **108**: p. 7228-7231.
5. Vargaftik, M.N., et al., *Giant palladium clusters as catalysts of oxidative reactions of olefins and alcohols.* Journal of Molecular Catalysis, 1989. **53**: p. 315-348.
6. Schmidt, T.J., et al, *Electrocatalytic activity of PtRu alloy colloids for CO and CO/H_2 electrooxidation: stripping voltammetry and rotating disk measurements.* Langmuir, 1997. **13**: p. 2591-2595.

7. Reetz, M.T., Breinbauer, R., Wedemann, P., Binger, P, *Nanostructured nickel-clusters as catalysts in [3+2]cycloaddition reactions.* Tetrahedron, 1998. **54**: p. 1233-1240.

8. Reetz, M.T., Breinbauer, R., Wanninger, K., *Suzuki and heck reactions catalysed by preformed palladium clusters and palladium/nickel bimetallic clusters.* Tetrahedron Letters, 1996. **37**: p. 4499-4502.

9. Reetz, M.T., Lohmer, G., *Propylene carbonate stabilized nanostructured palladium clusters as catalysts in Heck reactions.* Chemical Communications, 1996. **1996**: p. 1921-1922.

10. Alvarez, W.E., Kitiyanan, B., Borgna, A., Resasco, D. E., *Synergism of Co and Mo in the catalytic production of single-wall carbon nanotubes by decomposition of CO.* Carbon, 2001. **39**: p. 547-558.

11. Alvarez, W.E., et al., *Characterization of single-walled carbon nanotubes (SWNTs) produced by CO disproportionation on Co-Mo catalysts.* Chemistry of Materials, 2002. **14**: p. 1853-1858.

12. Bachillo, S.M., et al., *Narrow (n,m)-distribution of single-walled carbon nanotubesgrown using a solid supported catalyst.* Journal of the American Chemical Society, 2003. **125**: p. 11186-11187.

13. Herrera, J.E., et al., *Relationship between the structure/composition of Co-Mo catalysts and their ability to produce single-walled nanotubes by CO disproportionation.* Journal of Catalysis, 2001. **204**: p. 129-145.

14. Herrera, J.E., Resasco, D. E., *Loss of single-walled nanotube selectivity by disruption of the Co-Mo interaction in the catalyst.* Journal of Catalysis, 2004. **221**: p. 345-364.

15. Kitiyanan, B., Alvarez, W. E., Harwell, J. H., Resasco, D. E., *Controlled production of single-walled carbon nanotubes by catalytic decomposition of CO on bimetallic Co-Mo catalysts.* Chemical Physics Letters, 2000. **317**: p. 496-503.

16. Dai, H., et al., *Single-wall nanotubes produced by metal catalyzed disproportionation of carbon monoxide.* Chemical Physics Letters, 1996. **260**: p. 471-475.

17. Moisala, A., Nasibulin, A. G., Kauppinen, E. I., *The role of metal nanoparticles in the catalytic production of single-walled carbon nanotubes -- a review.* Journal of Physics: Condensed Matter, 2003. **15**: p. S3011-S3035.

18. Zhang, Y., et al., *Imaging as-grown single-walled carbon nanotubes originated from isolated catalytic nanoparticles.* Applied Physics A, 2002. **74**: p. 325-328.

19. Li, Y., et al., *Growth of single-walled carbon nanotubes from discrete catalytic nanoparticles of various sizes.* Journal of Physical Chemistry B, 2001. **105**: p. 11424-11431.

20. Choi, H.C., Woong, K., Wang, D., Dai, H., *Delivery of catalytic metal species onto surfaces with dendrimer carriers for the synthesis of carbon nanotubes with narrow diameter distribution.* Journal of Physical Chemistry B, 2002. **106**: p. 12361-12365.

21. Su, M., et al., *Lattice-oriented growth of single-walled carbon nanotubes.* Journal of Physical Chemistry B, 2000. **104**: p. 6505-6508.

22. An, L., Owens, J. M., McNeil, L. E., Liu, J., *Synthesis of nearly uniform single-walled carbon nanotubes using identical metal-containing molecular nanoclusters as catalysts.* Journal of the American Chemical Society, 2002. **124**: p. 13688-13689.

23. Cheung, C.L., Kurtz, A., Park, H., Lieber, C. M., *Diameter controlled synthesis of carbon nanotubes.* Journal of Physical Chemistry B, 2002. **106**: p. 2429-2433.

24. Prince, M.R., et al., *Dynamic gadolinimum -enhanced three-dimensional abdominal MR arteriography.* Journal of Magnetic Resonance Imaging, 1993. **3**: p. 877-881.

25. Leung, D.A. and J.F. Debatin, *Three-dimensional contrast enhanced magnetic resonance angiography of the thoracic vasculature.* European Radiology, 1997. **7**: p. 981-989.

26. Schmiedl, U., et al., *Albumen labled with Gd-DTPA as an intravascular, blood pool-enhancing agent for MR imaging studies.* Radiology, 1987. **162**: p. 205-210.

27. Brasch, R.C., *Rationale and applications for macromolecular Gd-based contrast agents.* Magnetic Resonance Medicine, 1991. **22**: p. 282-287.

28. Allkemper, T., et al., *Contrast-enhanced blood-pool MR angiography with optimized iron oxides: effect of size and dose on vascular contrast enhancement in rabbits.* Radiology, 2002. **223**(2): p. 432-438.

29. Edelstein, A.S., Cammarata, R. C., *Nanomaterials: Synthesis, properties, and applications*. 1996, Bristol, UK: Institute of Physics. 566.

30. Yang, C.S., et al., *Nanoparticle-based in vivo investigation on blood-brain barrier permeability following ischemia and reperfusion.* Analytical Chemistry, 2004. **76**: p. 4465-4471.

31. Firth, J.A., *Endothelial barriers: from hypothetical pores to membrane proteins.* Journal of Anatomy, 2002. **200**: p. 541-548.

32. Kereiakes, D.J., et al., *Usefulness of a cobalt chromium coronary stent alloy.* American Journal of Cardiology, 2003. **94**: p. 463-466.

33. Donachie, M., *Biomedical Alloys.* Advanced Materials & Processes, 1998. **154**(1): p. 63-65.

34. Hermanson, G.T., *Bioconjugate Techniques*. 1996, San Diego, CA: Academic.

35. Hayat, M., *Colloidal Gold: Principles, Methods, and Applications*. 1989, San Diego, CA: Academic.

36. Elghanian, R., et al., *Selective colorimetric detection of polynucleotides based on the distance-dependent optical properties of gold nanoparticles.* Science, 1997. **277**: p. 1078-1081.

37. Averitt, R.D., D. Sarkar, and N.J. Halas, *Plasmon resonance shifts of Au-coated Au2S nanoshells: insight into multicomponent nanoparticle growth.* Physical Review Letters, 1997. **78**: p. 4217-4220.

38. Hirsch, L.R., et al. *A rapid whole blood immunoassay using metal nanoshells*. in *Proceedings of the 25th Annual International Conference of IEEE EMBS*. 2003. Cancun, Mexico.

39. Ross, C.A., *Patterned magnetic recording media.* Annual Reviews in Materials Research, 2001. **31**: p. 203-235.

40. Chou, S.Y., *Patterned magnetic nanostructures and quantized data disks.* Proceedings of the IEEE, 1997. **85**: p. 652-671.

41. Ferre, R., et al., *Magnetization Processes in nickel and cobalt electrodeposited nanowires.* Physical Review B, 1997. **56**: p. 14066-14075.

42. Garcia, J.M., et al., *Magnetic behavior of an array of cobalt nanowires.* Journal of Applied Physics, 1999. **85**: p. 5480-5482.

43. Schwarzacher, W., et al., *Metal nanostructures prepared by template electrodeposition.* Journal of Magnetism and Magnetic Materials, 1999. **198**: p. 185-190.

44. Ross, C.A., et al., *Fabrication of patterned media for high density magnetic storage.* Journal of Vacuum Science and Technology B, 1999. **17**: p. 3168.

45. Pignard, S., et al., *Study of the magnetization reversal in individual nickel nanowires.* Journal of Applied Physics, 2000. **87**: p. 824-829.

46. Smyth, J.F., et al., *Hysteresis in lithographic arrays of permalloy particles: Experiment and theory (invited).* Journal of Applied Physics, 1991. **69**: p. 5262-5266.

47. Thielen, M., et al., *Magnetization reversal in nanostructured Co/Pt multilayer dots and films.* IEEE Trans. Magn., 1998. **34**: p. 1009-1011.

48. Cowburn, R.P., *Property variation with with shape in magnetic nanoelement.* Journal of Physics D: Applied Physics, 2000. **33**: p. R1-R16.

49. Evoy, S., et al., *Thickness dependent binary behavior of elongated single-domain cobalt nanostructures.* Journal of Applied Physics, 2000. **87**: p. 404-409.

50. Ross, C.A., et al., *Micromagnetic behavior of conical ferromagnetic particles.* Journal of Applied Physics, 2000. **89**: p. 1310-1319.

51. New, R.M.H., R.F.W. Pease, and R.L. White, *Submicron patterning of thin cobalt films for magnetic patterning.* Journal of Vacuum Science and Technology B, 1994. **12**: p. 3196.

52. Rousseaux, F., et al., *Study of large area high density magnetic dot arrays fabricated using synchrotron radiation based x-ray lithography.* Journal of Vacuum Science and Technology B, 1995. **13**: p. 2787.

53. Wernsdorfer, W., et al., *DC-SQUID magnetization measurements of single magnetic particles.* J. Magn. Magn. Mater., 1995. **145**: p. 33-39.

54. Haginoya, C., et al., *Thermomagnetic writing on 29 Gbit/in.^2 patterned magnetic media.* Applied Physics Letters, 1999. **75**: p. 3159-3161.

55. Walsh, M., et al., *Optimization of a lithographic and ion beam etching process for nanostructuring magnetoresistive thin film stacks.* Journal of Vacuum Science and Technology B, 2000. **18**: p. 3539.

56. Haast, M.A.M., et al., *Reversal mechanism of submicron patterned CoNi/Pt multilayers.* IEEE Trans. Magn., 1998. **34**: p. 1006-1008.

57. Haginoya, C., et al., *Magnetic nanoparticle array with perpendicular crystal magnetic anisotropy.* Journal of Applied Physics, 1999. **85**: p. 8327-8331.

58. Smith, H.I., *100 years of x-rays: Impact on micro- and nanofabrication.* Journal of Vacuum Science and Technology B, 1995. **13**: p. 2323.

59. Wegrowe, J.E., et al., *Arrays of ultrathin monocrystalline submicrometer-sized Fe dots: Néel–Brown relaxation and activation volume.* Journal of Applied Physics, 1999. **86**: p. 1028-1034.

60. Zangari, G. and D.N. Lambeth, *Porous aluminum oxide templates for nanometer-sized cobalt arrays.* IEEE Trans. Magn., 1997. **33**: p. 3010-3012.

61. Metzger, R.M., et al., *Magnetic nanowires in hexagonally ordered pores of alumina.* IEEE Trans. Magn., 2000. **36**: p. 30-35.

62. Bates, F.S., Fredrickson, G. H., *Block copolymer thermodynamics: Theory and experiment.* Annual Review of Physical Chemistry, 1990. **41**: p. 525-557.

63. Park, M., et al., *Block copolymer lithography: Periodic arrays of ~10^{11} holes in 1 square centimeter.* Science, 1997. **276**: p. 1401.

64. Lammertink, R.G.H., et al., *Nanostructured thin films of organic-organometallic block copolymers: one-step lithography with poly(ferrocenylsilanes) by reactive ion etching.* Advanced Materials, 2000. **12**: p. 98-103.

65. Thurn-Albrecht, T., et al., *Ultrahigh-density nanowire arrays grown in self-assembled diblock copolymer templates.* Science, 2000. **290**: p. 2126-2129.

66. Zhu, S., et al., *Microscopic magnetic characterization of submicron cobalt islands prepared using self-assembled polymer masking technique.* IEEE Trans. Magn., 1997. **33**: p. 3022-3024.

67. Sohn, B.H. and R.E. Cohen, *Processable optically transparent block copolymer films containing superparamagnetic iron oxide nanoclusters.* Chemistry of Materials, 1997. **9**: p. 264-269.

68. Schmid, G. and B. Corain, *Synthesis of single-walled carbon nanotubes using binary (Fe, Co, Ni) alloy nanoparticles prepared in situ by the reduction of oxide solid solutions.* Chemical Physics Letters, 2003. **300**(1,2): p. 236-242.

69. Schmid, G. and A. Lehnert, *Complexation of gold colloids.* Angewandte Chemie, 1989. **101**(6): p. 773-774.

70. Weare, W.W., et al., *Improved synthesis of small (dCORE ~ 1.5 nm) phosphine-stabilized gold nanoparticles.* Journal of the American Chemical Society, 2000. **122**(51): p. 12890-12891.

71. Leff, D.V., L. Brandt, and J.R. Heath, *Synthesis and characterization of hydrophobic, organically soluble gold nanocrystals functionalized with primary amines.* Langmuir, 1996. **12**(20): p. 4723-4730.

72. Brust, M., et al., *Langmuir-Blodgett films of alkane chalcogenide (S, Se, Te) stabilized gold nanoparticles.* Nano Letters, 2001. **1**(4): p. 189-191.

73. Yao, H., et al., *Stepwise size-selective extraction of carboxylate-modified gold nanoparticles from an aqueous suspension into toluene with tetraoctylammonium cations.* Chemistry of Materials, 2001. **13**(12): p. 4692-4697.

74. Corbierre, M.K., et al., *Polymer-stabilized gold nanoparticles and their incorporation into polymer matrices.* Journal of the American Chemical Society, 2001. **123**(42): p. 10411-10412.

75. Tan, Y., et al., *Preparation of gold, platinum, palladium and silver nanoparticles by the reduction of their salts with a weak reductant-potassium bitartrate.* Journal of Materials Chemistry, 2003. **13**(5): p. 1069-1075.

76. Heath, J.R., C.M. Knobler, and D.V. Leff, *Pressure/temperature phase diagrams and superlattices of organically functionalized metal nanocrystal monolayers: the influence of particle size, size distribution, and surface passivant.* Journal of Physical Chemistry B, 1997. **101**(2): p. 189-197.

77. He, S., et al., *Formation of silver nanoparticles and self-assembled two-dimensional ordered superlattice.* Langmuir, 2001. **17**(5): p. 1571-1575.

78. Li, X., et al., *Mercaptoacetic acid-capped silver nanoparticle colloids: formation, morphology, and SERS activity.* Langmuir, 2003. **19**(10): p. 4285-4290.

79. Tan, Y., Y. Li, and D. Zhu, *Preparation of silver nanocrystals in the presence of aniline.* Journal of Colloid and Interfacial Sciences, 2003. **258**(2): p. 244-251.

80. Pastoriza-Santos, I. and L.M. Liz-Marzan, *Formation and stabilization of silver nanoparticles through reduction by N,N-dimethylformamide.* Langmuir, 1999. **15**(4): p. 948-951.

81. Sondi, I., D.V. Goia, and E. Matijevic, *Preparation of highly concentrated stable dispersions of uniform silver nanoparticles.* Journal of Colloid and Interface Science, 2003. **260**(1): p. 75-81.

82. Lee, C.L., C.C. Wan, and Y.Y. Wang, *Preparation of highly concentrated stable dispersions of uniform silver nanoparticles.* Advanced Functional Materials, 2001. **11**(5): p. 344-347.

83. Ayyappan, S., et al., *Nanoparticles of Ag, Au, Pd, and Cu produced by alcohol reduction of the salts.* Journal of Materials Research, 1997. **12**(2): p. 398-401.

84. Shen, C.M., et al., *Synthesis and characterization of n-octadecyl mercaptan-protected palladium nanoparticles.* Chemical Physics Letters, 2003. **373**(1,2): p. 39-45.

85. Chen, S., K. Huang, and J.A. Stearns, *Alkanethiolate-protected palladium nanoparticles.* Chemistry of Materials, 2000. **12**(2): p. 540-547.

86. Yee, C., et al., *One-phase synthesis of thiol-functionalized platinum nanoparticles.* Langmuir, 1999. **15**(13): p. 4314-4316.

87. Chen, S. and K. Kimura, *Synthesis of Thiolate-Stabilized Platinum Nanoparticles in Protolytic Solvents as Isolable Colloids.* Journal of Physical Chemistry B, 2001. **105**(23): p. 5397-5403.

88. Perez, H., et al., *Synthesis and characterization of functionalized platinum nanoparticles.* Chemistry of Materials, 1999. **11**(12): p. 3460-3463.

89. Quiros, I., et al., *Preparation of alkanethiolate-protected palladium nanoparticles and their size dependence on synthetic conditions.* Langmuir, 2002. **18**(4): p. 1413-1418.

90. Teranishi, T. and M. Miyake, *Size control of palladium nanoparticles and their crystal structures.* Chemistry of Materials, 1998. **10**(2): p. 594-600.

91. Thomas, P.J., G.U. Kulkarni, and C.N.R. Rao, *An investigation of two-dimensional arrays of thiolized Pd nanocrystals.* Journal of Physical Chemistry B, 2000. **104**(34): p. 8138-8144.

92. Mandal, S., et al., *A new method for the synthesis of hydrophobized, catalytically active Pt nanoparticles.* Chemical Communications, 2002(24): p. 3002-3003.

93. Horswell, S.L., et al., *Alkyl isocyanide-derivatized platinum nanoparticles.* Journal of the American Chemical Society, 1999. **121**(23): p. 5573-5574.

94. Alvarez, J., et al., *Water-soluble platinum and palladium nanoparticles modified with thiolated b-cyclodextrin.* Chemical Communications, 2000(13): p. 1151-1152.

95. Zhu, T., et al., *Surface modification of citrate-reduced colloidal gold nanoparticles with 2-mercaptosuccinic acid.* Langmuir, 2003. **19**(22): p. 9518-9525.

96. Frens, G., *Controlled nucleation for the regulation of the particle size in monodisperse gold suspensions.* Nature, 1973. **241**(105): p. 20-22.

97. Turkevich, J., P.C. Stevenson, and J. Hillier, *The nucleation and growth processes in the synthesis of colloidal gold.* Discussions of the Faraday Society, 1951(11): p. 55-75.

98. Han, M.Y., et al., *A simple and effective chemical route for the preparation of uniform nonaqueous gold colloids.* Chemistry of Materials, 1999. **11**(4): p. 1144-1147.

99. Dai, X.T., Y.; Xu, J., *Formation of Gold Nanoparticles in the Presence of o-Anisidine and the Dependence of the Structure of Poly(o-anisidine) on Synthetic Conditions.* Langmuir, 2002. **18**(23): p. 9010-9016.

100. Sun, S. and C.B. Murray, *Synthesis of monodisperse cobalt nanocrystals and their assembly into magnetic superlattices.* Journal of Applied Physics, 1999. **85**(8, Pt. 2A): p. 4325-4330.

101. Murray, C.B., et al., *Colloidal synthesis of nanocrystals and nanocrystal superlattices.* IBM Journal of Research and Development, 2001. **45**(1): p. 47-56.

102. Puntes, V.F., K.M. Krishnan, and A.P. Alivisatos, *Synthesis, self-assembly, and magnetic behavior of a two-dimensional superlattice of single-crystal -Co nanoparticles.* Applied Physics Letters, 2001. **78**: p. 2187-2189.

103. Suslick, K.S., T. Hyeon, and M. Fang, *Nanostructured materials generated by high-intensity ultrasound: sonochemical synthesis and catalytic studies.* Chemistry of Materials, 1996. **8**(8): p. 2172-2179.

104. Shafi, K.V.P.M., A. Gedanken, and R. Prozorov, *Surfactant-assisted self-organization of cobalt nanoparticles in a magnetic fluid.* Advanced Materials, 1998. **10**(8): p. 590-593.

105. Hyeon, T., et al., *Synthesis of highly crystalline and monodisperse maghemite nanocrystallites without a size-selection process.* Journal of the American Chemical Society, 2001. **123**(51): p. 12798-12801.

106. Lisiecki, I. and M.P. Pileni, *Copper metallic particles synthesized "in situ" in reverse micelles: influence of various parameters on the size of the particles.* Journal of Physical Chemistry B, 1995. **99**(14): p. 5077-5082.

107. Pileni, M.P., *Reverse micelles as microreactors.* Journal of Physical Chemistry, 1993. **97**(27): p. 6961-6973.

108. Lisiecki, I. and M.P. Pileni, *Synthesis of copper metallic clusters using reverse micelles as microreactors.* Journal of the American Chemical Society, 1993. **115**(10): p. 3887-3896.

109. Chen, J.P., et al., *Enhanced magnetization of nanoscale colloidal cobalt particles.* Physical Review B: Condensed Matter, 1995. **51**(17): p. 11527-11532.

110. Chen, J.P., et al., *Magnetic properties of nanophase cobalt particles synthesized in inversed micelles.* Journal of Applied Physics, 1994. **76**(10, Pt. 2): p. 6316-6318.

111. Chen, J.P., et al., *Magnetic properties of microemulsion synthesized cobalt fine particles.* Journal of Applied Physics, 1994. **75**(10, Pt. 2A): p. 5876-5878.

112. Akthakul, A., Hochbaum, A. I., Stellacci, F, Mayes, A. M., *Size fractionation of metal nanoparticles by membrane filtration.* Advanced Materials, 2005. **17**(5): p. 532-535.

113. Schaff, G.T., Knight, G., Shafigullin, Khoury, J. T., Vezmar, R. L., Whetten, R. L., Cullen, W. G., First, P. N., *Isolation of smaller nanocrystal Au molecules: robust quantum effects in optical spectra.* Journal of Physical Chemistry B, 1997. **101**: p. 7885-7891.

114. Hicks, J.F., Templeton, A. C., Chen, S., Sheran, K. M., Jasti, R., Murray, R. W., *The monolayer thickness dependence of quantized double-layer capacitances of monolayer-protected gold clusters.* Analytical Chemistry, 1999. **71**: p. 3703-3711.

115. Whetten, R.L., et al., *Nanocrystal gold molecules.* Advanced Materials, 1996. **8**: p. 428-433.

116. Novak, J.P., Nickerson, C., Franzen, S., Feldheim, D. L., *Purification of molecularly bridged metal nanoparticle arrays centrifugation and size exclusion chromatography.* Analytical Chemistry, 2001. **73**: p. 5758-5761.

117. Jiminez, V.J., Loepold, M. C., Mazzitelli, C., Jorgenson, J. W., Murray, R. W., *HPLC of monolayer-protected gold nanoclusters.* Analytical Chemistry, 2003. **75**: p. 199-206.

118. Chen, S., Murray, R. W., Felgberg, S. W., *Quantized capacitance charging of monolayer-protected Au clusters.* Journal of Physical Chemistry B, 1998. **102**: p. 9898-9907.

119. Wilcoxson, J.P., Martin, J. E., Provencio, P., *Size distributions of gold nanoclusters studied by liquid chromatography.* Langmuir, 2000. **16**: p. 9912-9920.

120. Schaff, G.T., Knight, G., Shafigullin, M. N., Borkman, R. F., Whetten, R. L., *Isolation and selected properties of a 10.4 kDa gold:glutathione cluster compound.* Journal of Physical Chemistry B, 1998. **102**(52): p. 10643-10646.

121. Luckham, P.F., Ukeje, M. A., *Effect of particle size distribution on the rheology of dispersed systems.* Journal of Colloid and Interface Science, 1999. **220**: p. 347-356.

122. Lenggoro, I.W., Xia, B., Okuyama, K., *Sizing of colloidal nanoparticles by electrospray and differential mobility analyzer methods.* Langmuir, 2002. **18**: p. 4584-4591.

123. Hammouda, A., Gulik, Th., Pileni, M. P., *Synthesis of nanosize latexes by reverse micelle polymerization.* Langmuir, 1995. **11**: p. 3656-3659.

124. Qi, Z.-M., et al., *Characterization of gold nanoparticles synthesized using sucrose by seeding formation in the solid phase and seeding growth in aqueous solution.* Journal of Physical Chemistry B, 2004. **108**: p. 7006-7011.

125. Chu, B., Liu, T., *Characterization of nanoparticles by scattering techniques.* Journal of Nanoparticle Research, 2000. **2**: p. 29-41.

126. Bao, C., et al., *Preparation of Au nanoparticles in the presence of low generational polt(amidoamine) dendrimer with surface hydroxyl groups.* Materials Chemistry and Physics, 2003. **81**: p. 160-165.

127. Bao, C., et al., *Hyperbranched poly(amine-ester) templates for the synthesis of Au nanoparticles.* Materials Chemistry and Physics, 2003. **82**: p. 812-817.

128. Bogatyrev, V.A., Dykman, L. A., Khlebtsov, B. N., Khlebtsov, N., G., *Measurement of mean size and evaluation of polydispersity of gold nanoparticles from spectra of optical absorption and scattering.* Optics and Spectroscopy, 2004. **96**: p. 128-135.

129. Cecere, D., Bruno, A., Minutolo, P., D'Alessio, A., *DLS measurements on nanoparticles produced in laminar premixed flames.* Synthetic Metals, 2003. **139**: p. 653-656.

130. Egorove, E.M., Revina, A. A., *Optical properties and sizes of silver nanoparticles in micellar solutions.* Colloid Journal, 2002. **64**: p. 334-345.

131. Wilcoxson, J.P., Williamson, R. L., Baughman, R., *Optical properties of gold colloids formed in inverse micelles.* Journal of Chemical Physics, 1993. **98**(12): p. 9933-9950.

132. Grabar, K.C., et al, *Nanoscale characterization of gold colloid monalayers: a comparison of four techniques.* Analytical Chemistry, 1997. **69**: p. 471-477.

133. Carrot, G., et al, *Gold nanoparticle synthesis in graft copolymer micelles.* Colloid and polymer science, 1998. **276**: p. 853-859.

134. Petit, C., Taleb, A., Pileni, M. P., *Cobalt nanosized particles organized in a 2D superlattice: synthesis, characterization, and magnetic properties.* Journal of Physical Chemistry B, 1999. **103**: p. 1805-1810.

135. Chen, S., Kimura, K., *Synthesis and characterization of carboxylate-modified gold nanoparticle powders dispersible in water.* Langmuir, 1999. **15**: p. 1075-1082.

136. Buffat, P.A., *Electron diffraction and HRTEM studies of multiply-twinned structures and dynamical events in metal nanoparticles: facts and artifacts.* Materials Chemistry and Physics, 2003. **81**: p. 368-375.

137. Sangregorio, C., Galeotti, M., Bardi, U., Baglioni, P., *Synthesis of Cu_3Au nanocluster alloy in reverse micelles.* Langmuir, 1996. **12**: p. 5800-5802.

138. Arcoleo, V., Liveri, V. T., *AFM investigation of gold nanoparticles synthesized in water/AOT/n-heptane microemulsions.* Chemical Physics Letters, 1996. **258**: p. 223-227.

139. Narita, T., et al., *Preparation and characterization of core-shell nanoparticles hardened by gamma-ray.* Colloids and Surfaces B: Biointerfaces, 2004. **38**: p. 187-190.

140. Pecora, R., *Dynamic light scattering: Applications of photon correlation spectroscopy*. 1985, New York: Plenum Press. 420.

141. West, A.R., *Solid state chemistry and its applications*. 1984, New York: John Wiley and Sons.

142. Rosen, M., J, *Surfactants and Interfacial Phenomena*. 2nd ed. 1989, Ney York: John Wiley and Sons. 431.

143. Pileni, M.P., ed. *Structure and Reactivity in Reverse Micelles*. Studies in Physical and Theoretical Chemistry. Vol. 65. 1989, Elsevier: New York. 379.

144. Olla, M., Monduzzi, M., Ambrosone, L., *Microemulsions and emulsions in DDAB/W/oil systems.* Colloids and Surfaces A: Physiochemical and Engineering Aspects, 1999. **160**: p. 23-36.

145. Pileni, M.P., *Reverse micelles as microreactors.* Journal of Physical Chemistry, 1993. **97**: p. 6961-6973.

146. Evans, D.F., Mitchell, D. J., Ninham, B. W., *Oil, water, and surfactant: propreties and conjectured structure of simple microemulsions.* Journal of Physical Chemistry, 1986. **90**: p. 2817-2825.

147. Chen, S.J., Evans, D. F., Ninham, B. W., Mitchell, D. J., Blum, F. D., Pickup, S., *Curvature as a determinant of microstructure and microemulsions.* Journal of Physical Chemistry, 1986. **90**: p. 842-847.

148. Leung, R., Shah, D. O., *Solubilization and phase equilibria in water-in-oil microemulsions I. Effects of spontaneous curvature and elasticity of interfacial films.* Journal of Colloid and Interface Science, 1987. **120**: p. 320-329.

149. Safran, S.A., Turkevich, L. A., *Phase diagrams for microemulsions.* Physical Review Letters, 1983. **50**: p. 1930-1939.

150. Pileni, M.P., *Nanosized particles made in colloidal assemblies.* Langmuir, 1997. **13**: p. 3266.

151. Pileni, M.P., *Fabrication and properties of nanosized materials made by using colloidal assemblies as templates.* Crystal Research and Technology, 1998. **33**: p. 1155-1186.

152. Young, R.S., *Cobalt: its chemistry, metalurgy, and uses*. 1960, New York: Reinhold Publishing Corporation.

153. Bailar, J.C., Emeleus, H. J., Nyholm, R., Trotman-Dickenson, A. F., ed. *Comprehensive Inorganic Chemistry*. Vol. 3. 1973. 1387.

154. Verbeeck, A., Voortmans, G.,Jackers, C., De Schryver, F. C., *Characterization and stabilization of inverse micelles.* Langmuir, 1989. **5**: p. 766-776.

155. Trantler, R.L., *Design and Analysis in Chemical Research*. 1999, Boca Raton, FL: CRC Press. 558.

156. Del Vecchio, R.J., *Understanding Design of Experiments*. 1997, Cincinnati, OH: Hanser/Gardner Publications, Inc.

157. Davies, L., *Efficiency in Research, Development, and Production: The Statistical Design of Chemical Experiments*. 1993, Cambridge: The Royal Society of Chemistry. 180.

158. Anderson, R.L., *Practical Statistics for Analytical Chemists*. 1987, New York: Van Nostrand Reinhold Co. 316.

APPENDIX

A.1. Significance Test: No NaOH

The GLM Procedure

Class Level Information

Class	Levels	Values			
LOGDIAM	423				
-0.578034373	-0.435408984	-0.432322562	-0.429245637	-0.427710717	
-0.417031744	-0.295714244	-0.294371061	-0.291690094	-0.289016295	
-0.285018955	-0.283690051	-0.262664309	-0.175544573	-0.169602784	
-0.166054584	-0.16134315	-0.157824085	-0.151986357	-0.077961541	
-0.074723546	-0.071496002	-0.070422464	-0.069350078	-0.066139803	
-0.065071997	-0.06400533	-0.0629398	-0.060812139	-0.056570351	
-0.054456186	-0.050241216	-0.048140375	-0.046043939	-0.004008021	
0.0207825392	0.0217614918	0.022739487	0.0256677467	0.027615167	
0.0285874569	0.0295588022	0.030529205	0.0344014267	0.0363319292	
0.0372957847	0.0440168854	0.0459289319	0.0573250666	0.0713899961	
0.0843411484	0.0907543633	0.1034587084	0.1079571415	0.1106465201	
0.1115413747	0.1133286853	0.1160036758	0.1168937515	0.1186715297	
0.1213322852	0.124868982	0.1292723357	0.1484200051	0.1663615372	
0.1722712209	0.1781461854	0.1839868361	0.1864795669	0.1897935716	
0.1906203596	0.1914464646	0.19309663	0.1939206926	0.1955667835	
0.1972101693	0.2004888607	0.2013068567	0.2070141694	0.2086388651	
0.2126890934	0.2134971743	0.2151113796	0.2255406759	0.2303177551	
0.231905057	0.2468600779	0.2523139286	0.2569650998	0.2577381961	
0.2631331995	0.2639015438	0.2646692981	0.2677344346	0.268499253	
0.2783890255	0.2799018851	0.2836740511	0.2866815721	0.2911759617	
0.292669614	0.2956502421	0.3111544286	0.3169981268	0.3199072197	
0.3285840638	0.3321773123	0.3336110043	0.3371862674	0.3378997886	
0.3386128011	0.3400373028	0.3471295311	0.3499523982	0.3506568716	
0.353469813	0.354873322	0.3562748639	0.3597701488	0.3611648492	
0.3625576071	0.3632532593	0.3722529739	0.3770656336	0.3832194992	
0.3866220203	0.3913661837	0.3994470358	0.4007875186	0.4027948796	
0.4061315527	0.4107842696	0.4134332778	0.414755155	0.4167347004	
0.4226499329	0.4369637752	0.4434029474	0.452348694	0.4542552723	
0.4548899914	0.4561582224	0.4700036292	0.476234179	0.4768551042	
0.4774756441	0.4780957991	0.4811908186	0.4836599557	0.4922542382	
0.4928652984	0.5007752879	0.5050087384	0.5199835616	0.5353230954	
0.5376622777	0.5382462193	0.5388298202	0.5399960011	0.5405785819	
0.5504308784	0.5636078092	0.5664495275	0.587230955	0.5944312076	
0.5993858007	0.603222473	0.6070444815	0.6216511789	0.6259384309	
0.6349882664	0.6476266653	0.6486726905	0.6559643894	0.6637183699	
0.6906440503	0.6926470555	0.6966410698	0.7030975114	0.7100042976	

0.7134398838 0.7202758479 0.7294791098 0.7309245449 0.7357276281
0.73620667 0.737164066 0.7645371766 0.7677907236 0.777488329
0.7816158285 0.797056644 0.8002062529 0.8095959932 0.8285518176
0.8346467428 0.8462973601 0.8637334811 0.8645762962 0.8742179555
0.8829407522 0.903408106 0.9094675065 0.9146894505 0.9174900124
0.9620286235 0.9673640021 0.9775739603 0.9809542452 0.9861898593
0.9943622673 1.0126912262 1.0469680555 1.05535678 1.0763666797
1.0797692009 1.0818051704 1.0919233005 1.1102114245 1.11317244
1.1223288153 1.1271997455 1.1384738221 1.1451777578 1.1477198628
1.1521530556 1.1543623038 1.1575099299 1.1844841277 1.198155919
1.2017703808 1.2068686074 1.2278846244 1.2564703733 1.2627132993
1.2725655958 1.2764794951 1.2806560291 1.2845384522 1.285644953
1.2963696536 1.3007364728 1.305897424 1.3137236683 1.3365787689
1.3436477864 1.3470336472 1.3643043432 1.3782621894 1.4090338481
1.4238309646 1.4255150743 1.4298326631 1.4305504524 1.4372250898
1.4541866272 1.461865548 1.4681047363 1.4888509494

The GLM Procedure

1.5091754905 1.5208252541 1.5214806337 1.5216989981 1.5295285292
1.5325568681 1.5671565202 1.5804209634 1.5835045304 1.5898472627
1.600800719 1.6221566848 1.6235380368 1.6245235499 1.6249174833
1.6294365989 1.6323728837 1.6360798434 1.6524974019 1.6582280766
1.6620303626 1.6692151165 1.6739139316 1.6754129014 1.6791505248
1.6863989536 1.6952485688 1.6954321056 1.7065646232 1.710368631
1.7121749899 1.7134375025 1.7188302892 1.7208003803 1.7222307399
1.725085336 1.7277541393 1.7282870463 1.7332471982 1.7415182528
1.7448425494 1.74606451 1.7547496436 1.7549225792 1.7631885122
1.7649020151 1.7890892407 1.7909257885 1.7934247485 1.7942563494
1.798735083 1.801214628 1.805004696 1.8074687629 1.8081248233
1.8248718207 1.8295368336 1.8380067204 1.8394379045 1.8397556675
1.8457740575 1.851913392 1.8561417282 1.8586389981 1.8587948706
1.8592623423 1.8657841046 1.8693376039 1.8702625307 1.8704166021
1.8747209899 1.8797703466 1.8826660279 1.8864634047 1.8962696234
1.9001653431 1.907763145 1.9150090177 1.9167755425 1.9180983913
1.9182452665 1.928327912 1.93629262 1.9419021277 1.9474803442
1.9504711604 1.9517502055 1.9574151407 1.9627672661 1.9637500672
1.9724129689 1.9746364273 1.9772703791 1.9923847091 1.9944281674
1.9985025992 2.002965383 2.0434256875 2.0645816788 2.0647085421
2.0716613544 2.0731719287 2.0846778085 2.0978952203 2.1014476219
2.1020588315 2.104378027 2.1058400155 2.1068134885 2.1081504683
2.1227404661 2.1418293141 2.1432375998 2.1438238006 2.1488509931
2.1543170763 2.154433052 2.1795130954 2.1857141413 2.1931049924
2.2173539486 2.223325412 2.2387929599 2.2420917126 2.2452737263
2.2483400781 2.2637403092 2.2674759159 2.2695452389 2.2708880063
2.2844211224 2.2880804068 2.2893985312 2.302485088 2.3083683377
2.3303947936 2.3342775397 2.3351490839 2.3600989992 2.3620796648
2.3829662049 2.4028828143 2.4080256055 2.4083855119 2.4097340085
2.422055593 2.4344025176 2.4473778379 2.4567643438 2.4758659051
2.4773783834 2.5089486443 2.5156783085 2.5534216293 2.5830914817
2.5881399044 2.589416804 2.5912916405 2.6433338864 2.6965172853
2.7707745777 2.7747114676 2.8405393841 2.8745246306

SOL 4 1 2 3 4
Number of Observations Read 481

Number of Observations Used 481

0

The SAS System 02:57 Monday, June 6, 20053

The GLM Procedure

Dependent Variable: LOGDIAM

Source	OF	Sum of Squares	Mean Square	F Value	Pr > F
Model	3	243.0936160	81.0312053	378.78	<.0001
Error	477	102.0425291	0.2139256		
Corrected Total		480 345.1361450			

R-Square	Coeff Var	Root MSE	LOGDIAM Mean
0.704341	46.59430	0.462521	0.992656

Source	DF	Type I SS	Mean Square	F Value	Pr > F
SOL	3	243.0936160	81.0312053	378.78	<.0001

Source	DF	Type III SS	Mean Square	F Value	Pr > F
SOL	3	243.0936160	81.0312053	378.78	<.0001

The SAS System 02:57 Monday, June 6, 2005 4

The GLM Procedure

t Tests (LSD) for LOGDIAM

NOTE: This test controls the Type I comparisonwise error rate,
not the experimentwise error rate.

Alpha 0.05
Error Degrees of Freedom 477
Error Mean Square 0.213926
Critical Value of t 1.96495

Comparisons significant at the 0.05 level are indicated by***

SOL Comparison	Difference Between Means	95% Confidence Limits		
4 -3	0.61401	0.41811	0.80990	***
4 -2	1.48781	1.29475	1.68088	***
4 -1	2.19855	2.00788	2.38923	***
3 -4	-0.61401	-0.80990	-0.41811	***
3 -2	0.87381	0.76374	0.98387	***
3 -1	1.58455	1.47873	1.69036	***
2 -4	-1.48781	-1.68088	-1.29475	***
2 -3	-0.87381	-0.98387	-0.76374	***
2 -1	0.71074	0.61026	0.81121	***
1 -4	-2.19855	-2.38923	-2.00788	***
1 -3	-1.58455	-1.69036	-1.47873	***
1 -2	-0.71074	-0.81121	-0.61026	***

A.2. Significance Test: With Naoh

The SAS System 03:10 Monday, June 6, 2005 1
The GLM Procedure

Class Level Information

Class	Levels	Values
SOL	3	1 2 3
CONC	3	3.1 3.25 3.3

The SAS System 03:10 Monday, June 6, 2005 2

The GLM Procedure

Class Level Information

Class	Levels	Values
LOGDIAM	1083	

-1.087672349	-0.834710745	-0.823255866	-0.791863153	-0.597837001
-0.576253429	-0.569161201	-0.560366069	-0.495937011	-0.484508315
-0.479650006	-0.465215113	-0.458865885	-0.457284857	-0.441610555
-0.427710717	-0.412489723	-0.407968238	-0.393042588	-0.391562203
-0.387134151	-0.376877651	-0.372514008	-0.371063681	-0.338273859
-0.33128571	-0.328504067	-0.327116142	-0.32573014	-0.318828801
-0.303811454	-0.291690094	-0.282362911	-0.278392026	-0.265268478
-0.262664309	-0.258770729	-0.25747623	-0.253602759	-0.248461359
-0.247180129	-0.235722334	-0.224394333	-0.219400565	-0.214431611
-0.210721031	-0.196014884	-0.192371893	-0.180323554	-0.175544573
-0.168418652	-0.162518929	-0.15082289	-0.136965855	-0.131248287
-0.122167634	-0.119910297	-0.100925919	-0.089924708	-0.088831214
-0.086647807	-0.080126044	-0.075801713	-0.070422464	-0.06720875
-0.066139803	-0.06400533	-0.061875404	-0.060812139	-0.056570351
-0.05551271	-0.034591445	-0.032523192	-0.025317808	-0.015113638
-0.011060947	-0.010050336	-0.003004509	0.0009995003	0.0019980027
0.0049875415	0.0079681696	0.01093994	0.0119285709	0.0139029052
0.0178399181	0.0285874569	0.0295588022	0.0363319292	0.0372957847
0.0382587121	0.0392207132	0.0430594895	0.0449733656	0.0468835859
0.0497420919	0.0544881853	0.0573250666	0.0648509723	0.0732504617
0.0751074725	0.0861776962	0.0916671885	0.099845335	0.1052605107
0.1079571415	0.1186715297	0.1213322852	0.1231021971	0.1239859798
0.1257512053	0.1371498381	0.1388919989	0.1406311297	0.1423672413
0.1432341681	0.1501426584	0.1638180852	0.1663615372	0.1688985365
0.1722712209	0.1747932904	0.1756325686	0.177309015	0.1781461854
0.1831545431	0.1839868361	0.1881379421	0.1897935716	0.1906203596
0.196388814	0.1980308505	0.1996701951	0.2021241841	0.202940844
0.2037568375	0.2045721657	0.2110709701	0.2126890934	0.2134971743
0.2167229835	0.2175278125	0.2183319943	0.2199384204	0.2382291887
0.2390169005	0.245296356	0.2476410229	0.2507587183	0.2515366258
0.253866724	0.2561914054	0.2569650998	0.2592825979	0.2608246183
0.2639015438	0.2662030408	0.2669690309	0.2677344346	0.268499253
0.2707902048	0.2723145953	0.2799018851	0.2836740511	0.2866815721
0.2874320412	0.2889312919	0.2904282981	0.2919230667	0.2971372312
0.2986220125	0.3060130291	0.3067491352	0.3133498192	0.3184537311
0.3199072197	0.3206331726	0.3220834992	0.3228078744	0.3235317253
0.3300229129	0.3343270803	0.3364722366	0.3378997886	0.3393253056
0.3407487934	0.3421702577	0.3435897044	0.3457151037	0.3471295311

0.3485419607 0.3492474281 0.3499523982 0.3506568716 0.3513608491
0.3520643314 0.354873322 0.3569748989 0.3604677422 0.3660310389
0.3674170405 0.370183294 0.3729419164 0.3777512695 0.3791211328
0.3825376035 0.3839009302 0.3859424416 0.3866220203 0.3893357262
0.3906898225 0.3913661837 0.3940670632 0.3947411447 0.3974329364
0.4021262068 0.4027948796 0.4041308851 0.4061315527 0.4067975533
0.4081282255 0.4087928982 0.4107842696 0.415415439 0.4167347004
0.4187103349 0.4200252594 0.4246139269 0.4259211167 0.4265740713
0.4298324646 0.4317824164 0.4324315563 0.4330802751 0.4350239103
0.4356709502 0.4363175716 0.4369637752 0.4414755456 0.4459670514
0.447885824 0.4491629634 0.4504384738 0.4517123593 0.4548899914
0.4567917353 0.4586898693 0.4593217809 0.4605844073 0.4612151232
0.4656190309

The GLM Procedure

0.4681268692 0.4700036292 0.4725005094 0.4737466155 0.4774756441
0.4818086747 0.4842762885 0.4855078158 0.4861230111 0.4879663296
0.4891933236 0.4898062565 0.4910309964 0.4928652984 0.4934759854
0.4946962418 0.4965238391 0.4971322966 0.4977403842 0.4983481023
0.4989554512 0.5001690436 0.5007752879 0.5013811649 0.5019866751
0.5031965966 0.5038010088 0.5050087384 0.5074198306 0.5080216964
0.5092243424 0.5104255437 0.5122246447 0.5134222496 0.5152159721
0.5158131653 0.5164100021 0.517602608 0.5193888544 0.5199835616
0.5205779152 0.5211719158 0.5217655638 0.5229518036 0.5276827408
0.5306282511 0.5318040302 0.5323914017 0.5329784284 0.5335651107
0.5364933705 0.5370779949 0.5376622777 0.5394130806 0.5399960011
0.5405785819 0.5411608236 0.5429055172 0.5440669575 0.5452270505
0.5463857992 0.5481214085 0.5492768101 0.5498540107 0.5510074134
0.5521594873 0.5544596608 0.5556077665 0.5573274574 0.559044196
0.5596157879 0.5601870533 0.5613286059 0.5692831933 0.5704144152
0.5709795466 0.5715443588 0.5721088522 0.5749265492 0.5760514087
0.5771750043 0.577736329 0.5782973389 0.5794184152 0.5799784825
0.5810976768 0.5816568045 0.5844477636 0.5877866649 0.5905605918
0.5927742064 0.5944312076 0.5949829318 0.5960854677 0.5966362802
0.5982868995 0.5993858007 0.6004834957 0.6043159669 0.6048622657
0.6054082663 0.6081338062 0.6130211361 0.6135627012 0.6141039732
0.6146449524 0.6195006404 0.6200387087 0.6227247163 0.6232610531
0.6248683398 0.6286086594 0.6302073808 0.6318035503 0.6397464038
0.6413274318 0.6418538862 0.6465795447 0.6481498146 0.649195293
0.6497176226 0.6502396795 0.6507614641 0.652325186 0.6528458838
0.6538864666 0.6554453134 0.6564831962 0.6580380034 0.6585557358
0.6590732002 0.6611403844 0.6616565135 0.664747706 0.6652619771
0.6657759838 0.6662897264 0.6678293726 0.668854488 0.6698785536
0.6709015716 0.6714126884 0.6729444732 0.6754922453 0.6770177986
0.6775257997 0.6805683984 0.6820862332 0.6841064359 0.6851150089
0.6866259636 0.6881346387 0.6891391592 0.6896410412 0.6906440503
0.6911451779 0.6921466802 0.6931471806 0.6941466809 0.6946460567
0.6966410698 0.6971392018 0.6986321108 0.6991292522 0.7011153502
0.701611259 0.7021069219 0.7035924384 0.7045815582 0.7050757514
0.7060634058 0.7085282826 0.7104958189 0.7119689348 0.7124594916
0.7144193158 0.7149086723 0.7153977895 0.7173518693 0.719302138
0.7256143707 0.7260982807 0.7265819566 0.7270653988 0.7280315824
0.7328485474 0.7333289702 0.7347688553 0.7352483566 0.7357276281
0.7366854826 0.7376424204 0.7400307665 0.7419373447 0.7433648967

0.7457396307 0.7476353658 0.7481087386 0.7485818874 0.749527514
0.7509442793 0.7514160887 0.7523590402 0.7528301827 0.7565913531
0.7589349211 0.7603384301 0.760805829 0.7622067165 0.7631395524
0.7654678421 0.7668622184 0.7687183674 0.7701082217 0.7710337192
0.771496147 0.7742662318 0.7770286645 0.777488329 0.778866056
0.7811580579 0.7829878846 0.7839015438 0.7843580606 0.7852704694
0.7870927934 0.787547856 0.7898200678 0.7911809208 0.7916341273
0.7920871284 0.7934449019 0.7938970837 0.7943490611 0.7948008343
0.7952524035 0.797056644 0.7975071959 0.7997569156 0.8020015855
0.8037937006 0.8046885553 0.8060293376 0.8064758659 0.8069221948
0.810485673 0.8127064156 0.8149222375 0.8184573715 0.8193392058
0.8202202631 0.8211005449 0.8228587871 0.8237367503 0.824175443
0.8246139433 0.8250522514 0.8254903675 0.8259282918 0.8285518176
0.8289884035 0.8294247989 0.8298610039 0.8316039237 0.8320391794
0.8324742458 0.8333438111 0.8372475245 0.8381129508 0.8394096875
0.8398415597

The GLM Procedure

0.8407047449 0.8428594538 0.8441500541 0.8475835339 0.8480118911
0.8488680556 0.8497234876 0.8501509294 0.8510052652 0.8548407696
0.85526603 0.8590852581 0.8599319982 0.8603550995 0.8612007656
0.8616233305 0.8624679252 0.8628899551 0.8637334811 0.8671004877
0.8683601981 0.8687797492 0.8708748683 0.8712933659 0.8721298361
0.8725478089 0.8729656071 0.8733832309 0.8746350566 0.8763017237
0.8783811588 0.8792117236 0.8804562789 0.8808707866 0.8812851227
0.8821132801 0.8837675402 0.8854190682 0.88747965 0.8878912574
0.8883026953 0.8911780311 0.8936360413 0.8948627845 0.8960880246
0.8964961045 0.8973117653 0.8985340103 0.8993480111 0.9005677714
0.9017860457 0.9021918075 0.9066443548 0.9074517832 0.9086617047
0.9126842363 0.9134868045 0.9162907319 0.9190868192 0.9222728036
0.9230677162 0.9254486697 0.9258449447 0.9262410627 0.9282193027
0.9290095043 0.9297990819 0.9309822806 0.9313763693 0.9337376455
0.934916196 0.9353087377 0.9360933592 0.9380522237 0.9392257032
0.9400072585 0.9415685391 0.9427379019 0.9431273858 0.9458495341
0.9474017269 0.9501122803 0.9512717008 0.9516578757 0.9524297785
0.955511445 0.9570487243 0.958200135 0.9593502213 0.9597332897
0.9608816152 0.9616464336 0.9624106675 0.9631743178 0.968883182
0.9696419074 0.9704000575 0.972292922 0.9730490657 0.9738046381
0.978701992 0.97907772 0.9809542452 0.9813291281 0.9817038704
0.9828272557 0.9861898593 0.9873082191 0.987680728 0.9895411936
0.9902844118 0.9906558138 0.991027078 0.992881334 0.9936220748
0.9962103551 0.9965795631 0.9984235614 0.9991602097 0.9998963157
1.0024684281 1.0028353333 1.0032021039 1.0050339417 1.0053999069
1.0057657383 1.0061314359 1.0068624301 1.0072277269 1.0075928903
1.0079579204 1.009781075 1.0101453073 1.0112372092 1.0119644819
1.0123279201 1.0155929329 1.017040635 1.0174022332 1.0184862442
1.0195690813 1.0210110426 1.0228105753 1.0231700935 1.0235294825
1.0242478734 1.0246068754 1.0253244929 1.0267581849 1.027116287
1.0292622105 1.0299764963 1.0301192922 1.0317599817 1.0349622616
1.0353174383 1.0363822121 1.0385083646 1.0413362208 1.0416891413
1.0430995787 1.0452115119 1.0483710722 1.0490718431 1.0501220795
1.0504719133 1.0508216248 1.0532661869 1.05535678 1.0557047877
1.0570956085 1.0581374561 1.0588314187 1.062985111 1.0643658499
1.064710737 1.069183478 1.0712410919 1.0719260234 1.0729525419

1.0732944807 1.0773886522 1.0787496596 1.0807877038 1.0818051704
1.0868770324 1.0872142437 1.0892351269 1.089571544 1.090580117
1.0932646823 1.0946042673 1.0959420601 1.0972780657 1.0989455665
1.1006102913 1.100942904 1.1012754061 1.1019400788 1.1045943603
1.1059188639 1.10757203 1.1085626195 1.1102114245 1.1115285139
1.1121864087 1.1141575 1.1154694057 1.1161247138 1.1164522068
1.1167795926 1.1177611075 1.11874166 1.1213517756 1.1255787369
1.1262274557 1.1265516574 1.1291414937 1.1323693855 1.1352656063
1.1362291522 1.136550128 1.1381534633 1.1384738221 1.139114232
1.1400740785 1.1403938227 1.1407134647 1.1416717781 1.1439042779
1.1454958746 1.1467673306 1.148988496 1.1512047388 1.1549926221
1.1568811968 1.1600209168 1.1612740498 1.1615870878 1.1637756146
1.1640878706 1.1672050801 1.1687600486 1.1721724918 1.1789626413
1.1795776475 1.1826470176 1.1878434224 1.188148254 1.1893666519
1.1899752947 1.1902794772 1.192406168 1.1933162241 1.1954364733
1.1963437772 1.1972502586 1.1987592373 1.1996635327 1.2002659424
1.201168877 1.2014696741 1.2074666936 1.2092588088 1.2095571826
1.2143190964 1.2190584417 1.2193539064 1.2214197179 1.2225982684
1.2237754316 1.2249512107 1.2340169257 1.234889907 1.2360526978
1.2372141381 1.238084334 1.2386640441 1.2398224572 1.2412685891
1.244154594

The GLM Procedure

1.2447307968 1.248181059 1.2581768583 1.2627132993 1.2644091731
1.268917493 1.2703221849 1.2725655958 1.273125663 1.2739651761
1.2742448573 1.2745244603 1.2748039851 1.2809338455 1.285644953
1.2867502308 1.2881301123 1.2892326483 1.2897834607 1.290609111
1.291159166 1.2919836816 1.2930819794 1.2933563655 1.2963696536
1.2974631474 1.2982824838 1.2993738891 1.3031844544 1.3039991184
1.3088732142 1.3091433019 1.3096832587 1.3121094629 1.3129168913
1.3156036205 1.3180155204 1.3209555198 1.3268097143 1.3273402183
1.3286652483 1.3291947691 1.3297240096 1.3305173457 1.3323660191
1.3339478807 1.3350010667 1.3386785072 1.3394647738 1.3397267253
1.3407738458 1.3423424736 1.3454723666 1.3457327494 1.3509262173
1.351961682 1.3537711694 1.3545456628 1.3568655504 1.3591800686
1.3614892422 1.3711807233 1.3739687114 1.3752334138 1.3795214768
1.3855440797 1.3932699749 1.3994573476 1.399704048 1.4038886695
1.4043798287 1.4051161154 1.4075664964 1.4117184135 1.4124493186
1.412692835 1.4141526892 1.4146388341 1.4190035355 1.4243124283
1.4264761508 1.4276761989 1.4303112465 1.431984487 1.4346082214
1.4365120773 1.4379375943 1.4388868112 1.4426746946 1.4433833281
1.4436194277 1.4473894605 1.4487995665 1.4504421809 1.4523161567
1.4537193374 1.4553538971 1.4569857892 1.4572186995 1.4620973245
1.463023894 1.4653365685 1.469485952 1.4699459336 1.4761350651
1.4811498921 1.4822861268 1.4836479064 1.485687105 1.4926793518
1.4933534334 1.4962692143 1.4989531793 1.5014071682 1.5040773968
1.5047438413 1.5056317437 1.5149074286 1.5166645123 1.5203880956
1.524315659 1.5271426697 1.5273598014 1.5277939234 1.5297451435
1.5340676054 1.5411590717 1.5432981099 1.5456457793 1.5494755713
1.5505368045 1.5507489161 1.5515969127 1.5522324387 1.5545592509
1.5612975371 1.5619269298 1.5623463049 1.5631845279 1.564858869
1.5721513276 1.5733961411 1.5765014122 1.5824777309 1.5841201044
1.5890311027 1.5918847532 1.5947302836 1.5979724343 1.599185536
1.6074359098 1.6082371919 1.6092378924 1.6110366338 1.6170091779

1.6195862435 1.6205756568 1.6237352171 1.6241294612 1.6294365989
1.633740205 1.6370530795 1.6382197139 1.6397731122 1.6409365795
1.6415178059 1.6422922493 1.6453840392 1.6476966246 1.6547936142
1.6718491726 1.6720370542 1.6729759332 1.6735388378 1.675225653
1.6754129014 1.6878793387 1.6904647511 1.6961659159 1.6983641216
1.7029282555 1.7056567702 1.7083778603 1.7137979278 1.7190095489
1.7240158171 1.7293520091 1.7381828683 1.7404661748 1.7469364256
1.7504165057 1.7654154939 1.7671251883 1.7798555647 1.7965811595
1.8045111532 1.8051691561 1.8054979953 1.8154759958 1.8179144267
1.8190503295 1.8221270058 1.8226119327 1.8229350867 1.8256776874
1.829055254 1.8314608361 1.8327414509 1.8386430551 1.8394379045
1.8399145111 1.8445100346 1.8446681249 1.8500283774 1.8515994696
1.8562979904 1.8609745382 1.8751810774 1.8767131751 1.8768662559
1.8808381523 1.8929613497 1.8941656251 1.8985190058 1.9025551874
1.90434383 1.9050881545 1.9055344835 1.9068722763 1.9073178099
1.9148616664 1.9252700283 1.9290546034 1.9344157696 1.9410411719
1.9434786239 1.9437649927 1.9469096494 1.9477655696 1.9507555341
1.9589673882 1.9661328562 2.0031003084 2.0070052484 2.015036345
2.0377076732 2.0380985781 2.0440733978 2.04691835 2.0588561081
2.0594939039 2.0786912603 2.0836825359 2.0926045282 2.1085147892
2.1379462711 2.158483749 2.1649309277 2.1891924056 2.2264597026
2.2372996263 2.2515023028 2.2603037007 2.2815657258 2.3083683377
2.3782489969 2.427630582 2.4321210143 2.4346654334 2.4817349586
2.4923786646

The GLM Procedure

2.5367081484 2.6096285189 6.4754327167

Number of Observations Read 1233
Number of Observations Used 1233

The GLM Procedure

Dependent Variable: LOGDIAM

Source	DF	Sum of Squares	Mean Square	F Value	Pr > F
Model	2	32.3825870	16.1912935	48.27	<.0001
Error	1230	412.5844093	0.3354345		
Corrected Total	1232	444.9669962			

R-Square	Coeff Var	Root MSE	LOGDIAM Mean
0.072775	67.11543	0.579167	0.862942

Source	DF	Type I SS	Mean Square	F Value	Pr > F
SOL	2	32.38258698	16.19129349	48.27	<.0001

Source	DF	Type III SS	Mean Square	F Value	Pr > F
SOL	2	32.38258698	16.19129349	48.27	<.0001

The GLM Procedure

t Tests (LSD) for LOGDIAM

NOTE: This test controls the Type I comparisonwise error rate, not the experimentwise error

rate.

Alpha 0.05
Error Degrees of Freedom 1230
Error Mean Square 0.335434
Critical Value of t 1.96189

Comparisons significant at the 0.05 level are indicated by

SOL Comparison	Difference Between Means	95% Confidence Limits	
3 - 1	0.33188	0.24845	0.41531
3 - 2	0.36795	0.28967	0.44624
1 - 3	-0.33188	-0.41531	-0.24845
1 - 2	0.03607	-0.04197	0.11411
2 - 3	-0.36795	-0.44624	-0.28967
2 - 1	-0.03607	-0.11411	0.04197

A.3. ANOVA & Model: Diameter

The SAS System 1

The GLM Procedure

Class Level Information

Class Levels Values

SOL 8 1 2 3 4 5 6 7 8

The SAS System 2

The GLM Procedure

Class Level Information

Class Levels Values

LOGDIAM 225

0.1016536537	0.1466943792	0.1756325686	0.2963940131
0.4246139269	0.5323914017	0.5743636446	0.6054082663
0.6318035503	0.6371057897	0.6481498146	0.659590397
0.6780335427	0.6820862332	0.7070500857	0.7820733898
0.7852704694	0.7997569156	0.8055826099	0.8073683246
0.8294247989	0.8363813486	0.8467262685	0.8522854019
0.8771340167	0.905836274	0.9182887345	0.929404371
0.9597332897	0.9604989865	0.9673640021	0.9685036033
0.9839493803	0.9843231423	0.9906558138	0.9913982044
0.9917691931	1.0202903219	1.0249657485	1.0321162974
1.0452115119	1.0518700261	1.0529173294	1.0722683133
1.0885619528	1.1108701861	1.1138292545	1.1281710909
1.1301109557	1.1537315879	1.1540469956	1.1665824151

1.1687600486 1.1712429797 1.1826470176 1.184178177
1.1844841277 1.1869283697 1.202070997 1.2071676952
1.2077656026 1.222303761 1.2395329797 1.246169853
1.2464574159 1.2675108251 1.2706028866 1.2739651761
1.2748039851 1.2837077723 1.2873024119 1.2881301123
1.2908841763 1.292807518 1.2947271676 1.2977363341
1.3056264581 1.3086030534 1.3113013821 1.3131858893
1.3196202279 1.3233545613 1.3268097143 1.3402504226
1.344430157 1.3501489145 1.354803694 1.3660916538
1.3759914681 1.3885418337 1.3925249109 1.3927733272
1.4016754632 1.4029056269 1.4068320123 1.4073217283
1.4090338481 1.4160958524 1.4334164682 1.4353225922
1.4362742934 1.4395981331 1.441729068 1.448329752
1.4525501569 1.4574515554 1.4576843572 1.4595448229
1.4662601428 1.4720132365 1.4727013889 1.4736181893
1.4777334214 1.485234309 1.4859134261 1.4865920824
1.4895276158 1.4902038245 1.4906543764 1.4929040962
1.4991765182 1.5002924652 1.5016299598 1.5045217425
1.5049658908 1.5082907304 1.5175418977 1.5201694447
1.5267082648 1.5295285292 1.5319087099 1.5385861715
1.5390154481 1.5403021736 1.540944916 1.5413731815
1.5415872455 1.5435117623 1.5541365966 1.557302158
1.559196696 1.5631845279 1.5748464677 1.5806268306
1.5837097639 1.5845302767 1.5898472627 1.5904589458
1.5912739418 1.5945272997 1.5963526729 1.5987813322
1.5999934536 1.6005989638 1.6028160361 1.6056306741
1.6082371919 1.6090378324 1.6104374128 1.611835037
1.6130314479 1.6158175194 1.6172076497 1.6191902039
1.6231435595 1.6257048849 1.6262950295 1.6302204516
1.6345206928 1.6446119874 1.6459626871 1.6496197021
1.6576564847 1.6582280766 1.6584185347 1.6589896913
1.6593702812 1.6607012064 1.6610811456 1.6631682349
1.6643048139 1.6656291921 1.6699684122 1.6767226592
1.6845453849 1.6880642329 1.6932274382 1.6935952204
1.6956156087 1.6961659159 1.7110915662 1.7231236768
1.7252634779 1.7259757287 1.7311244307 1.7387102481
1.7453664297 1.7455409954 1.7491998548 1.7504165057
1.7611284257 1.7652443636 1.7655865949 1.7690024821

The GLM Procedure

1.7739348843 1.8010495161 1.8040173666 1.8280913985
1.829055254 1.8338606452 1.8348189587 1.8364141098
1.8448261902 1.8470364847 1.878090059 1.904045945
1.905236953 1.9276006921 1.9345602679 2.0151696517
2.0253812648

PKWDTH 226

0.1168	0.1437	0.1465	0.1551	0.1696	0.1763	0.1826	0.1876
0.1888	0.1925	0.1962	0.1979	0.2039	0.2049	0.2068	0.2082
0.2123	0.2125	0.2166	0.2178	0.2185	0.2276	0.2303	0.2343
0.2363	0.2371	0.2403	0.2405	0.2458	0.2479	0.2489	0.2541
0.2606	0.2641	0.2681	0.2707	0.2727	0.2731	0.2761	0.2781

0.2784 0.28 0.2836 0.2837 0.2863 0.2885 0.2897 0.2943
0.2959 0.3027 0.3038 0.304 0.3138 0.3167 0.3366 0.3419
0.3449 0.3469 0.3489 0.3495 0.3515 0.3537 0.3594 0.3601
0.3629 0.3638 0.3641 0.3662 0.3687 0.3709 0.3812 0.3822
0.3872 0.3881 0.3894 0.3916 0.3944 0.3946 0.3948 0.3952
0.3962 0.4032 0.4034 0.4036 0.4047 0.4062 0.4082 0.4102
0.4114 0.4157 0.4175 0.4199 0.42 0.4216 0.4257 0.4267
0.4271 0.4276 0.4311 0.4344 0.4373 0.4383 0.4436 0.4447
0.4466 0.4493 0.4527 0.4548 0.4549 0.4566 0.4571 0.4613
0.4667 0.4691 0.4699 0.47 0.4704 0.477 0.4782 0.4795
0.4808 0.4813 0.4866 0.4873 0.4889 0.489 0.4915 0.4919
0.4922 0.4958 0.4968 0.5051 0.5147 0.5185 0.5203 0.5204
0.5227 0.5233 0.5258 0.5278 0.5293 0.5314 0.535 0.5384
0.5414 0.5423 0.5426 0.5448 0.5467 0.5471 0.5478 0.5481
0.5543 0.5593 0.5594 0.5603 0.5608 0.5637 0.5704 0.5705
0.5708 0.5716 0.5757 0.5759 0.5842 0.5845 0.585 0.5854
0.589 0.5905 0.5933 0.6 0.6008 0.6027 0.6112 0.6113
0.6152 0.6174 0.6288 0.6341 0.6345 0.6348 0.6392 0.6407
0.643 0.6444 0.6483 0.6607 0.6631 0.6638 0.6661 0.6664
0.6837 0.6905 0.6932 0.73 0.739 0.7546 0.759 0.7732
0.7951 0.8189 0.8282 0.8307 0.8491 0.8697 0.8718 0.873
0.8794 0.8969 0.9004 0.9138 0.9445 0.9466 0.9609 1.001
1.04 1.047 1.072 1.097 1.099 1.105 1.11 1.135
1.216 1.246

TRTA	2	0 1
TRTB	2	0 1
TRTC	2	0 1

Number of Observations Read	240
Number of Observations Used	232

The GLM Procedure

Dependent Variable: LOGDIAM

Source	DF	Sum of Squares	Mean Square	F Value	Pr > F
Model	6	18.32477508	3.05412918	61.02	<.0001
Error	225	11.26162217	0.05005165		
Corrected Total	231	29.58639725			

R-Square	Coeff Var	Root MSE	LOGDIAM Mean
0.619365	16.18154	0.223722	1.382577

Source	DF	Type I SS	Mean Square	F Value	Pr > F
TRTA	1	0.57234981	0.57234981	11.44	0.0008
TRTB	1	10.02983427	10.02983427	200.39	<.0001
TRTC	1	1.03512230	1.03512230	20.68	<.0001
TRTA*TRTB	1	0.05828949	0.05828949	1.16	0.2817
TRTA*TRTC	1	0.00126416	0.00126416	0.03	0.8739
TRTB*TRTC	1	6.62791504	6.62791504	132.42	<.0001

Source	DF	Type III SS	Mean Square	F Value	Pr > F
TRTA	1	0.45751632	0.45751632	9.14	0.0028
TRTB	1	10.06131880	10.06131880	201.02	<.0001
TRTC	1	1.13124233	1.13124233	22.60	<.0001
TRTA*TRTB	1	0.05870873	0.05870873	1.17	0.2800
TRTA*TRTC	1	0.01067189	0.01067189	0.21	0.6447
TRTB*TRTC	1	6.62791504	6.62791504	132.42	<.0001

Contrast	DF	Contrast SS	Mean Square	F Value	Pr > F
B	1	10.06131880	10.06131880	201.02	<.0001
C	1	1.13124233	1.13124233	22.60	<.0001
B*C	1	6.62791504	6.62791504	132.42	<.0001

Parameter		Estimate	Standard Error	t Value	Pr > Itl
Intercept		1.479101207 B	0.04006669	36.92	<.0001
TRTA	0	-0.134313295 B	0.05123806	-2.62	0.0094
TRTA	1	0.000000000 B			
TRTB	0	0.046803973 B	0.05123806	0.91	0.3620
TRTB	1	0.000000000 B			
TRTC	0	-0.491547486 B	0.05209443	-9.44	<.0001
TRTC	1	0.000000000 B			
TRTA*TRTB	0 0	0.063687482 B	0.05880469	1.08	0.2800
TRTA*TRTB	0 1	0.000000000 B			

The GLM Procedure

Dependent Variable: LOGDIAM

Parameter		Estimate	Standard Error	t Value	Pr > Itl
TRTA*TRTB	1 0	0.000000000 B			
TRTA*TRTB	1 1	0.000000000 B			
TRTA*TRTC	0 0	0.027149643 B	0.05879667	0.46	0.6447
TRTA*TRTC	0 1	0.000000000 B			
TRTA*TRTC	1 0	0.000000000 B			
TRTA*TRTC	1 1	0.000000000 B			
TRTB*TRTC	0 0	0.676472540 B	0.05878560	11.51	<.0001
TRTB*TRTC	0 1	0.000000000 B			
TRTB*TRTC	1 0	0.000000000 B			
TRTB*TRTC	1 1	0.000000000 B			

NOTE: The X'X matrix has been found to be singular, and a generalized inverse was used to solve the normal equations. Terms whose estimates are followed by the letter 'B' are not uniquely estimable.

The GLM Procedure
t Tests (LSD) for LOGDIAM
NOTE: This test controls the Type I comparisonwise error rate, not the experimentwise error rate.

Alpha 0.05
Error Degrees of Freedom 225
Error Mean Square 0.050052
Critical Value of t 1.97056
Least Significant Difference 0.0579
Harmonic Mean of Cell Sizes 115.9224
NOTE: Cell sizes are not equal.
Means with the same letter are not significantly different.

t Grouping	Mean	N	TRTA
A	1.43355	113	1
B	1.33418	119	0

The GLM Procedure
t Tests (LSD) for LOGDIAM
NOTE: This test controls the Type I comparisonwise error rate, not the experimentwise error rate.

Alpha 0.05
Error Degrees of Freedom 225
Error Mean Square 0.050052
Critical Value of t 1.97056
Least Significant Difference 0.0579
Harmonic Mean of Cell Sizes 115.9655

NOTE: Cell sizes are not equal.

Means with the same letter are not significantly different.

t Grouping	Mean	N	TRTB
A	1.58816	118	0
B	1.16978	114	1

The GLM Procedure

t Tests (LSD) for LOGDIAM

NOTE: This test controls the Type I comparisonwise error rate, not the experimentwise error rate.

Alpha 0.05
Error Degrees of Freedom 225
Error Mean Square 0.050052
Critical Value of t 1.97056
Least Significant Difference 0.0579
Harmonic Mean of Cell Sizes 115.9914

NOTE: Cell sizes are not equal.

Means with the same letter are not significantly different.

t Grouping	Mean	N	TRTC

A	1.45055	117	1
B	1.31342	115	0

The GLM Procedure
Least Squares Means

LOGDIAM TRTA	LSMEAN	Standard Error	HO:LSMEAN=O Pr > Itl	HO:LSMeanl= LSMean2 Pr > Itl
0	1.33695285	0.02051043	<.0001	0.0028
1	1.42584759	0.02106775	<.0001	

TRTA	LOGDIAM LSMEAN	95% Confidence	Limits
0	1.336953	1.296536	1.377370
1	1.425848	1.384332	1.467363

Least Squares Means for Effect
TRTA

i		Difference Between Means	95% Confidence Limits for LSMean(i)-LSMean(j)	
1	2	-0.088895	-0.146834	-0.030956

TRTB	LOGDIAM LSMEAN	Standard Error	HO:LSMEAN=O Pr > Itl	HO:LSMeanl= LSMean2 Pr > Itl
0	1.58984221	0.02059826	<.0001	<.0001
1	1.17295823	0.02098259	<.0001	

TRTB	LOGDIAM LSMEAN	95% Confidence	Limits
0	1.589842	1.549252	1.630432
1	1.172958	1.131611	1.214306

Least Squares Means for Effect
TRTB

i		Difference Between Means	95% Confidence Limits for LSMean(i)-LSMean(j)	
1	2	0.416884	0.358943	0.474825

TRTC	LOGDIAM LSMEAN	Standard Error	HO:LSMEAN=O Pr > Itl	HO:LSMeanl= LSMean2 Pr > Itl
0	1.31153202	0.02087389	<.0001	<.0001
1	1.45126842	0.02070092	<.0001	

The SAS System 10

The GLM Procedure

Least Squares Means

TRTC	LOGDIAM LSMEAN	95% Confidence	Limits
0	1.311532	1.270399	1.352665
1	1.451268	1.410476	1.492061

Least Squares Means for Effect TRTC

i		Difference Between Means	95% Confidence Limits for LSMean(i)-LSMean(j)	
1	2	-0.139736	-0.197657	-0.081816

TRTA	TRTB	LOGDIAM LSMEAN	Standard Error	Pr > Itl	LSMEAN Number
0	0	1.56131672	0.02912932	<.0001	1
0	1	1.11258899	0.02888242	<.0001	2
1	0	1.61836771	0.02912932	<.0001	3
1	1	1.23332746	0.03044474	<.0001	4

Least Squares Means for effect TRTA*TRTB
Pr > Itl for HO: LSMean(i)=LSMean(j)

Dependent Variable: LOGDIAM

i/j	1	2	3	4
1		<.0001	0.1674	<.0001
2	<.0001		<.0001	0.0044
3	0.1674	<.0001		<.0001
4	<.0001	0.0044	<.0001	

TRTA	TRTB	LOGDIAM LSMEAN	95% Confidence	Limits
0	0	1.561317	1.503916	1.618718
0	1	1.112589	1.055674	1.169504
1	0	1.618368	1.560967	1.675769
1	1	1.233327	1.173334	1.293321

Least Squares Means for Effect TRTA*TRTB

i		Difference Between Means	95% Confidence Limits for LSMean(i)-LSMean(j)	
1	2	0.448728	0.367894	0.529562
1	3	-0.057051	-0.138226	0.024124

The SAS System

The GLM Procedure
Least Squares Means
Least Squares Means for Effect
TRTA*TRTB

i		Difference Between Means	95% Confidence Limits for LSMean(i)-LSMean(j)	
1	4	0.327989	0.244959	0.411020
2	3	-0.505779	-0.586613	-0.424945
2	4	-0.120738	-0.203434	-0.038043
3	4	0.385040	0.302010	0.468071

NOTE: To ensure overall protection level, only probabilities associated with
pre-planned comparisons should be
used.

TRTA	TRTC	LOGDIAM LSMEAN	Standard Error	Pr > Itl	LSMEAN Number
0	0	1.27387207	0.02912932	<.0001	1
0	1	1.40003364	0.02888242	<.0001	2
1	0	1.34919198	0.02991029	<.0001	3
1	1	1.50250319	0.02966340	<.0001	4

Least Squares Means for effect
TRTA*TRTC
Pr > Itl for HO: LSMean(i)=LSMean(j)

Dependent Variable:
LOGDIAM

i/j	1	2	3	4
1		0.0024	0.0726	<.0001
2	0.0024		0.2227	0.0141
3	0.0726	0.2227		0.0003
4	<.0001	0.0141	0.0003	

TRTA	TRTC	LOGDIAM LSMEAN	95% Confidence Limits	
0	0	1.273872	1.216471	1.331273
0	1	1.400034	1.343119	1.456948
1	0	1.349192	1.290252	1.408132
1	1	1.502503	1.444050	1.560957

Least Squares Means for Effect
TRTA*TRTC

i		Difference Between Means	95% Confidence Limits for LSMean(i)-LSMean(j)	
1	2	-0.126162	-0.206996	-0.045327
1	3	-0.075320	-0.157599	0.006959

The GLM Procedure
Least Squares
Means

Least Squares Means for Effect
TRTA*TRTC

i		Difference Between Means	95% Confidence Limits for LSMean(i)-LSMean(j)	
1	4	-0.228631	-0.310547	-0.146715
2	3	0.050842	-0.031093	0.132776
2	4	-0.102470	-0.184054	-0.020885
3	4	-0.153311	-0.236302	-0.070321

NOTE: To ensure overall protection level, only probabilities associated with pre-planned comparisons should be used.

TRTB	TRTC	LOGDIAM LSMEAN	Standard Error	Pr > Itl	LSMEAN Number
0	0	1.68909215	0.02937617	<.0001	1
0	1	1.49059227	0.02888242	<.0001	2
1	0	0.93397189	0.02966340	<.0001	3
1	1	1.41194456	0.02966340	<.0001	4

Least Squares Means for effect
TRTB*TRTC
Pr > Itl for HO: LSMean(i)=LSMean(j)

Dependent Variable:
LOGDIAMI

i/j	1	2	3	4
1		<.0001	<.0001	<.0001
2	<.0001		<.0001	0.0588
3	<.0001	<.0001		<.0001
4	<.0001	0.0588	<.0001	

TRTB	TRTC	LOGDIAM LSMEAN	95% Confidence	Limits
0	0	1.689092	1.631205	1.746980
0	1	1.490592	1.433678	1.547507
1	0	0.933972	0.875518	0.992426
1	1	1.411945	1.353491	1.470398

Least Squares Means for Effect
TRTB*TRTC

i		Difference Between Means	95% Confidence Limits for LSMean(i)-LSMean(j)	
1	2	0.198500	0.117320	0.279680

1	3	0.755120	0.672854	0.837387

The SAS System 13

The GLM Procedure
Least Squares
Means

Least Squares Means for Effect
TRTB*TRTC

i		Difference Between Means	95% Confidence Limits for LSMean(i)-LSMean(j)	
1	4	0.277148	0.194881	0.359414
2	3	0.556620	0.475035	0.638205
2	4	0.078648	-0.002937	0.160233
3	4	-0.477973	-0.560609	-0.395336

NOTE: To ensure overall protection level, only probabilities associated with pre-planned comparisons should be used.

The SAS System 14

---------- TRTA=O ----------

The MEANS Procedure

Analysis Variable :
LOGDIAM

N	Mean	Std Dev	Minimum	Maximum
119	1.3341764	0.3024340	0.4246139	1.7491999

---------- TRTA=1 ----------

Analysis Variable :
LOGDIAM

N	Mean	Std Dev	Minimum	Maximum
113	1.4335479	0.4033456	0.1016537	2.0253813

The SAS System 15

---------- TRTB=O ----------

The MEANS Procedure

Analysis Variable :

LOGDIAM

N	Mean	Std Dev	Minimum	Maximum
118	1.5881600	0.1697547	1.1687600	2.0253813

---------- TRTB=1 ----------

Analysis Variable :
LOGDIAM

N	Mean	Std Dev	Minimum	Maximum
114	1.1697809	0.3770576	0.1016537	1.8448262

The SAS System 16

---------- TRTC=O ----------

The MEANS Procedure

Analysis Variable :
LOGDIAM

N	Mean	Std Dev	Minimum	Maximum
115	1.3134174	0.4581268	0.1016537	2.0253813

---------- TRTC=1 ----------

Analysis Variable :
LOGDIAM

N	Mean	Std Dev	Minimum	Maximum
117	1.4505548	0.1984715	0.7070501	1.8448262

REGRESSION MODEL 17
The REG Procedure
Model: MODEL1
Dependent Variable:
LOGDIAM

Number of Observations Read 240
Number of Observations Used 232
Number of Observations with Missing Values 8

Analysis of Variance

Source	DF	Sum of Squares	Mean Square	FValue	Pr > F
Model	4	18.25581	4.56395	91.44	<.0001
Error	227	11.33058	0.04991		
Corrected Total	231	29.58640			

Root MSE	0.22342	R-Square		0.6170
Dependent Mean	1.38258	Adj R-Sq	0.6103	
Coeff Var	16.15935			

Parameter Estimates

Variable	DF	Parameter Estimate	Standard Error	t Value	Pr > Itl
Intercept	1	1.64488	0.03280	50.14	<.0001
TRTA	1	0.08842	0.02936	3.01	0.0029
TRTB	1	-0.75561	0.04168	-18.13	<.0001
TRTC	1	-0.19850	0.04114	-4.82	<.0001
TRTBC	1	0.67576	0.05868	11.52	<.0001

A.4 ANOVA & Model: Peakwidth

The SAS System

The GLM Procedure

Class Level Information

Class	Levels	Values
SOL	8	1 2 3 4 5 6 7 8

The SAS System 2

The GLM Procedure

Class Level Information

Class	Levels	Values
LOGDIAM	225	

0.1016536537	0.1466943792	0.1756325686	0.2963940131
0.4246139269	0.5323914017	0.5743636446	0.6054082663
0.6318035503	0.6371057897	0.6481498146	0.659590397
0.6780335427	0.6820862332	0.7070500857	0.7820733898
0.7852704694	0.7997569156	0.8055826099	0.8073683246
0.8294247989	0.8363813486	0.8467262685	0.8522854019
0.8771340167	0.905836274	0.9182887345	0.929404371
0.9597332897	0.9604989865	0.9673640021	0.9685036033
0.9839493803	0.9843231423	0.9906558138	0.9913982044
0.9917691931	1.0202903219	1.0249657485	1.0321162974
1.0452115119	1.0518700261	1.0529173294	1.0722683133
1.0885619528	1.1108701861	1.1138292545	1.1281710909
1.1301109557	1.1537315879	1.1540469956	1.1665824151
1.1687600486	1.1712429797	1.1826470176	1.184178177
1.1844841277	1.1869283697	1.202070997	1.2071676952
1.2077656026	1.222303761	1.2395329797	1.246169853
1.2464574159	1.2675108251	1.2706028866	1.2739651761
1.2748039851	1.2837077723	1.2873024119	1.2881301123
1.2908841763	1.292807518	1.2947271676	1.2977363341

1.3056264581 1.3086030534 1.3113013821 1.3131858893
1.3196202279 1.3233545613 1.3268097143 1.3402504226
1.344430157 1.3501489145 1.354803694 1.3660916538
1.3759914681 1.3885418337 1.3925249109 1.3927733272
1.4016754632 1.4029056269 1.4068320123 1.4073217283
1.4090338481 1.4160958524 1.4334164682 1.4353225922
1.4362742934 1.4395981331 1.441729068 1.448329752
1.4525501569 1.4574515554 1.4576843572 1.4595448229
1.4662601428 1.4720132365 1.4727013889 1.4736181893
1.4777334214 1.485234309 1.4859134261 1.4865920824
1.4895276158 1.4902038245 1.4906543764 1.4929040962
1.4991765182 1.5002924652 1.5016299598 1.5045217425
1.5049658908 1.5082907304 1.5175418977 1.5201694447
1.5267082648 1.5295285292 1.5319087099 1.5385861715
1.5390154481 1.5403021736 1.540944916 1.5413731815
1.5415872455 1.5435117623 1.5541365966 1.557302158
1.559196696 1.5631845279 1.5725664377 1.5733961411
1.5736034594 1.5740179672 1.5748464677 1.5806268306
1.5837097639 1.5845302767 1.5898472627 1.5904589458
1.5912739418 1.5945272997 1.5963526729 1.5987813322
1.5999934536 1.6005989638 1.6028160361 1.6056306741
1.6082371919 1.6090378324 1.6104374128 1.611835037
1.6130314479 1.6158175194 1.6172076497 1.6191902039
1.6231435595 1.6257048849 1.6262950295 1.6302204516
1.6345206928 1.6446119874 1.6459626871 1.6496197021
1.6576564847 1.6582280766 1.6584185347 1.6589896913
1.6593702812 1.6607012064 1.6610811456 1.6631682349
1.6643048139 1.6656291921 1.6699684122 1.6767226592
1.6845453849 1.6880642329 1.6932274382 1.6935952204
1.6956156087 1.6961659159 1.7110915662 1.7231236768
1.7252634779 1.7259757287 1.7311244307 1.7387102481
1.7453664297 1.7455409954 1.7491998548 1.7504165057
1.7611284257 1.7652443636 1.7655865949 1.7690024821

The GLM Procedure

1.7739348843 1.8010495161 1.8040173666 1.8280913985
1.829055254 1.8338606452 1.8348189587 1.8364141098
1.8448261902 1.84703,64847 1.878090059 1.904045945
1.905236953 1.9276006921 1.9345602679 2.0151696517
2.0253812648

PKWDTH 226

0.1168	0.1437	0.1465	0.1551	0.1696	0.1763	0.1826	0.1876
0.1888	0.1925	0.1962	0.1979	0.2039	0.2049	0.2068	0.2082
0.2123	0.2125	0.2166	0.2178	0.2185	0.2276	0.2303	0.2343
0.2363	0.2371	0.2403	0.2405	0.2458	0.2479	0.2489	0.2541
0.2606	0.2641	0.2681	0.2707	0.2727	0.2731	0.2761	0.2781
0.2784	0.28	0.2836	0.2837	0.2863	0.2885	0.2897	0.2943
0.2959	0.3027	0.3038	0.304	0.3138	0.3167	0.3366	0.3419
0.3449	0.3469	0.3489	0.3495	0.3515	0.3537	0.3594	0.3601
0.3629	0.3638	0.3641	0.3662	0.3687	0.3709	0.3812	0.3822
0.3872	0.3881	0.3894	0.3916	0.3944	0.3946	0.3948	0.3952
0.3962	0.4032	0.4034	0.4036	0.4047	0.4062	0.4082	0.4102

0.4114 0.4157 0.4175 0.4199 0.42 0.4216 0.4257 0.4267
0.4271 0.4276 0.4311 0.4344 0.4373 0.4383 0.4436 0.4447
0.4466 0.4493 0.4527 0.4548 0.4549 0.4566 0.4571 0.4613
0.4667 0.4691 0.4699 0.47 0.4704 0.477 0.4782 0.4795
0.4808 0.4813 0.4866 0.4873 0.4889 0.489 0.4915 0.4919
0.4922 0.4958 0.4968 0.5051 0.5147 0.5185 0.5203 0.5204
0.5227 0.5233 0.5258 0.5278 0.5293 0.5314 0.535 0.5384
0.5414 0.5423 0.5426 0.5448 0.5467 0.5471 0.5478 0.5481
0.5543 0.5593 0.5594 0.5603 0.5608 0.5637 0.5704 0.5705
0.5708 0.5716 0.5757 0.5759 0.5842 0.5845 0.585 0.5854
0.589 0.5905 0.5933 0.6 0.6008 0.6027 0.6112 0.6113
0.6152 0.6174 0.6288 0.6341 0.6345 0.6348 0.6392 0.6407
0.643 0.6444 0.6483 0.6607 0.6631 0.6638 0.6661 0.6664
0.6837 0.6905 0.6932 0.73 0.739 0.7546 0.759 0.7732
0.7951 0.8189 0.8282 0.8307 0.8491 0.8697 0.8718 0.873
0.8794 0.8969 0.9004 0.9138 0.9445 0.9466 0.9609 1.001
1.04 1.047 1.072 1.097 1.099 1.105 1.11 1.135
1.216 1.246

TRTA	2	0 1
TRTB	2	0 1
TRTC	2	0 1

Number of Observations Read	240
Number of Observations Used	232

The GLM Procedure

Dependent Variable: PKWDTH

Source	DF	Sum of Squares	Mean Square	F Value	Pr > F
Model	6	10.15002262	1.69167044	167.12	<.0001
Error	225	2.27753723	0.01012239		
Corrected Total	231	12.42755984			

R-Square	Coeff Var	Root MSE	PKWDTH Mean
0.816735	20.22145	0.100610	0.497541

Source	DF	Type I SS	Mean Square	F Value	Pr > F
TRTA	1	2.06407015	2.06407015	203.91	<.0001
TRTB	1	4.01470964	4.01470964	396.62	<.0001
TRTC	1	0.03213565	0.03213565	3.17	0.0761
TRTA*TRTB	1	0.70847429	0.70847429	69.99	<.0001
TRTA*TRTC	1	0.06559890	0.06559890	6.48	0.0116
TRTB*TRTC	1	3.26503399	3.26503399	322.56	<.0001

Source	DF	Type III SS	Mean Square	F Value	Pr > F
TRTA	1	1.87484414	1.87484414	185.22	<.0001
TRTB	1	4.16969664	4.16969664	411.93	<.0001
TRTC	1	0.02361589	0.02361589	2.33	0.1281
TRTA*TRTB	1	0.71140017	0.71140017	70.28	<.0001
TRTA*TRTC	1	0.04346143	0.04346143	4.29	0.0394

TRTB*TRTC	1	3.26503399	3.26503399	322.56	<.0001
Contrast	DF	Contrast SS	Mean Square	F Value	Pr > F
B	1	4.16969664	4.16969664	411.93	<.0001
C	1	0.02361589	0.02361589	2.33	0.1281
B*C	1	3.26503399	3.26503399	322.56	<.0001

Parameter	Estimate	Standard Error	t Value	Pr > Itl
Intercept	0.4925026272 B	0.01801838	27.33	<.0001
TRTA 0	-.0417083249 B	0.02304225	-1.81	0.0716
TRTA 1	0.0000000000 B			
TRTB 0	0.1418250084 B	0.02304225	6.15	<.0001
TRTB 1	0.0000000000 B			
TRTC 0	-.1898126617 B	0.02342737	-8.10	<.0001
TRTC 1	0.0000000000 B			
TRTA*TRTB 0 0	-.2216969462 B	0.02644504	-8.38	<.0001
TRTA*TRTB 0 1	0.0000000000 B			

The GLM Procedure

Dependent Variable: PKWDTH

Parameter	Estimate	Standard Error	t Value	Pr > Itl
TRTA*TRTB 1 0	0.0000000000 B			
TRTA*TRTB 1 1	0.0000000000 B			
TRTA*TRTC 0 0	-.0547892760 B	0.02644144	-2.07	0.0394
TRTA*TRTC 0 1	0.0000000000 B			
TRTA*TRTC 1 0	0.0000000000 B			
TRTA*TRTC 1 1	0.0000000000 B			
TRTB*TRTC 0 0	0.4747943687 B	0.02643645	17.96	<.0001
TRTB*TRTC 0 1	0.0000000000 B			
TRTB*TRTC 1 0	0.0000000000 B			
TRTB*TRTC 1 1	0.0000000000 B			

NOTE: The X'X matrix has been found to be singular, and a generalized inverse was used to solve the normal equations. Terms whose estimates are followed by the letter 'B' are not uniquely estimable.

The GLM Procedure

t Tests (LSD) for PKWDTH

NOTE: This test controls the Type I comparisonwise error rate, not the experimentwise error rate.

Alpha	0.05
Error Degrees of Freedom	225
Error Mean Square	0.010122
Critical Value of t	1.97056
Least Significant Difference	0.026
Harmonic Mean of Cell Sizes	115.9224

NOTE: Cell sizes are not equal.

Means with the same letter are not significantly different.

t Grouping	Mean	N	TRTA
A	0.59434	113	1
B	0.40563	119	0

The SAS System 7

The GLM Procedure

t Tests (LSD) for PKWDTH

NOTE: This test controls the Type I comparisonwise error rate, not the experimentwise error rate.

Alpha	0.05
Error Degrees of Freedom	225
Error Mean Square	0.010122
Critical Value of t	1.97056
Least Significant Difference	0.026
Harmonic Mean of Cell Sizes	115.9655

NOTE: Cell sizes are not equal.

Means with the same letter are not significantly different.

t Grouping	Mean	N	TRTB
A	0.62924	118	0
B	0.36123	114	1

The SAS System 8

The GLM Procedure

t Tests (LSD) for PKWDTH

NOTE: This test controls the Type I comparisonwise error rate, not the experimentwise error rate.

Alpha	0.05
Error Degrees of Freedom	225
Error Mean Square	0.010122
Critical Value of t	1.97056
Least Significant Difference	0.026
Harmonic Mean of Cell Sizes	115.9914

NOTE: Cell sizes are not equal.

Means with the same letter are not significantly different.

t Grouping	Mean	N	TRTC
A	0.50827	115	0
A			
A	0.48700	117	1

The GLM Procedure
Least Squares Means

TRTA	PKWDTH LSMEAN	Standard Error	HO:LSMEAN=O Pr > Itl	HO:LSMeanl= LSMean2 Pr > Itl
0	0.40725596	0.00922374	<.0001	<.0001
1	0.58720739	0.00947437	<.0001	

TRTA	PKWDTH LSMEAN	95% Confidence	Limits
0	0.407256	0.389080	0.425432
1	0.587207	0.568538	0.605877

Least Squares Means for Effect
TRTA

i		Difference Between Means	95% Confidence Limits for LSMean(i)-LSMean(j)	
1	2	-0.179951	-0.206007	-0.153896

TRTB	PKWDTH LSMEAN	Standard Error	HO:LSMEAN=O Pr > Itl	HO:LSMeanl= LSMean2 Pr > Itl
0	0.63141853	0.00926324	<.0001	<.0001
1	0.36304481	0.00943608	<.0001	

TRTB	PKWDTH LSMEAN	95% Confidence	Limits
0	0.631419	0.613165	0.649672
1	0.363045	0.344450	0.381639

Least Squares Means for Effect
TRTB

i		Difference Between Means	95% Confidence Limits for LSMean(i)-LSMean(j)	
1	2	0.268374	0.242317	0.294430

TRTC	PKWDTH LSMEAN	Standard Error	HO:LSMEAN=O Pr > Itl	HO:LSMeanl= LSMean2 Pr > Itl
0	0.50732662	0.00938719	<.0001	0.1281
1	0.48713673	0.00930940	<.0001	

The GLM Procedure
Least Squares Means

TRTC	PKWDTH LSMEAN	95% Confidence	Limits
0	0.507327	0.488829	0.525825
1	0.487137	0.468792	0.505482

Least Squares Means for Effect TRTC

i	i	Difference Between Means	95% Confidence Limits for LSMean(i)-LSMean(j)	
1	2	0.020190	-0.005857	0.046237

TRTA	TRTB	PKWDTH LSMEAN	Standard Error	Pr > Itl	LSMEAN Number
0	0	0.48601858	0.01309974	<.0001	1
0	1	0.32849333	0.01298871	<.0001	2
1	0	0.77681849	0.01309974	<.0001	3
1	1	0.39759630	0.01369130	<.0001	4

Least Squares Means for effect TRTA*TRTB
Pr > Itl for HO: LSMean(i)=LSMean(j)

Dependent Variable: PKWDTH

i/j	1	2	3	4
1		<.0001	<.0001	<.0001
2	<.0001		<.0001	0.0003
3	<.0001	<.0001		<.0001
4	<.0001	0.0003	<.0001	

TRTA	TRTB	PKWDTH LSMEAN	95% Confidence	Limits
0	0	0.486019	0.460205	0.511832
0	1	0.328493	0.302898	0.354088
1	0	0.776818	0.751005	0.802632
1	1	0.397596	0.370617	0.424576

Least Squares Means for Effect TRTA*TRTB

i		Difference Between Means	95% Confidence Limits for LSMean(i)-LSMean(j)	
1	2	0.157525	0.121173	0.193877
1	3	-0.290800	-0.327305	-0.254295

Least Squares Means
Least Squares Means for Effect
TRTA*TRTB

i		Difference Between Means	95% Confidence Limits for LSMean(i)-LSMean(j)	
1	4	0.088422	0.051083	0.125762
2	3	-0.448325	-0.484677	-0.411973
2	4	-0.069103	-0.106292	-0.031914
3	4	0.379222	0.341883	0.416562

NOTE: To ensure overall protection level, only probabilities associated with pre-planned comparisons should be used.

TRTA	TRTC	PKWDTH LSMEAN	Standard Error	Pr > It	LSMEAN Number
0	0	0.40365358	0.01309974	<.0001	1
0	1	0.41085833	0.01298871	<.0001	2
1	0	0.61099965	0.01345095	<.0001	3
1	1	0.56341513	0.01333992	<.0001	4

Least Squares Means for effect
TRTA*TRTC
Pr > Itl for HO: LSMean(i)=LSMean(j)

Dependent Variable:
PKWDTH

i/j		1	2	3	4
	1		0.6965	<.0001	<.0001
	2	0.6965		<.0001	<.0001
	3	<.0001	<.0001		0.0127
	4	<.0001	<.0001	0.0127	

TRTA	TRTC	PKWDTH LSMEAN	95% Confidence	Limits
0	0	0.403654	0.377840	0.429467
0	1	0.410858	0.385263	0.436453
1	0	0.611000	0.584494	0.637506
1	1	0.563415	0.537128	0.589702

Least Squares Means for Effect
TRTA*TRTC

i		Difference Between Means	95% Confidence Limits for LSMean(i)-LSMean(j)	
1	2	-0.007205	-0.043557	0.029147
1	3	-0.207346	-0.244348	-0.170344

The SAS System 12

The GLM Procedure
Least Squares
Means

Least Squares Means for Effect
TRTA*TRTC

i	i	Difference Between Means	95% Confidence Limits for LSMean(i)-LSMean(j)	
1	4	-0.159762	-0.196600	-0.122923
2	3	-0.200141	-0.236988	-0.163295
2	4	-0.152557	-0.189246	-0.115867
3	4	0.047585	0.010263	0.084906

NOTE: To ensure overall protection level, only probabilities associated with pre-planned comparisons should be used.

TRTB	TRTC	PKWDTH LSMEAN	Standard Error	Pr > Itl	LSMEAN Number
0	0	0.76021207	0.01321075	<.0001	1
0	1	0.50262500	0.01298871	<.0001	2
1	0	0.25444116	0.01333992	<.0001	3
1	1	0.47164846	0.01333992	<.0001	4

Least Squares Means for effect
TRTB*TRTC
Pr > Itl for HO: LSMean(i)=LSMean(j)

Dependent Variable:
PKWDTH

i/j	1	2	3	4
1		<.0001	<.0001	<.0001
2	<.0001		<.0001	0.0976
3	<.0001	<.0001		<.0001
4	<.0001	0.0976	<.0001	

TRTB	TRTC	PKWDTH LSMEAN	95% Confidence	Limits
0	0	0.760212	0.734179	0.786245
0	1	0.502625	0.477030	0.528220
1	0	0.254441	0.228154	0.280728
1	1	0.471648	0.445361	0.497936

Least Squares Means for Effect TRTB*TRTC

		Difference Between Means	95% Confidence Limits for LSMean(i)-LSMean(j)	
1	2	0.257587	0.221079	0.294095
1	3	0.505771	0.468775	0.542767

The GLM Procedure
Least Squares Means

Least Squares Means for Effect TRTB*TRTC

i		Difference Between Means	95% Confidence Limits for LSMean(i)-LSMean(j)	
1	4	0.288564	0.251567	0.325560
2	3	0.248184	0.211494	0.284873
2	4	0.030977	-0.005713	0.067666
3	4	-0.217207	-0.254370	-0.180045

NOTE: To ensure overall protection level, only probabilities associated with pre-planned comparisons should be used.

The SAS System 14

---------- TRTA=O

The MEANS Procedure

Analysis Variable : PKWDTH

N	Mean	Std Dev	Minimum	Maximum
119	0.4056269	0.1198863	0.1465000	0.6664000

---------- TRTA=1 ----------

Analysis Variable : PKWDTH

N	Mean	Std Dev	Minimum	Maximum
113	0.5943363	0.2781878	0.1168000	1.2460000

The SAS System 15

---------- TRTB=O ----------

The MEANS Procedure

Analysis Variable :
PKWDTH

N	Mean	Std Dev	Minimum	Maximum
118	0.6292356	0.2240253	0.2943000	1.2460000

---------- TRTB=1 ----------

Analysis Variable :

PKWDTH

N	Mean	Std Dev	Minimum	Maximum
114	0.3612263	0.1454562	0.1168000	0.7590000

---------- TRTC=O ----------

The MEANS Procedure

Analysis Variable :
PKWDTH

N	Mean	Std Dev	Minimum	Maximum
115	0.5082670	0.3093280	0.1168000	1.2460000

---------- TRTC=1 ----------

Analysis Variable :
PKWDTH

N	Mean	Std Dev	Minimum	Maximum
117	0.4869991	0.1134633	0.2303000	0.7590000

REGRESSION MODEL 17
The REG Procedure
Model: MODEL1
Dependent Variable:
PKWDTH

Number of Observations Read	240
Number of Observations Used	232
Number of Observations with Missing Values	8

Analysis of Variance

Source	DF	Sum of Squares	Mean Square	FValue	Pr > F
Model	6	10.15002	1.69167	167.12	<.0001
Error	225	2.27754	0.01012		
Corrected Total	231	12.42756			

Root MSE	0.10061	R-Square	0.8167
Dependent Mean	0.49754	Adj R-Sq	0.8118
Coeff Var	20.22145		

Parameter Estimates

Variable	DF	Parameter Estimate	Standard Error	t Value	Pr > Itl
Intercept	1	0.60111	0.01748	34.39	<.0001
TRTA	1	0.31819	0.02289	13.90	<.0001
TRTB	1	-0.39492	0.02276	-17.35	<.0001

TRTC	1	-0.23019	0.02276	-10.11	<.0001
TRTAB	1	-0.22170	0.02645	-8.38	<.0001
TRTAC	1	-0.05479	0.02644	-2.07	0.0394
TRTBC	1	0.47479	0.02644	17.96	<.0001

VITA

KEVIN NAKIA BARBER

Candidate for the Degree of

Master of Science

Thesis: SIZE CONTROLLED REVERSE MICELLE SYNTHESIS OF METALLIC COBALT NANOPARTICLES

Major Field: Chemical Engineering

Education:

BS Chemical Engineering, University of Oklahoma, 1999
MS Chemical Engineering, Oklahoma State University, 2005

Experience:

Engineering Co-op, Nuclear Licensing, Arkansas Nuclear One, Russellville, AR, 1995
Engineering Co-op, Engineering Training, Arkansas Nuclear One, Russellville, AR, 1995
Research Engineer, NewMan Technologies, Norman, OK, 2000 – 2002
Head Teaching Assistant, Fluid Mechanics, Oklahoma State University, School of Chemical Engineering, 2003-2004.
Tutor, Engineering and Chemistry, Oklahoma State University, CEAT Student Services, 2004.
Research Assistant, Oklahoma State University, School of Chemical Engineering, Inorganic Synthesis and Ceramics Processing, 2002-2005.

Professional Memberships:

American Association for the Advancement of Science, 2003 - 2005

Name: Kevin Nakia Barber Date of Degree: July, 2005

Institution: Oklahoma State University Location: Stillwater, Oklahoma

Title of Study: SIZE CONTROLLED REVERSE MICELLE SYNTHESIS OF METALLIC COBALT NANOPARTICLES

Pages in Study: 140 Candidate for the Degree of Master of Science
Major Field: Chemical Engineering

Scope and Method of Study:

This study examined the effects of process variables on the particle size distribution of metallic cobalt nanoparticles synthesized by a reverse micelle process. The factors examined were metal salt concentration, reducing agent to metal ion ratio, and water content. The range of interest for the cobalt particle diameter was 1 – 5 nm. Characterization methods used to determine the particle diameter included dynamic light scattering (DLS) and tapping mode-atomic force microscopy (TM-AFM).

Findings and Conclusions:

The following effects were determined for the experimental system: (1) Average particle diameter increases with increasing metal salt concentration. (2) Average particle diameter decreases as the reducing agent to metal salt ratio increases. (3) Average particle diameter increases with increasing water content. (4) One two-way interaction exists between the reducing agent ratio and the water content. The effects for the polydispersity of the particles, embodied in the peak width of the distribution, were similarly determined as follows: (1) Average peak width increases with increasing metal salt concentration. (2) Average peak width decreases as the reducing agent to metal salt ratio increases. (3) Average peak width decreases with increasing water content. (4)Three two-way interactions for all three factors.

ADVISER'S APPROVAL: Dr. James E. Smay